Phase Diagram for Liquid Crystalline Polymer/ Polycarbonate Blends

by

Gang Huang

A Thesis submitted to the Faculty of Graduate Studies and Research in partial
fulfillment of the requirements of the degree of Master of Engineering

November 2001

Department of Chemical Engineering

McGill University, Montreal

0-612-79076-2

Canadä

To my parents

Abstract

Blends containing a thermotropic liquid crystalline polymer and an engineering thermoplastic polymer have recently received considerable attention, because liquid crystalline polymers display low melt viscosity, excellent chemical resistance, thermal stability and mechanical performance. A novel mechanism to form binary polymer blends is through phase separation by spinodal decomposition in the unstable region of the phase diagram. The overall objective of this work is to investigate the effects of thermally induced phase separation by spinodal decomposition on the morphology development of liquid crystalline polymer/polycarbonate blends and to obtain a thermodynamic binary phase diagram. The blends were obtained using a twin-screw extruder at various processing melt temperatures. To study miscibility of the blends and the resulting morphology, techniques such as differential scanning calorimetry and scanning electron microscopy were used. The liquid crystalline polymer/polycarbonate blend undergoes phase separation during thermally induced spinodal decomposition exhibiting a miscibility window reminiscent of a lower critical solution temperature. The blend is found to be miscible, when blend T_g slightly decreases. On the other hand, the blend is found to be immiscible as blend T_g increases. A thermodynamic two-phase transition curve phase diagram was obtained using an innovative practical experimental technique in conjunction with twin screw extrusion and scanning electron microscopy.

Résumé

Les mélanges contenant un polymère cristallin liquide thermotropique et un polymère d'ingénierie thermoplastique ont reçu récemment une attention considérable, parce que les polymères cristallins liquides affichent de basses viscosités de fonte, d'excellentes résistances chimiques, thermique et performances mécaniques. Un nouveau mécanisme pour créer des mélanges binaires de polymères consiste en une séparation spinodal dans la région instable du diagramme de phase. L'objectif global de ce travail est d'investiguer les effets de la décomposition spinodal de phase, induite de façon thermale, sur le développement de la morphologie de mélanges de polymères/poly carbonates liquides cristallins et d'obtenir un diagramme de phase thermodynamique binaire. Les mélanges ont été obtenus en utilisant une extrudeuse double vis co-rotative fonctionnant à différentes températures de fontes. Pour étudier la miscibilité des mélanges et leurs résultantes morphologies, des techniques tel que la calorimétrie différentielle et la microscopie électronique ont été utilisées. Le mélange polymère/poly carbonate cristallin liquide subit une séparation de phase lors de la décomposition spinodal induite de façon thermale exhibe une fenêtre de miscibilité réminiscente à une température de solution critique inférieure. Le mélange apparaît être miscible, quand T_g du mélange diminue légèrement. D'un autre coté, le mélange apparaît être non miscible a mesure que T_g du mélange augmente. Un diagramme thermodynamique de transition de phases a été obtenu en utilisant une technique expérimentale pratique innovante en conjonction avec l'extrudeuse double vis co-rotative jumeler et la microscopie électronique.

Acknowledgments

Table of Contents

List of Figures

List of Tables

Nomenclature

Symbols

d_m	droplet diameter
D_i	droplet diameter of particles i
$<D>_n$	number average droplet size
$<D>_w$	weight average droplet size
f	Flory-Huggins' free energy density of mixing
F	total free energy
ΔG_m	Gibbs free energy of mixing
H_m	enthalpy of mixing
k_B	Boltzmann's constant
m	mass
M	mobility
M_0	structure unit molecular weight
M_n	number average molar mass
M_w	weight average molar mass
N	degree of polymerization of polymer
N_i	number of droplets
p	pressure
PD	particle distribution
$R(k)$	amplification factor
S_m	entropy of mixing

t	time
T	temperature
T_c	critical temperature
T_g	glass transition temperature
T_i	initial temperature
T_f	final temperature
T_{pm}	processing melt temperature
v	volume of a cell or segment
V	volume
V_T	total volume
x,y,z	rectangular coordinates (parallel, transverse, and plumb to flow respectively)

χ	Flory-Huggins' interaction parameter
χ_c	Flory-Huggins' interaction parameter at critical point
ϕ_i	volume fraction of component i
ϕ_0	average volume fraction
ϕ_c	critical volume fraction
κ	gradient energy parameter
λ_m	wavelength
ρ	density

DSC	differential scanning calorimetery
LC	liquid crystal
LCP	liquid crystalline polymer
LCST	lower critical solution temperature
PLM	polarized light microscopy
SALS	small-angle light scattering
SEM	scanning electron microscopy
SD	spinodal decomposition
TIPS	thermally induced phase separation
TSE	twin screw extruder
UCST	upper critical solution temperature
XRD	X-ray diffraction

Chapter 1

Introduction

1.1   Introduction to Liquid Crystals

Liquid crystals are certain organic materials that do not show a single transition from the solid to liquid phase, but rather exhibit a certain state of transitions involving a new phase. This new phase is called the liquid crystal mesophase, and has both solid-like molecular order and liquid-like fluidity.

There are two classification systems for liquid crystals (LCs). In the first system, LCs can be classified in three major groups. They are nematic, cholesteric and smectic. These types of structures are shown in Figure 1-1. The nematic phase, which is the Greek word for thread, has been formed when the molecules tend to align parallel to each other with the director **n** as shown in Figure 1-1. The director **n** is a unit vector that gives the preferred average molecular orientation in the neighborhood of any point. The most common examples of molecules forming the liquid crystal phase are closely associated with cholesterol, which is the reason why the second class is called cholesteric. Lastly, the third class is called smectic, which is the Greek word for soap. There are at least ten identified smectic phases and the best known are the smectic-A and smectic-C phases. For example, in multiple transition thermotropic (to be defined below) systems, the increase in temperature leads to changes from the most order to the least order state: crystal(k) $\rightarrow$ smectic (s) $\rightarrow$ nematic (n) $\rightarrow$ isotropic (i).

In the second classification system, LCs can be classified according to the method of phase transition. They are thermotropic and lyotropic liquid crystals. The term "thermotropic" arises because transitions involving these mesophases are most naturally effected by changing temperature. Cyanobiphenyls and cholesterol esters are examples of

(A)   **(B)**

(C)   **(D)**
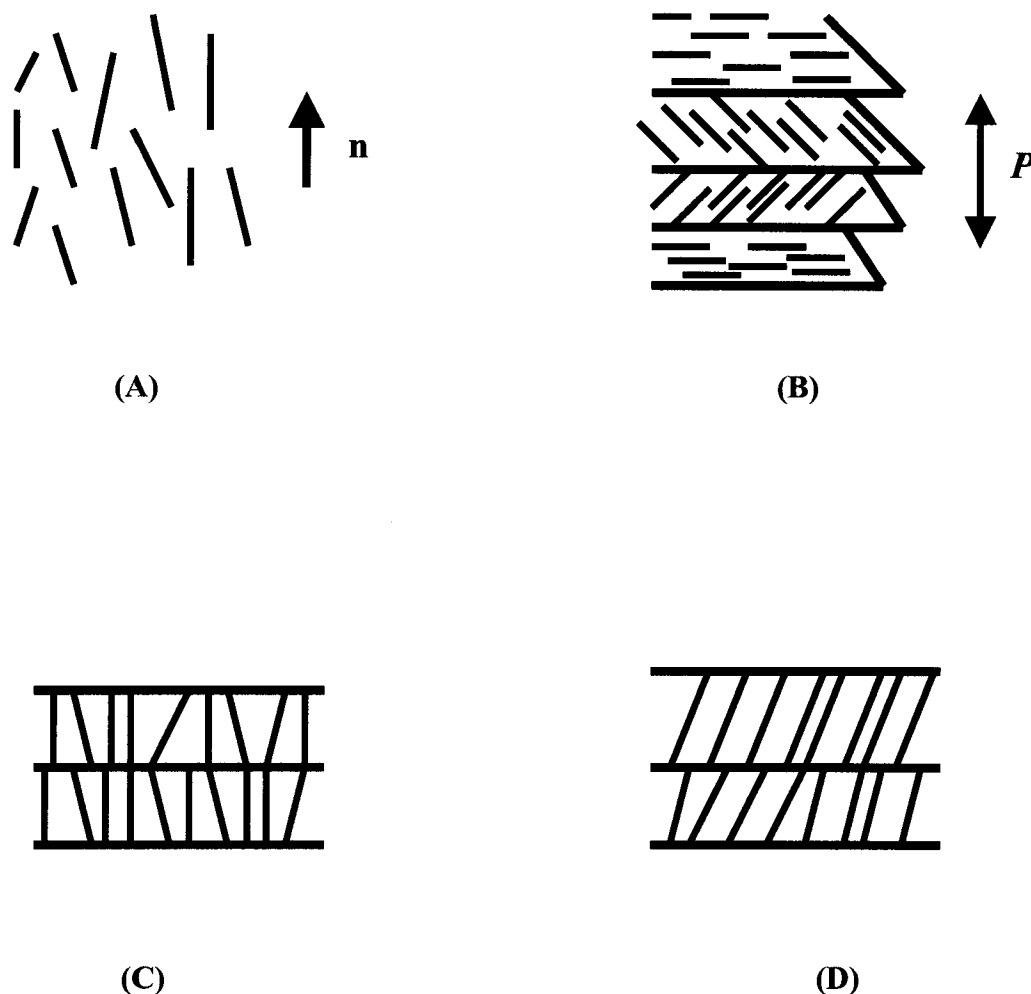
Figure 1-1: Schematic representations of the (A) nematic, (B) cholesteric, (C) smectic-A, and (D) smectic-C liquid crystalline phases. **n** is the director and P is the period.

thermotropic ordered fluid mesophases, which are obtained through temperature changes. In this type of liquid crystal, every molecule participates on an equal basis in the long range ordering. On the other hand, lyotropic liquid crystals are obtained by concentration changes. Generally, solutions of rod-like entities in a normally isotropic solvent often form liquid crystal phases at sufficiently high solute concentrations. Deoxyribonucleic acid (DNA), certain viruses (e.g., tobacco mosaic virus (TMV)), and many synthetic polypeptides all form lyotropic mesophases when dissolved in an appropriate solvent (usually water) in suitable concentrations.

1.2 Liquid Crystalline Polymer/Polycarbonate Blends

Polymer blends are mixtures of at least two polymers or copolymers. They are widely used in engineering applications [1], such as blends of thermoplastic polyesters poly(ethyleneterephthalate) (PET), poly(p-hydroxybenzoic acid) (PHB) with engineering plastics polycarbonate (PC), acrylonitrile-butadiene-styrene copolymer (ABS), styrene-maleic anhydride copolymer (SMA) and acrylonitrile-styrene-acrylates copolymer (ASA). There are two major reasons for polymer blending. The primary and most important reason is cost. For this reason, the manufacturer must use a material, which can be produced at a lower cost with properties meeting desired specifications, to remain competitive [2]. Secondly, polymer blending is a well-established strategy for improving material physical properties, such as impact resistance, toughness, high modulus and elasticity. Usually, the excellent properties of an expensive resin can be extended by blending with a cheaper polymer without the need to develop completely new polymers.

Blends of engineering thermoplastic polycarbonate (PC) and thermotropic liquid crystalline polymer (LCP) have recently received considerable attention [2,3,4], because the blends can take advantage of the high performance engineering properties of both components. LEXAN polycarbonate, manufactured by General Electric Plastics, is an amorphous engineering thermoplastic that combines high levels of mechanical, optical, electrical and thermal properties. This outstanding combination of engineering properties and processing versatility have made it the ideal resin for many applications, including compact discs, light covers, automotive headlamp lenses and housings for electrical applications.

On the other hand, liquid crystalline polymers (LCPs) represent a new class of engineering plastics with unique chemical and physical properties [4]. For instance, LCPs are highly resistant to most solvents at moderate to elevated temperatures (200°C). They have extremely rigid, rod-like molecules, which results in unique processing advantages compared with amorphous and semi-crystalline plastics. LCPs exhibit high ordered in both the melt and solid state. Therefore, LCPs find broad use in the electrical/electronic, health care, telecommunication and packaging industries.

3

Although many macroscopic properties of LCPs are very advantageous, the costs associated with production of these materials are high. The market price for a commercial grade LCP is US$12/lb. The blending of a conventional resin, such as LEXAN polycarbonate with a LCP can produce improvements in cost effectiveness and can yield novel chemical and physical properties. The spectrum of these composite materials exhibits a wide range of interesting peculiarities [4]. Since polycarbonate is an amorphous polymer, it has randomly oriented chains in both melt and solid phases. These amorphous polymers exhibit high impact strength, but relatively low stiffness and load bearing capacity. To compensate for poor mechanical performance, amorphous materials are usually polymerized to high molecular weights; however, this increases the melt viscosity and decreases the flowability. Addition of small amounts of LCP has been found to impart low melt viscosity and to minimize shrinkage during solidification. This is due to the highly ordered structure of LCPs. Because an outstanding significant feature of these blends is their ability to form a fibrillar structure and give a self-reinforcing effect after being processed, the blends are widely used in many automotive applications, in surgical devices and in telecommunications for network interface devices.

Despite poor interface adhesion and difficulty in controlling phase morphology, liquid crystalline polymer/polycarbonate blends can be obtained through a novel phase separation mechanism by spinodal decomposition (SD). The spinodal decomposition is defined as an active and irreversible process taking place spontaneously and continuously inside the unstable region of the thermodynamic phase diagram. The thorough study of SD theory will be presented in section 2.4, which could be well understood in terms of the Flory-Huggins and Cahn-Hilliard theories.

Our work is mainly concerned with the thermodynamic phase diagram for the LCP/PC blend system. Thus, it is of interest to determine the two-phase transition temperature points and construct a phase diagram based on these temperatures. Once this problem has been resolved, it is of further interest to evaluate the diagram in relation to phase separation theories.

1.3 Thesis Objectives

The objectives of this research thesis are listed below:

1. To develop a practical experimental technique for the determination of the thermodynamic binary phase diagram of liquid crystalline polymer/polycarbonate blends.

2. To evaluate the effects of various factors on phase separation, including processing temperature and shear rate.

3. To characterize the effect of processing temperature on the morphology of liquid crystalline polymer/polycarbonate blends during the phase separation process.

4. To compare the experimental phase diagram of liquid crystalline polymer /polycarbonate blends with the theoretical phase diagram obtained using the Flory-Huggins theory.

5. To compare the experimental droplet size distribution of liquid crystalline polymer/polycarbonate blends with the theoretical droplet size distribution obtained using the Cahn-Hilliard theory.

1.4 Thesis Organization

Chapter 2 summarizes the relevant technical background. The experimental techniques generally used to obtain the thermodynamic phase diagram of binary liquid crystalline polymer/polycarbonate blend systems are described. A novel approach is introduced, which is based on the thermally induced spinodal decomposition (SD)

method, for forming binary polymer blends. Two types of phase diagram for binary polymer blends are also introduced.

Chapter 3 describes the various experimental techniques used in this study to determine the phase diagram of liquid crystalline polymer/polycarbonate blend systems.

The phase diagram is presented in Chapter 4. The diagram and other results are discussed in terms of existing theories of phase separation.

Chapter 5 presents the general conclusions of this thesis and suggestions for future work.

Chapter 2

Technical Background

This chapter introduces the basic phase separation method and theory of spinodal decomposition (SD). We describe a novel mechanism to form binary polymer blends by SD due to temperature variations. Two types of phase diagram for binary polymer blends are presented in detail. The experimental techniques to obtain these thermodynamic phase diagrams are introduced as well.

2.1   Introduction

As mentioned previously, a polymer blend is a mixture of at least two polymers or copolymers. Immiscible and miscible blends are the two major types. As can be seen in Figure 2-1 [5], these blends are differentiated according to the Gibbs free energy of mixing ΔG_m. The majority of polymer blends are immiscible. These heterogeneous polymer blends have a positive ΔG_m value. In some cases, two polymers are soluble. However, they tend towards phase separation to form multiphase at some temperature and molecular weight. In many applications, miscibility of the phases is not desired or required. Therefore, phase separation methods have been one of the practical methods to obtain multi-component polymer blends. For example, the desired morphology of the blends can be obtained by controlling the polymer concentration and processing conditions such as temperature, shear rate and pressure. In order to obtain the heterogeneous mixtures and control their phase morphology, it is fundamentally important to understand the phase separation method. In addition, phase separation is an important field of polymer formation, modification and processing [6].
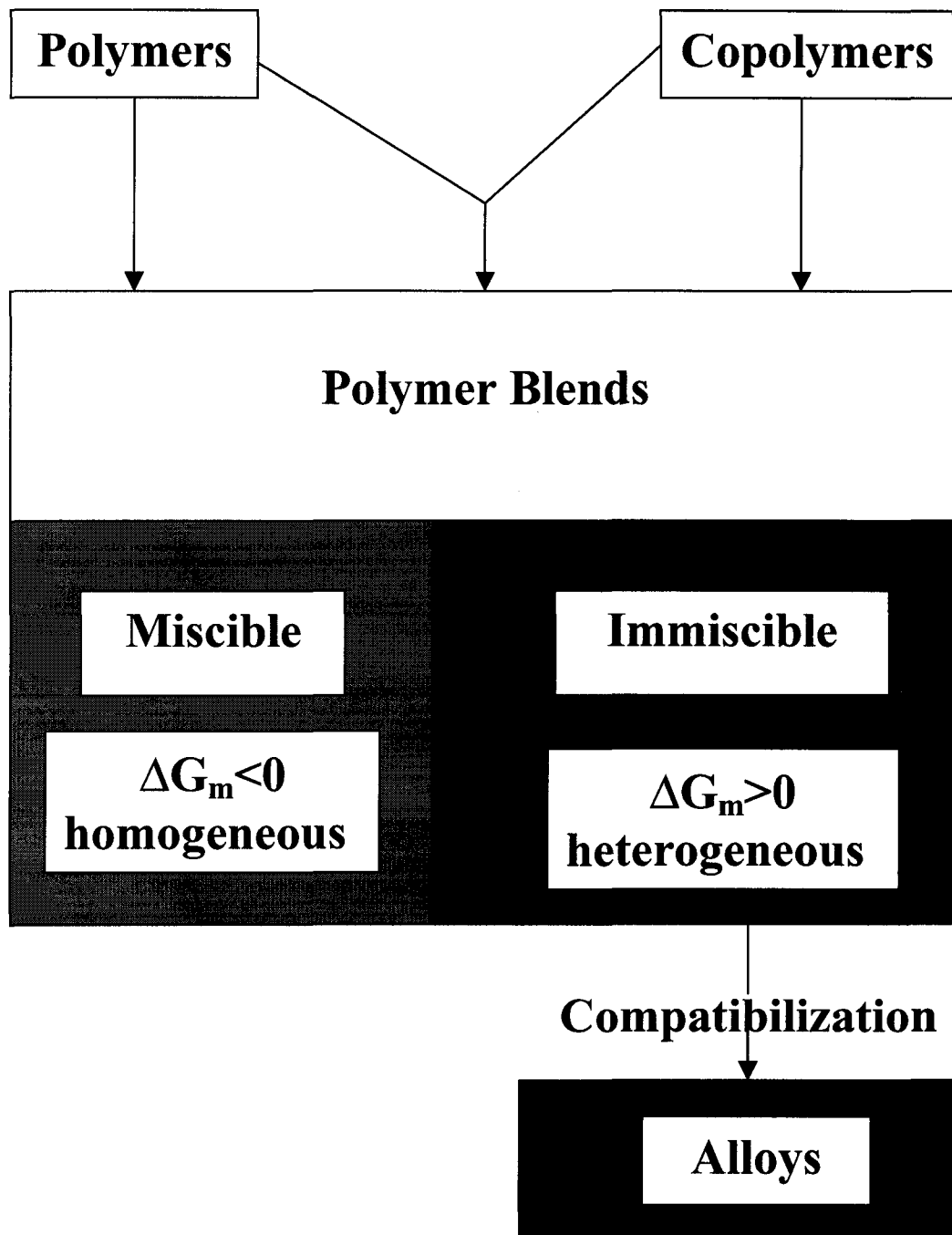
Figure 2-1: Schematic diagram of the interrelation between the different types of polymer blends [5].

2.2 Phase Separation Thermodynamics

Thermodynamics is a fundamental factor in determining polymer-polymer miscibility [7,8]. Based on the second law of thermodynamics, miscibility takes place when the Gibbs free energy of mixing is negative; i.e., $\Delta G_m < 0$. In addition, the second partial derivative of free energy with respect to composition is positive; i.e., $[\partial^2 \Delta G_m / \partial \phi_i^2]_{T,P,\phi_{j \neq i}} > 0$, where ϕ_i is the volume fraction of the ith component. The Gibbs free energy of mixing ΔG_m is expressed as:

$$\Delta G_m = \Delta H_m - T\Delta S_m \qquad (2\text{-}1)$$

where ΔH_m and ΔS_m are the enthalpy and entropy of mixing, respectively. T is the temperature. Generally, the distinctive property of polymers is their large molecular weight that can be used to control the miscibility of a multi-component mixture. The mixing entropy ΔS_m of a large molecular weight polymer almost equals zero. On the other hand, the enthalpy of mixing ΔH_m is always positive in most polymers, at least for non-polar polymer systems [5]. Therefore, the Gibbs free energy of mixing is seldom negative, which means that phase separation always occurs in polymer blends.

In the case of binary polymer blend systems (components 1 and 2), the Gibbs free energy of mixing ΔG_m versus volume fraction of component 1, ϕ_1, diagram can be constructed as a function of temperature. As shown in Figure 2-2, the shape of the free energy of mixing curve and the onset of phase separation varies by changing the temperature values from T_1 to T_5 ($T_1 < T_c < T_3 < T_4 < T_5$). T_2 is considered as the critical temperature T_c shown in Figure 2-2. In phase separation mechanism, the miscible polymer blend at an initial temperature T_1 goes through the critical temperature T_c, eventually becomes a totally immiscible system at temperature T_5. In the upper part of this diagram, the binodal (cloud-point) curve is formed by determining the projected points, which are shown in Figure 2-2. The dashed line is the common tangential line for the free energy curve T_5. Meanwhile, the spinodal curve is obtained by the projection of the inflection points. The thermodynamic requirements for binodal (equation 2-2) and spinodal (equation 2-3) can be given as,
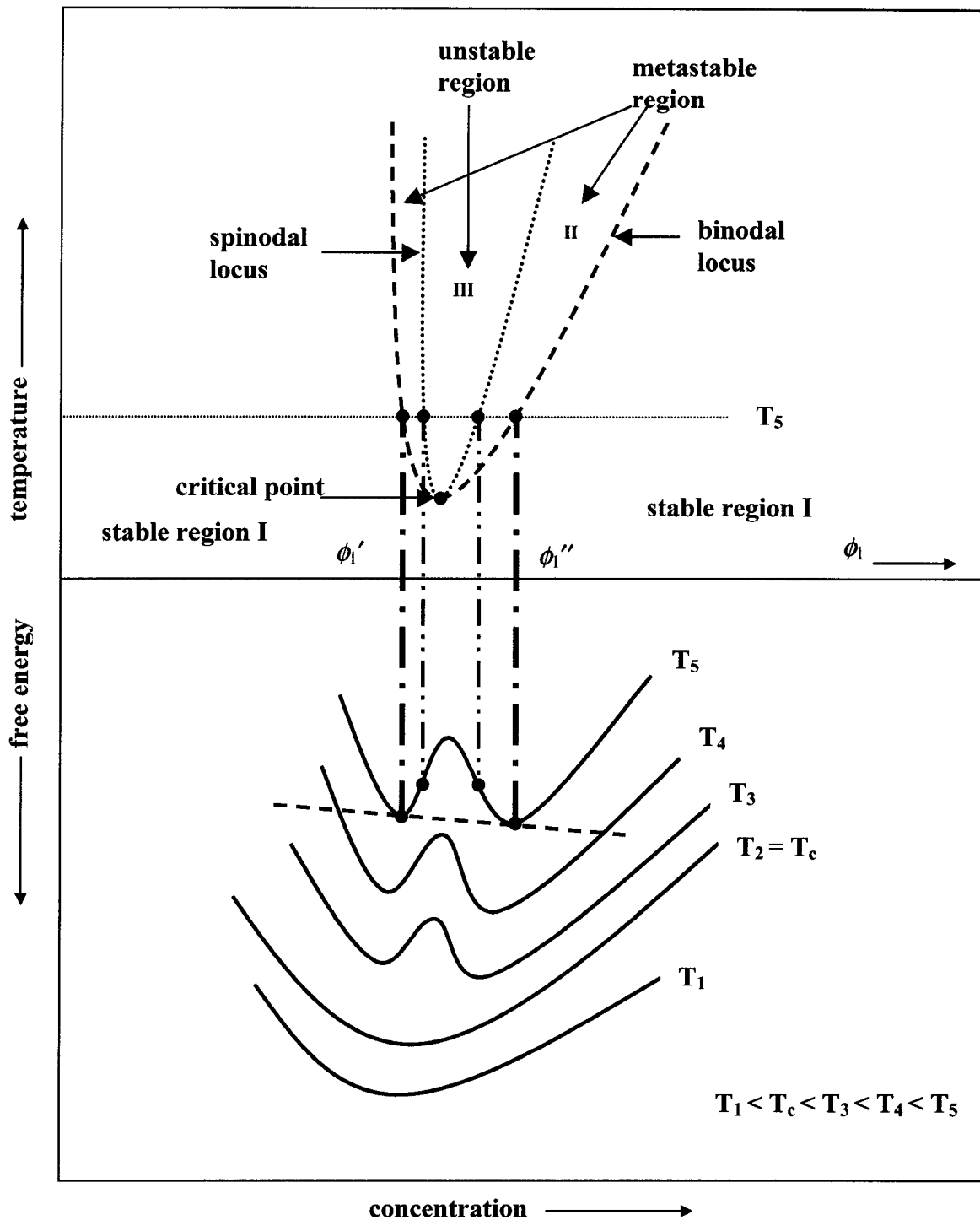
Figure 2-2: Schematic diagram of Gibbs free energy of mixing ΔG_m as a function of the volume fraction ϕ_1 of a binary polymer blend. The dashed (dotted) curves represent the binodal (spinodal) lines. This diagram indicates the one phase stable region I, the metastable region II and the unstable region III.

$$\left(\partial \Delta G_m / \partial \phi_1\right)_{P,T,\phi_2}^{\text{first phase}} = \left(\partial \Delta G_m / \partial \phi_1\right)_{P,T,\phi_2}^{\text{second phase}} \qquad (2\text{-}2)$$

$$\left(\partial^2 \Delta G_m / \partial \phi_1^2\right)_{P,T,\phi_2} = 0 \qquad (2\text{-}3)$$

where ΔG_m and ϕ_i are the Gibbs free energy of mixing and the volume fraction of the ith component, respectively. The lower half of Figure 2-2 shows that phase separation happens only when the slope change of volume fraction is positive and ΔG_m is negative.

In Figure 2-2, outside the binodal curve (region I), the system is a completely miscible, one-phase polymer blend. Inside the spinodal curve (region III), the system is unstable and undergoes spontaneous irreversible phase separation. The metastable region (II) is between the binodal and spinodal curves. The system in Figure 2-2 depicts a phase diagram exhibiting a lower critical solution temperature (LCST). The mixture can become miscible by lowering the temperature to region I. Depending on the nature of the polymers, binary polymer blends may display either upper critical solution temperature or lower critical solution temperature type of phase behavior.

The critical temperature T_c, which is the intersection point of the binodal and spinodal curves, is an important quantity for binary polymer blend phase diagrams. It is defined as,

$$[\partial \Delta G_m / \partial \phi_1]_{T,P,\phi_2} = [\partial^2 \Delta G_m / \partial \phi_1^2]_{T,P,\phi_2} = [\partial^3 \Delta G_m / \partial \phi_1^3]_{T,P,\phi_2} = 0 \qquad (2\text{-}4)$$

Thus, once the Gibbs free energy of mixing is known at various temperatures, the phase diagram can be defined.

2.3   Phase Separation Methods

In the phase separation methods, phase separation occurs when an initial single-phase blend enters the two-phase region. Phase separation phenomena in miscible polymer-polymer blends are generally brought about by variations in temperature, pressure, shearing, and composition. Among these techniques, temperature and solvent

induced phase separation, which are also called TIPS and SIPS, respectively, are useful methodologies in forming membranes and processing many thermoplastic polymers. In the SIPS method, a single phase can be formed with the acid of an organic solvent to solubilize the polymers. Phase separation occurs when the organic solvent evaporates. Polymerization-induced phase separation (PIPS) takes place when the length of polymer chains increases due to heat or radiation. In PIPS, a homogeneous system is thrust into the two-phase region with increasing conversion and decreasing solubility.

It should be noted that both shear-induced phase separation and pressure-induced phase separation take place during the processing of polymer blends in melt extruders [6]. They are schematically represented in Figure 2-3. In shear-induced phase separation, a homogeneous mixture enters the two-phase region with increasing shear rate. Usually, phase separation takes place at high screw speeds in melt extrusion. However, pressure levels in twin screw extrusion are not strong enough to cause phase separation. In pressure-induced phase separation, pressure changes can be brought about uniformly and very fast throughout the bulk of a mixture. This technique can be observed in injection-molding and it is also an unavoidable effect in near-critical or supercritical fluid process [6].
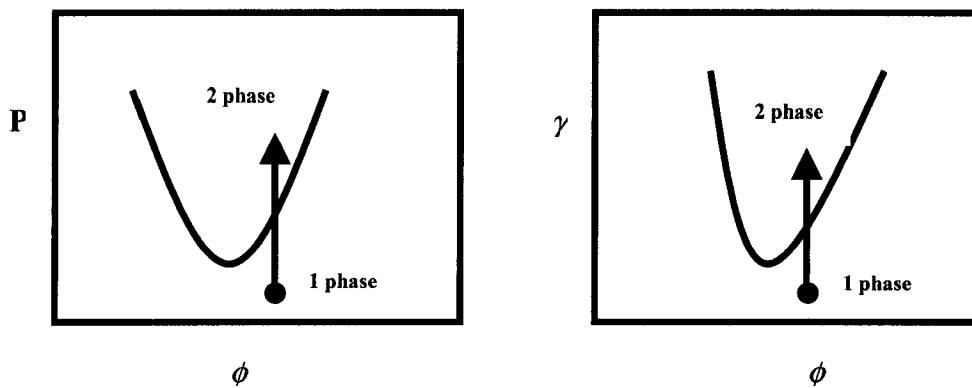
Figure 2-3: Schematic representation of phase separation processes. Left: pressure-induced phase separation, right: shear-induced phase separation. ϕ is polymer concentration, γ is shear rate and P is pressure.

2.3.1 Thermally Induced Phase Separation (TIPS)

The phase diagram for the TIPS process is a plot of concentration ϕ as a function of temperature T. In the TIPS process, a single-phase mixture is prepared at a certain temperature. When the mixture is thrust into the unstable or metastable region due to temperature variation, usually one component separates from the other.

Figure 2-4 (a) shows schematically a typical phase diagram for a binary polymer blend with a lower critical solution temperature (LCST). The dashed (dotted) curve represents the binodal (spinodal) line, where T_i, T_f, ϕ_0, and ϕ_c are initial temperature, final temperature, the average concentration and the critical concentration, respectively. The area between binodal and spinodal curves is called the metastable region, where phase separation occurs by nucleation and growth. At the beginning, a thermoplastic mixture in a homogeneous phase is formed at initial low temperature T_i at some average concentration ϕ_0 that is denoted by the dot. When the mixture is heated to high temperature T_f, phase separation takes place. When the thermoplastic solidifies, the phase separation is terminated. Two types of morphology can be obtained in the unstable region according to the average concentration ϕ_0. If $\phi_0 = \phi_c$ ($\phi_0 \neq \phi_c$), then the interconnected structure (droplet-type morphology) forms. Figure 2-4 (b) shows another type of phase diagram for a binary polymer blend with an upper critical solution temperature (UCST). The basic principle is the same for both types. Phase separation occurs due to temperature variation. Besides the morphology, the droplet size in the TIPS process can also be controlled by the rate of cooling or heating. In addition, there are other factors affecting the droplet sizes, such as the rate of diffusion, viscosity, and chemical potential of both components. Although the TIPS method seems simple, care must be taken to consider the process history and high temperature due to the unstable region in SD, which will be discussed in next section.

13
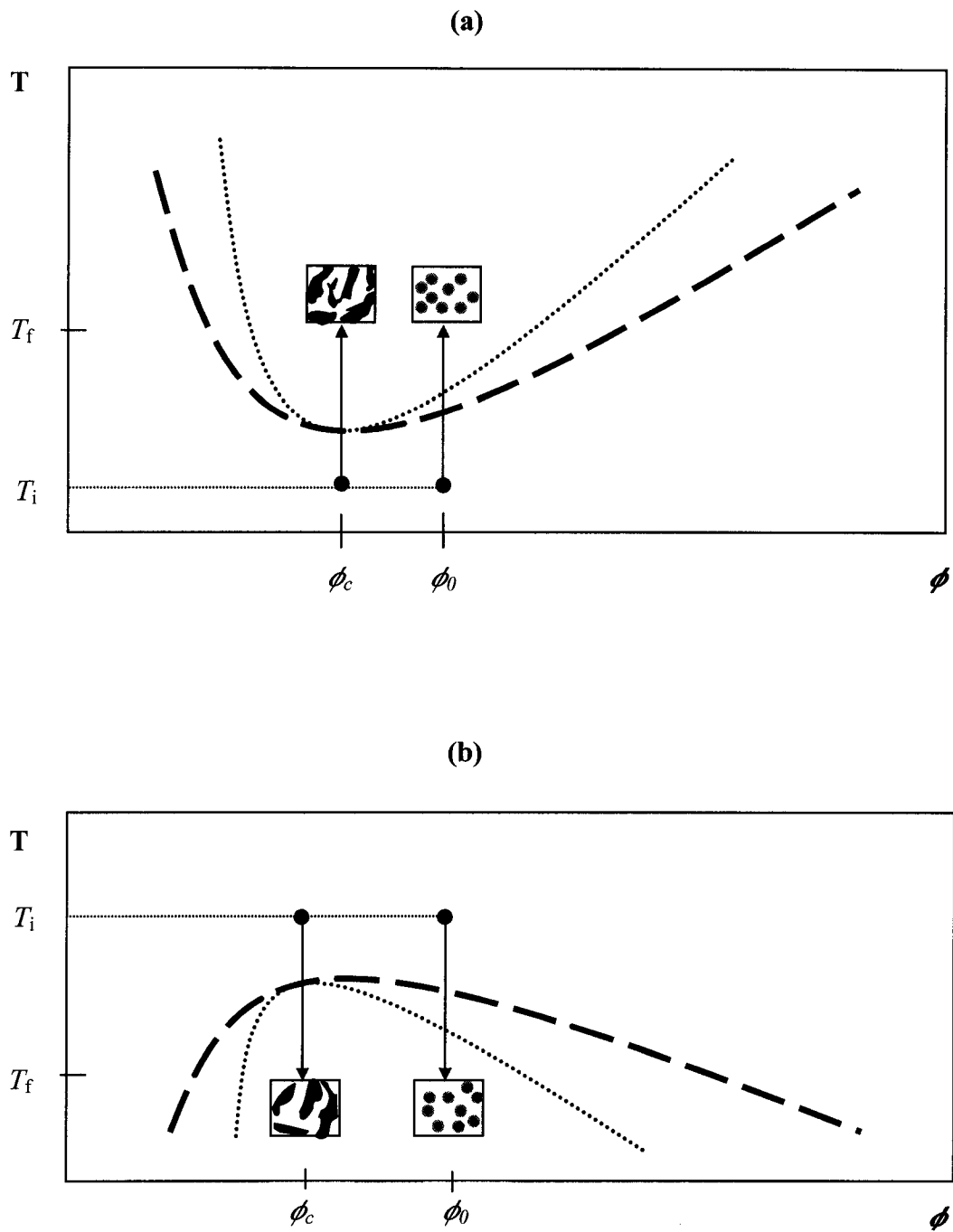
Figure 2-4: TIPS type phase diagram for the (a) lower critical solution temperature (LCST) and (b) upper critical solution temperature (UCST). The dashed (dotted) curves represent the binodal (spinodal) lines where ϕ_o and ϕ_c are the average and critical concentrations; T_i and T_f are the initial and final temperatures, respectively. The phase separation phenomena take place when the initially prepared one-phase mixtures are transferred into the two-phase region by TIPS (a) increasing T or (b) decreasing T.

14

2.4 Spinodal Decomposition Theory

Phase separation in the TIPS method often occurs via spinodal decomposition (SD) [9,10]. The phase separation mechanism for spinodal decomposition may be classified into the following three regimes: (a) early stage, (b) intermediate stage, and (c) late stage. These stages are schematically represented in Figure 2-5. In the early stage (S1), which occurs immediately after a temperature rises from the single-phase region I to the two-phase region III (see Figure 2-2). At the same time, fluctuations in the average concentration ϕ_0 lead to a change in the Gibbs free energy that can only decrease due to the fact $\partial^2 G_m / \partial \phi_1^2 < 0$. In the intermediate stage (S2), the nonlinear effects on the time evolution of the average concentration fluctuations become increasingly important with time. The droplet size and composition increase gradually with time. As a consequence, growth of the fluctuations is governed by the nonlinear time evolution equation. In the late stage (S3), phase separation is terminated by the minimization condition of the Gibbs free energy of mixing and the wavelength of the droplets is fixed by the scale of phase-separated structure. In SD, the diffusion coefficient determined by the sign of the curvature $\partial^2 G_m / \partial \phi_1^2$ is negative. Thus, molecules diffuse toward higher concentrations from lower concentration.

2.4.1 Cahn-Hilliard Equation

The theory of phase separation by spinodal decomposition (SD) was first introduced by Cahn and Hilliard [11]. The Cahn-Hilliard equation is based on the assumption that the total free energy of an inhomogeneous, binary mixture is expressed as a sum of two terms:

$$F = \int_v [f(\phi) + \frac{\kappa}{2}(\nabla \phi)^2] dv \qquad (2-5)$$

where ϕ is the volume fraction of one component in the binary mixture, κ is the gradient energy parameter, and $f(\phi)$ is the free energy of a homogeneous mixture.
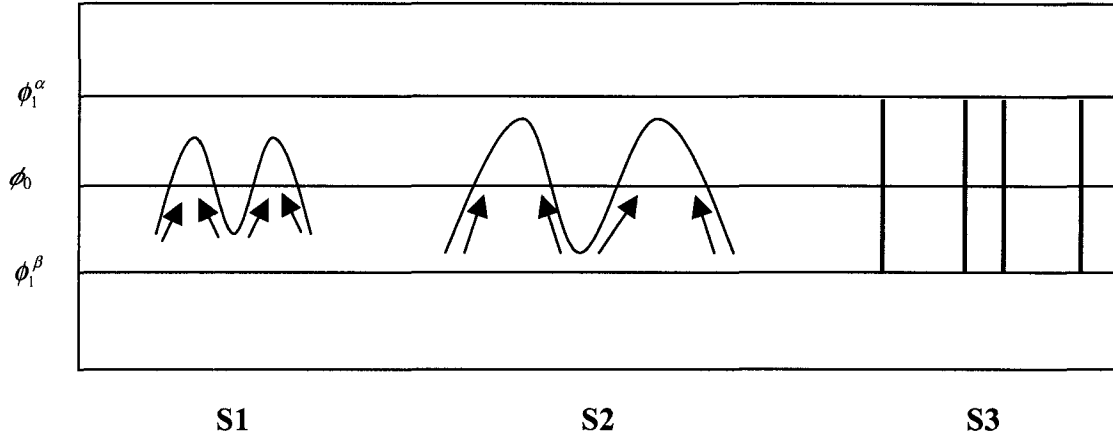
Figure 2-5: Schematic representation of the three regimes for spinodal decomposition. ϕ_0 is the average concentration, and ϕ_1^{α}, ϕ_1^{β} represent the concentration in phases α and β in the early (S1), intermediate (S2) and late (S3) stages, respectively. The arrows indicate the direction of the diffusion of the molecules. The diffusion coefficient is negative in spinodal decomposition.

The linear C-H equation can be given as:

$$\frac{\partial \phi}{\partial t} = M \left[\left. \frac{\partial^2 f(\phi)}{\partial \phi^2} \right|_{\phi_0} \nabla^2 \phi - 2\kappa \nabla^4 \phi \right] \qquad (2\text{-}6)$$

where ϕ_o is the initial average concentration. The general solution for Equation (2-6) is expressed as:

$$\phi - \phi_0 = \sum_k [A(k)\cos(\mathbf{k} \cdot \mathbf{r}) + B(k)\sin(\mathbf{k} \cdot \mathbf{r})]e^{R(k)t} \qquad (2\text{-}7)$$

where $k_i = 2\pi / \lambda_i$ (λ_i is the wavelength for fluctuation i) and

$$R(k) = -Mk^2 \left[\left. \frac{\partial^2 f(\phi)}{\partial \phi^2} \right|_{\phi_0} + 2\kappa k^2 \right] \qquad (2\text{-}8)$$

$R(k)$ is the amplification factor whose value is positive in the unstable region. The wavelength is obtained from Equation (2-6) and is expressed as

16

$$\lambda_m = 2\sqrt{2}\pi\left[\left(-\frac{1}{2\kappa}\right)\frac{\partial^2 f(\phi)}{\partial\phi^2}\bigg|_{\phi_0}\right]^{-\frac{1}{2}}$$ (2-9)

The morphological features study, such as the phase structure type and droplet size distribution, is the most important aspect of the TIPS process. Depending on initial average concentration, two different types of morphology are formed: the interconnected structure morphology and the droplet-type morphology. Therefore, Equation (2-9) is a key methodology to predict the morphological features of polymer blends in off critical TIPS. The predicted droplet diameter ($d_m \propto \lambda_m/2$) can be calculated in advance in order that the desired and required phase structure can be obtained at an initial concentration. Figure 2-6 schematically shows relationship between the droplet diameter d_m and the wavelength λ_m.
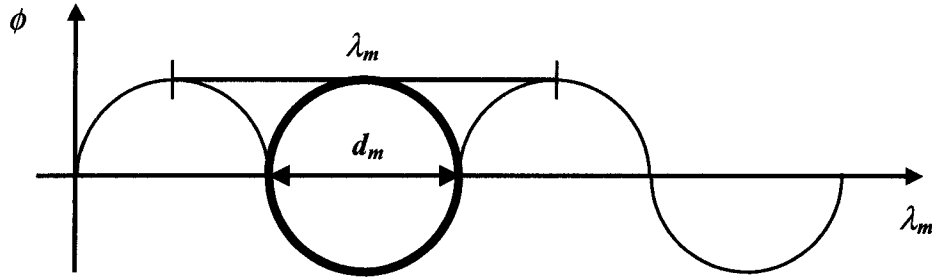
Figure 2-6: Schematic representation of the relationship for droplet diameter d_m and wavelength λ_m. ϕ is the average concentration, and λ is the wavelength. In two-dimensions, the circle represents a polymer droplet, since the droplet diameter equals half of the wavelength ($d_m = \lambda_m/2$).

2.4.2 The Flory-Huggins Theory and Phase Diagram

The phase stability of a binary mixture of two components (binary polymer blends system) can be well understood in terms of the lattice theory of Flory [12] and Huggins [13]. Thus, the Flory-Huggins free energy Equation (2-10 and 2-11) is the most widely and successfully used theory in phase equilibrium studies [8]. The Flory-Huggins

17

treatment represents the free energy density of mixing, f, as a sum of the configurational entropy and enthalpy of mixing [14]. The starting point of the model is the Gibbs free energy of mixing, ΔG_m, given by Equation (2-1). For mixing of the two components to occur, $\Delta G_m < 0$. According to the F-H theory, ΔS_m is

$$\Delta S_m = -\frac{k_B}{v}[\frac{(1-\phi)\ln(1-\phi)}{N_2} + \frac{\phi\ln\phi}{N_1}] \qquad (2\text{-}10)$$

where N_1 and N_2 are the degrees of polymerization of components 1 and 2, respectively, ϕ is the volume fraction of component 1, k_B is Boltzmann's constant, and v is the volume of a cell or segment.

The F-H enthalpy of mixing can be expressed as

$$\Delta H_{mix} = \frac{k_B}{v}T\chi\phi(1-\phi) \qquad (2\text{-}11)$$

where χ is the well-known Flory-Huggins interaction parameter. The temperature dependence of χ is often given by [8]

$$\chi(T) = a + \frac{b}{T} \qquad (2\text{-}12)$$

where a and b are frequently taken to be constants. The χ parameter measures the solubility of polymer blends; when the solubility power increases, χ decreases to -1. Equation (2-12) introduces the temperature dependence into the F-H equation, thus providing a direct T-ϕ relationship. The F-H free energy density of mixing is obtained by combining Equation (2-1) with Equations (2-10) and (2-11), which is expressed as [14],

$$f(\phi) = \frac{k_B T}{v}[\frac{\phi}{N_1}\ln\phi + \frac{(1-\phi)}{N_2}\ln(1-\phi) + \chi\phi(1-\phi)] \qquad (2\text{-}13)$$

Based on the condition for phase equilibrium that the chemical potential of each component is the same in all phases at a specified temperature and pressure, the two binodal points are calculated by solving a pair of nonlinear algebraic equations. Under the same equilibrium condition, the two spinodal points at the same temperature are obtained

by solving a quadratic equation [8,15]. At the critical point, the volume fraction ϕ_c and interaction parameter χ_c are given by [15]:

$$\phi_c = [1 + (\frac{N_1}{N_2})^{\frac{1}{2}}]^{-1} \tag{2-14}$$

$$\chi_c = \frac{1}{2}(N_1^{-\frac{1}{2}} + N_2^{-\frac{1}{2}})^2 \tag{2-15}$$

2.5 Thermodynamic Phase Diagram for Binary Polymer Blends Containing Liquid Crystalline Polymer (LCP)

The phase behavior of blends containing a liquid crystalline polymer (LCP) has been widely studied using experimental techniques such as differential scanning calorimetery (DSC), scanning electron microscopy (SEM), small-angle light scattering (SALS), polarized light microscopy (PLM) and X-ray diffraction (XRD) [16-23]. However, the thermal properties of LCP/PC blends are complex due to their multiphase character. The multiphase behavior also reflects the processing history dependence of the dispersed phase properties. There are many practical difficulties to obtain the blend thermodynamic phase diagram. Therefore, numerous researchers have studied the miscibility behavior of the commercial blend system incorporating LCP copolyesters of poly(ethylene terephthalate) (PET) and p-hydroxybenzoic (PHB) with other engineering thermoplastic polymers [16-19,21-23]. Kimura and Porter [16] used DSC to study the miscibility of blends of PET/PHB with poly(butylene terephthalate) PBT. They found that the PHB-rich phase of the copolyester was immiscible with PBT, whereas the PET-rich phase was miscible. This is because the copolyester PET/PHB itself exhibits two phases: one is a PHB-rich phase, the other is PET-rich. On the other hand, Huang *et al.* [24] reported that polycarbonate was only partially miscible with the PET-rich phase of the copolyester.

The determination of the glass transition temperature (T_g) of polymer blends is a generally accepted way to confirm the miscibility of polymer blends [9]. Zhuang et al. [17] studied the blends of PET/PHB with thermoplastic polymers such as polystyrene (PS), polycarbonate (PC), and PET. Among these blends, the PC and PET blend systems were found to be partially miscible whereas PS blends were completely immiscible. Hsieh et al. [25] investigated the T_g of blends of polycarbonate (PC) and a liquid crystalline copolyester Vectra A950, which consists of 73 mol% p-hydroxybenzoic acid (HBA) and 27 mol% 2-hydroxy-6-naphthoic acid (HNA). Using both DSC and dynamic mechanical analysis (DMA) techniques, they showed that the blends were found to be generally immiscible when T_g of the PC phase increased. The variation of free volume behavior in the blends could be explained in terms of this phenomenon. The phenomenon has also been reported to be the reason for phase separation in blend systems with similar components [26-28]. Malik et al. [26] also used DSC to study the miscibility behavior in the blends of Vectra and PC (Lexan 130-111). The blends processed at 280°C were found to have limited miscibility due to the slightly lowered T_g in PC-rich phase. Turek et al. [27] also reported the miscibility of the PC (Lexan134) blended with 25% Vectra. The miscibility was supported by the observation that the T_g of the PC-rich phase was slightly lower than that of the pure PC. However, Engberg et al. [28] studied the T_g of the PC-rich phase in PC (Lexan 141R) blended with low concentration (up to 40%) Vectra system. The T_g increased since the blend system was immiscible. In addition to T_g, the polymer-polymer interaction parameter χ of LCP in the LCP/PC blends was investigated by Lee et al. [29]. The studied blends were prepared by screw extrusion and were intensively investigated by DSC. From the measured T_gs of the blends, the polymer-polymer interaction parameter χ in the blends was calculated by the "T_g method", which helps to determine the apparent PC weight fractions in the PC-rich and LCP-rich phases. Based on these experimental PC weight fractions and Flory's lattice theory, the χ parameters for flexible chain polymer (PC) and rod-like conformation (LCP) blends are evaluated to be 0.076 ± 0.008 at 250°C.

Nakai et al. [18] and Kyu and Zhuang [19] investigated the phase behavior of solvent cast films of blends of 40 mol% PET/60 mol% PHB with PET and PC. A single-phase blend was prepared with liquid crystalline copolyesters (60mol% PHB/PET) and

amorphous polycarbonate (PC) via a mixed solvent of 60/40 (by weight) phenol/tetrachloroethane [19]. The optically clear and homogeneous as-cast films were brought into the spinodal decomposition (SD) two-phase region when heated above the cloud point temperature. A binodal (cloud point) curve with a lower critical solution temperature (Figure 2-7 [19]) was constructed by annealing the films and identifying the cloud point temperatures using small-angle light scattering (SALS). Polarized light micrographs showed that the blends were grossly phase separated with a high level of interconnectivity, which is characteristic of spinodal decomposition. Figure 2-7 shows a typical phase behavior of LCP/PC blends. Most LCP/PC blends normally have the LCST type of phase diagram in terms of their physical characteristics, such as degree of polymerization, polymer-polymer interaction parameter, *etc* [4].

In summary, the essential characteristic features of LCP/PC blend phase behavior in literature may be described as follows:

1. Preparation of LCP/PC blends can be accomplished by either mechanical mixing or dissolution in co-solvent followed by film casting, freezing or spray drying;

2. The experimental techniques to study LCP/PC blend phase behavior involve differential scanning calorimetery (DSC), scanning electron microscopy (SEM), small-angle light scattering (SALS), polarized microscopy (PLM) and X-ray diffraction (XRD);

3. Most LCP/PC blends exhibit a lower critical solution temperature (LCST) type phase behavior. Thermally induced phase separation (TIPS) occurs via a spinodal decomposition (SD) mechanism;

4. PC and LCP can form either miscible or immiscible blends. The blends are found to be generally immiscible (miscible) when T_g of the PC phase increases (decreases).
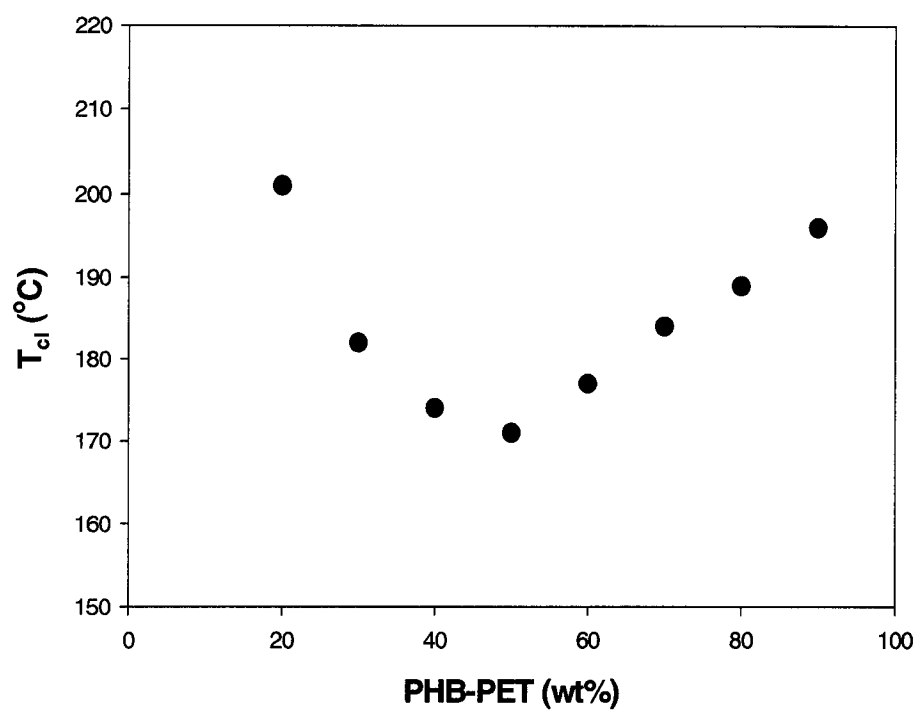
Figure 2-7: A cloud point phase diagram of PC/PHB-PET blends obtained at 2 °C/min
[19].

Chapter 3

Experimental Techniques

This chapter introduces various techniques such as twin screw extrusion blending, differential scanning thermal analysis and scanning electron microscopy to study the phase diagram of liquid crystalline polymer/polycarbonate blend systems. Both the mechanical mixing and co-solvent film casting for the preparation of blend samples are also presented.

3.1   Resin Selection

In this study, two commercial and readily available industrial grade resins were used. LEXAN 141-111N, a derivative of bisphenol A, is an amorphous, general-purpose polycarbonate (PC) (Figure 3-1A) manufactured by General Electric Plastics. The second resin is unfilled THERMX LCP LN001, which is a nematic liquid crystalline polymer (LCP). It consists of 80 mol% poly(ethylene terephthalate) (PET) and 20 mol% p-hydroxybenzoic acid (PHB) (Figure 3-1B). The LCP resin was supplied by Tennessee Eastman Kodak. The two resins were obtained in the form of pellets. Because of the hygroscopicity of the material, the pellets were always dried overnight at $100^{\circ}C$ in a vacuum oven before use. A summary of the properties of the two resins is given in Table 3-1.
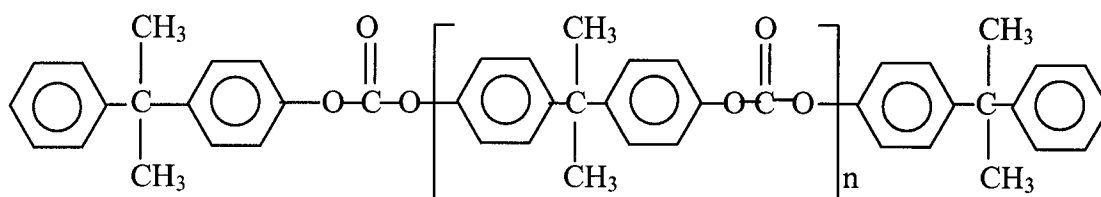
(A) Polycarbonate
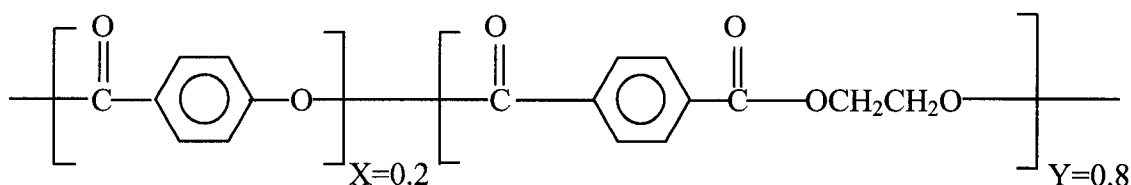
PHB   PET
(B) THERMX LCP LN001

Figure 3-1: Chemical structure of the polymers: (A) polycarbonate and (B) copolyester LCP. n is the degree of polymerization. X and Y represent the mole fraction of PHB and PET, respectively.

Table 3-1: Material Properties of the Polymers Used*

Properties	LCP	PC
M_0 (g/mol)	182	254
M_w (g/mol)	36,942	64,000
M_n (g/mol)	10,365	24,000-25,000
M_w/M_n	3.56	2.67-2.56
Glass Transition Temperature ($^{\circ}$C)	61.7	147.6
Melting Point ($^{\circ}$C)	325	NA
Density (kg/m^3)	1.38	1.2

*The number (M_n) and weight (M_w) average molar masses of LCP were measured by Eastman Kodak laboratories. The structured unit molar mass (M_0) was calculated based on Figure 3-1. Glass transition temperature (T_g) data were obtained using DSC (Figure 3-2). Other data were as updated in the suppliers' data sheets.
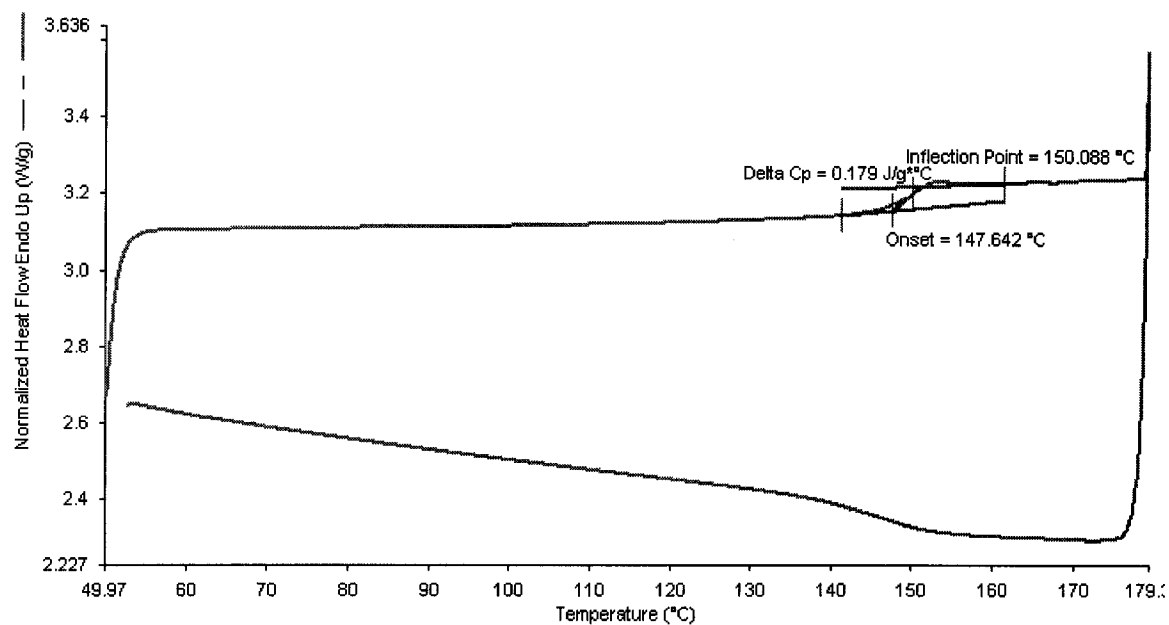
(A)
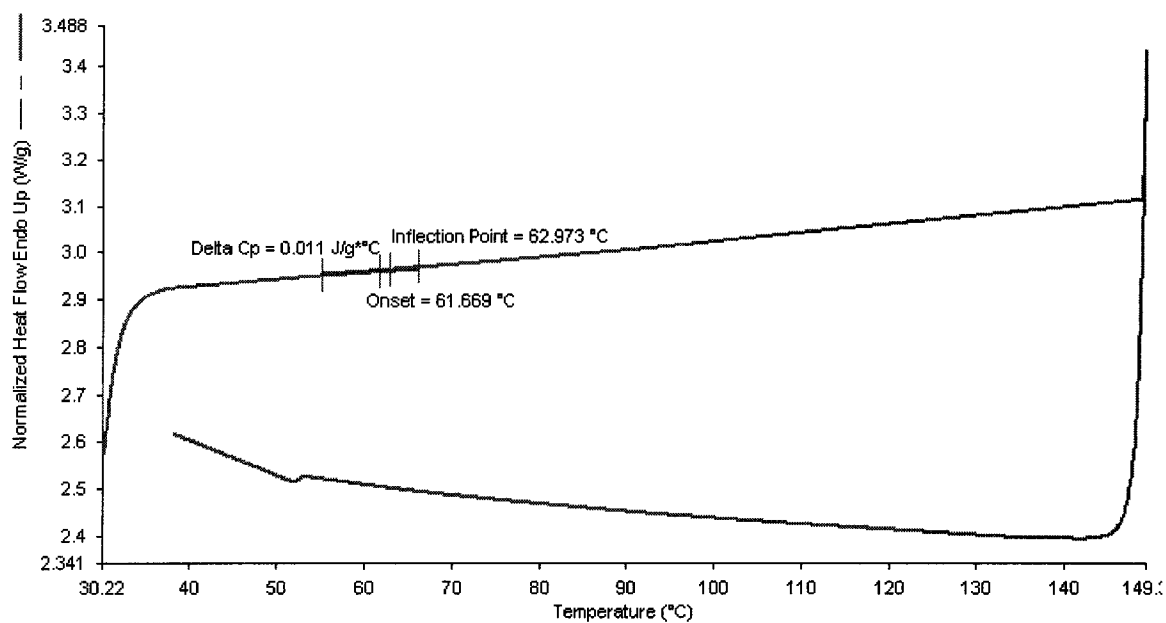
(B)

Figure 3-2: DSC thermograms for (A) PC and (B) LCP.

3.2 Blend Sample Preparation

As discussed previously in section 2.5, the preparation of LCP/PC blends can be accomplished by either (1) mechanical mixing or (2) co-solvent film casting. For economic and environmental reasons, mechanical blending predominates over solvent casting in polymer processing [2]. However, the mixing effectiveness of solvent casting is much better than that of the mechanical blending process. Moreover, the majority of the LCPs are wholly aromatic, high-melting materials. This will limit the available temperature range (processing window) of the blending process. Therefore, a number of blends processing techniques were tried in this work.

3.2.1 Haake Mixer

A Haake Buchler – Rheocord System 40 batch mixer was used for mechanical mixing. This mixer consists of three independent temperature controlled sections. Temperature in every section is maintained at a constant level. The blend melt temperature is measured by a melt thermocouple immersed in the specimens. In addition, a high-resolution torque transducer is situated directly behind the mixer. The torque applied to the molten blend specimen is kept constant. Specimens can be readily taken out of the mixer for analysis. The specimen chamber has a capacity of about 50 g. It is easy to clean due to its small capacity. No special preparation method is required to prepare the specimens. Specimen pellets as well as powder are introduced to the mixer without any loss of sample. Under normal operating conditions, intensive mixing and shearing action can be applied to the specimens.

3.2.1.1 Experimental Procedure

The blending conditions are given in Table 3-2. The experimental procedure is outlined in the following chart:

```
┌─────────────────────┐
│   Dry materials     │
└─────────────────────┘
          │
          ▼
┌─────────────────────┐
│ Weigh dried pellet  │
└─────────────────────┘
          │
          ▼
┌─────────────────────┐
│ Put specimens into  │
│    the chamber      │
└─────────────────────┘
          │
          ▼
┌─────────────────────┐
│     Switch on       │
│  processor and      │
│    drive units      │
└─────────────────────┘
          │
          ▼
┌─────────────────────┐
│     Input the       │
│    operational      │
│ conditions listed in│
│     Table 3-2       │
└─────────────────────┘
          │
          ▼
┌─────────────────────┐
│  Print out data at  │
│  every six seconds  │
└─────────────────────┘
```
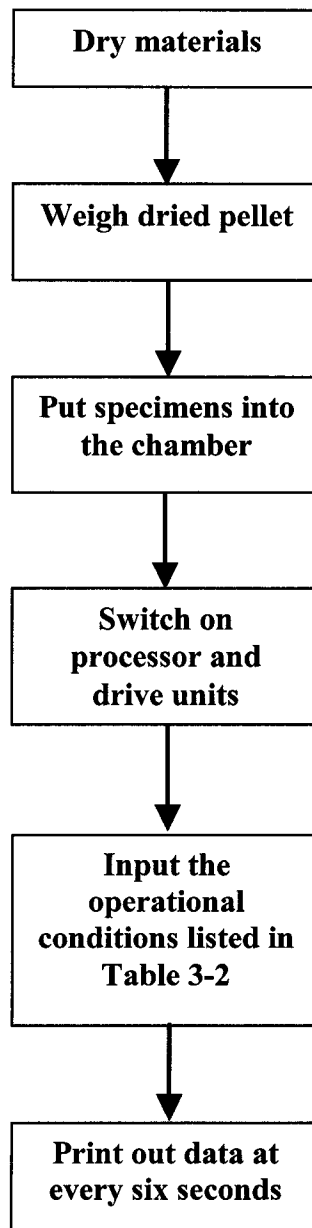
Table 3-2 Blending Conditions for LCP/PC Blends

Condition	Value
Zone 1 Temperature T_1 ($^\circ$C)	330
Zone 2 Temperature T_2 ($^\circ$C)	330
Zone 3 Temperature T_3 ($^\circ$C)	330
Screw Speed (rev min^{-1})	60
Residence Time (min)	6
Torque (Nm)	10,000

As mentioned before, there are three independent temperature controllers in the Haake mixer. The temperatures were all set at 330°C because the melting point of LCP is 325°C. In addition, the temperature is also kept constant due to the small chamber capacity.

3.2.2 Solvent Casting Technique

The solvent casting technique is a standard method to obtain films of LCP/PC blends. This method is usually used to study the phase behavior of the LCP/PC blends [18,19].

3.2.2.1 Phenol and 1,1,2,2- tetrachloroethane Solvent System

Phenol crystals (Code 5520-1) supplied by Caledon Co. have a melting point of 40.9°C and a boiling point of 181.8°C. 1,1,2,2-tetrachloroethane (98% purity) supplied by Aldrich Chemical Co. Inc., has a melting point of -43°C and a boiling point of 147°C.

The solvent casting experimental procedure is as follows:

```
┌─────────────────────────────────┐
│      Set up a flux condenser     │
└─────────────────────────────────┘
                 │
                 ▼
┌─────────────────────────────────┐
│    Prepare 1 g of LCP and 1 g    │
│             of PC                │
└─────────────────────────────────┘
                 │
                 ▼
┌─────────────────────────────────┐
│        Prepare 60 g of phenol    │
│      crystals and 40 g of 98%    │
│      1,1,2,2-tetrachloroethane   │
└─────────────────────────────────┘
                 │
                 ▼
┌─────────────────────────────────┐
│     Put these materials into a   │
│    250 ml round-bottomed flask   │
│                                  │
└─────────────────────────────────┘
                 │
                 ▼
┌─────────────────────────────────┐
│       Set up a water bath        │
│        apparatus (80°C)          │
│                                  │
└─────────────────────────────────┘
                 │
                 ▼
┌─────────────────────────────────┐
│      Start magnetic stirring     │
│                                  │
│                                  │
└─────────────────────────────────┘
                 │
                 ▼
┌─────────────────────────────────┐
│      Keep running for a week     │
│                                  │
└─────────────────────────────────┘
```
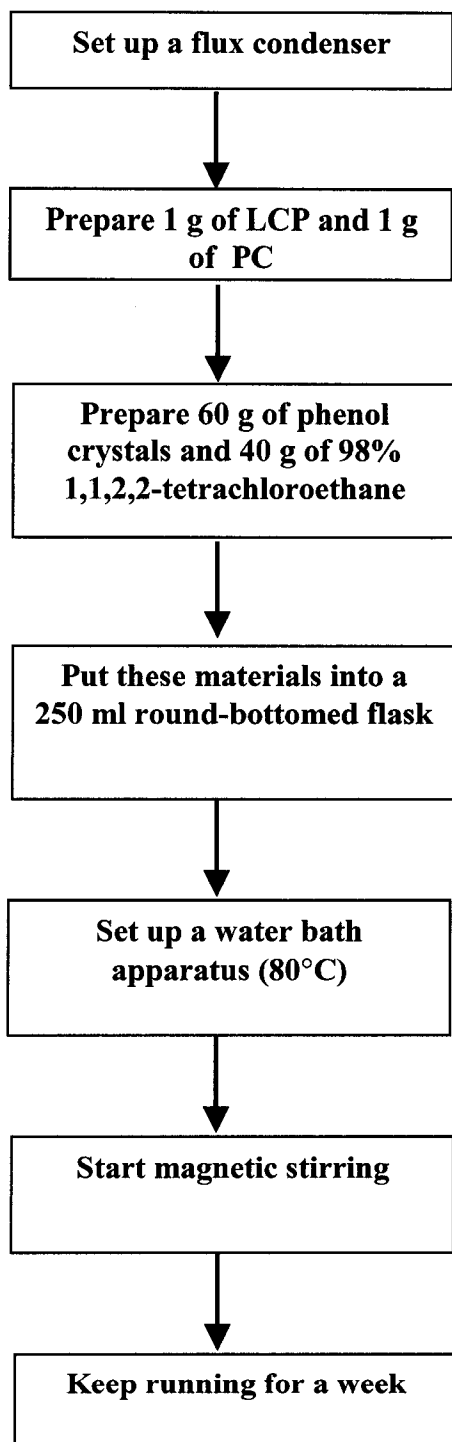
3.2.2.2 Trifluoroacetic acid - Chloroform Solvent System

Trifluoroacetic acid (D4901-500 UN2699), which was supplied by Fisher Scientific, has a melting point of -15.2°C and a boiling point of 73°C. Chloroform (C298-1 UN1888), which was also supplied by Fisher Scientific, has a melting point of -63°C and a boiling point of 61°C.

The experimental procedure was exactly the same as described in section 3.2.2.1, except for the preparation of a mixed solvent of 100ml (20/80 by volume) trifluoroacetic acid/chloroform.

For protection and as safety measure, the operator should wear a lab coat, safety glasses and plastic gloves during the operation.

3.2.3   Twin Screw Extruder (TSE)

The mechanical mixing was also carried out using a Berstorff ZE-25 twin screw extruder. The external diameter of the screw is 25 mm and L/D (length/diameter of screw) is 28 [30]. The machine consists of conveying, shearing and mixing screw elements. In order to achieve high blending processing performance, the individual parts were assembled again so as to form an appropriate blending screw configuration (see appendix Figure A-1). These screw elements consist of conveying elements, kneading blocks and toothed blocks. The conveying elements push forward the pellets that flow gravitationally from the hopper into the internal screw channel. The kneading blocks provide higher shearing energy than the conveying elements, thus providing further mixing. The toothed blocks are the best mixing elements that ensure uniform distribution of the component, even at low concentrations. Thus, intensive mixing and shearing action may be achieved in the twin screw extruder.

3.2.3.1 Feeder Calibration

Before operating the twin screw extrusion machine for the very first time, the processing part must be cleaned. For this purpose, polycarbonate is dosed into the feed opening manually and at low screw speed – approximately 50 rpm. The machine must not be running at maximum load, since it would be switched-off automatically due to excessive current consumption. After filling the processing part with polycarbonate over its total length, the machine should be operated at a higher speed for sufficient cleaning time until there are no impurities exiting the die.

The calibration of both feeders was performed after the cleaning process of the TSE barrel. Feed rate vs. feed speed is shown in Figure 3-3. The feed speed, which can be set on the switch desk board, is the motor speed of the hopper. The feed rate is obtained by measuring the rate of flow out of this hopper. For example, the feed speed of hopper #1 was set at 100 rpm, and the ratio of hopper #2 was set at 0.3. The measured feed rates of hoppers #1 and #2 were 32 g/min and 10 g/min, respectively. Therefore, the weight percentage under this condition was 23.8 wt% LCP (10/(32+10) = 23.8%). This value is the actual percentage of LCP in the feed. However, it is hard to precisely obtain this desired actual value in every independent experiment. For example, if we intend to prepare a 25 wt% LCP blend sample, we can only obtain samples in the actual weight percentage range between 23% and 26% based on the reproducibility of the outputs using the setting conditions established in the calibration procedures. Hence, we take this desired value as the nominal value for a 25% blend. A summary of all blending ratio conditions is given in Table 3-3. All the LCP/PC blending samples used in this work were prepared based on this table.

As can be seen in Figure 3-3B, the calibration line is nonlinear especially in the central part. There are many effects caused by the operation of the machine itself, but the major reason for the nonlinear region is the slow motor speed of hopper #2 during the calibration. However, the unstable flow rate in this nonlinear region introduces significant errors in obtaining the exact composition of the desired blends. In order to analyze the differences between actual values and nominal values of the output of the hoppers, a study of feeder calibration was performed (Figure 3-4). Initial weight of 3.0 kg

31

Feed Rate vs. Feed Speed of Master Hopper #1

(A)

Feed Rate vs. Feed Speed of Hopper #2
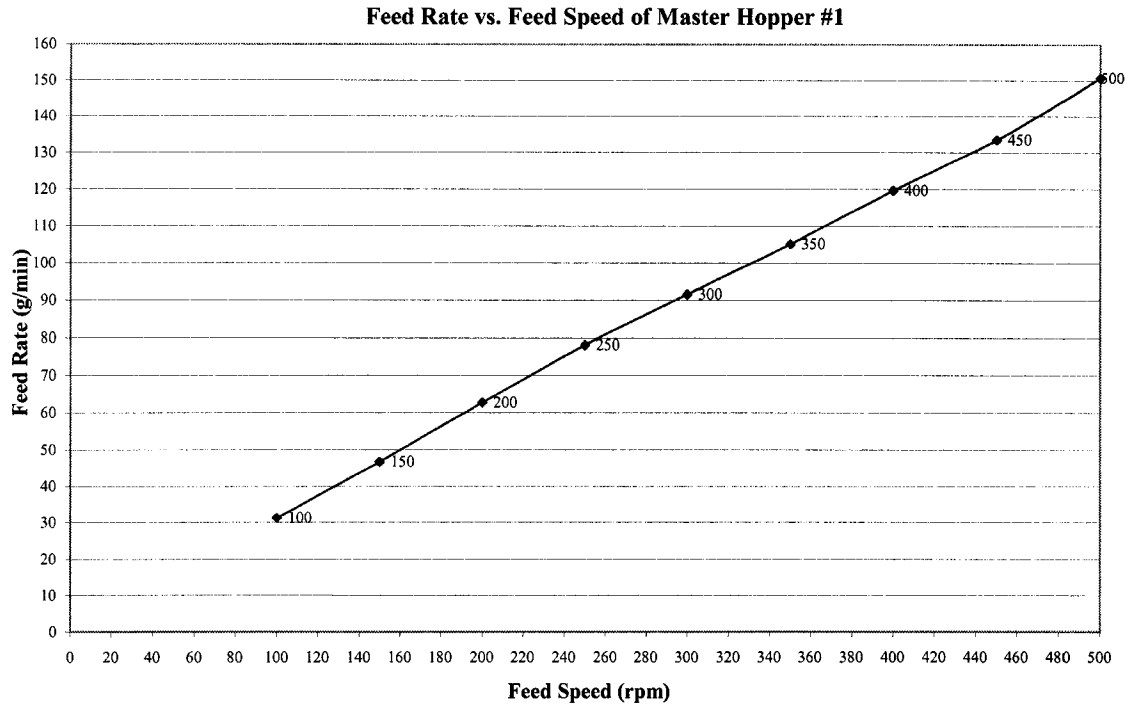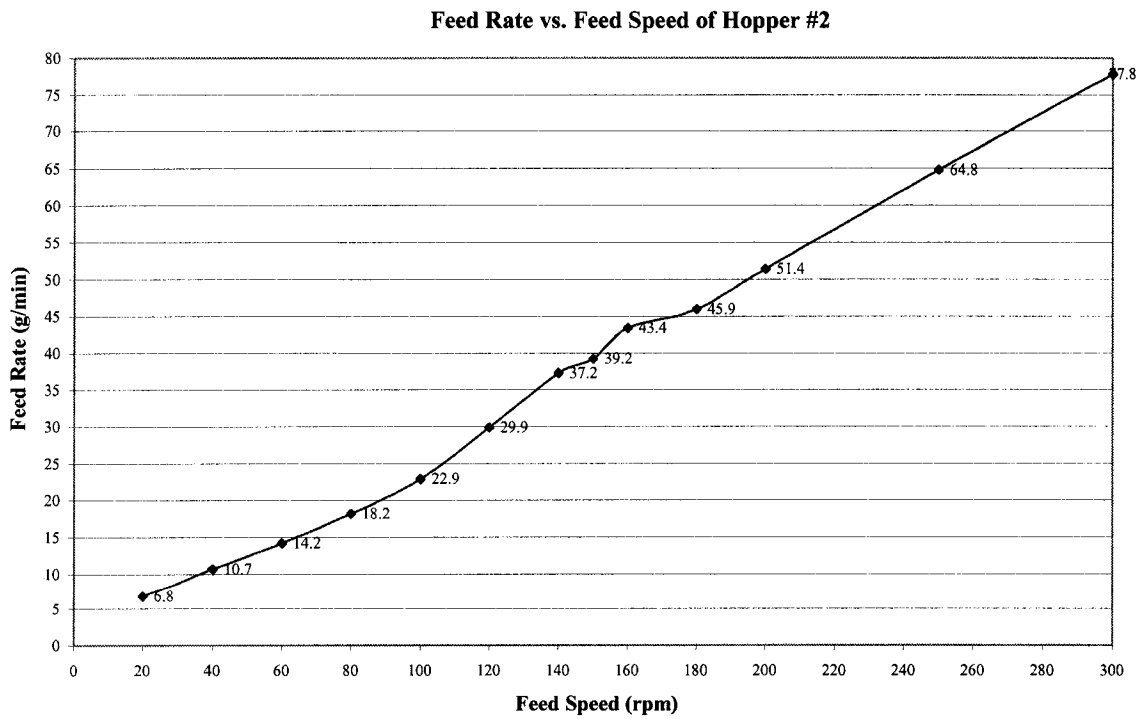
(B)

Figure 3-3: Feed rate vs. feed speed of TSE, (A) PC master hopper #1 and (B) LCP minor hopper #2.

32

Table 3-3: Summary of Blending Ratio Conditions for LCP/PC Blend

(A)

Feeder #1 (PC)* Speed	Feeder #2 (LCP)* Speed Ratio	LCP wt%***
250 rpm	0.112	10%
200 rpm	0.19	15%
200 rpm	0.29	20%
100 rpm	0.3	25%
100 rpm	0.5	30%
100 rpm	0.8	40%
100 rpm	1.1	50%

(B)

Feeder #1 (LCP)** Speed	Feeder #2 Ratio (PC)** Speed Ratio	LCP wt%***
100 rpm	0.8	60%
100 rpm	0.56	70%
200 rpm	0.24	80%
200 rpm	0.16	85%
200 rpm	0.08	90%

* Initial weight of LCP is 1.0 kg and PC is 3.0 kg.

** Initial weight of LCP is 2.0 kg and PC is 1.0 kg.

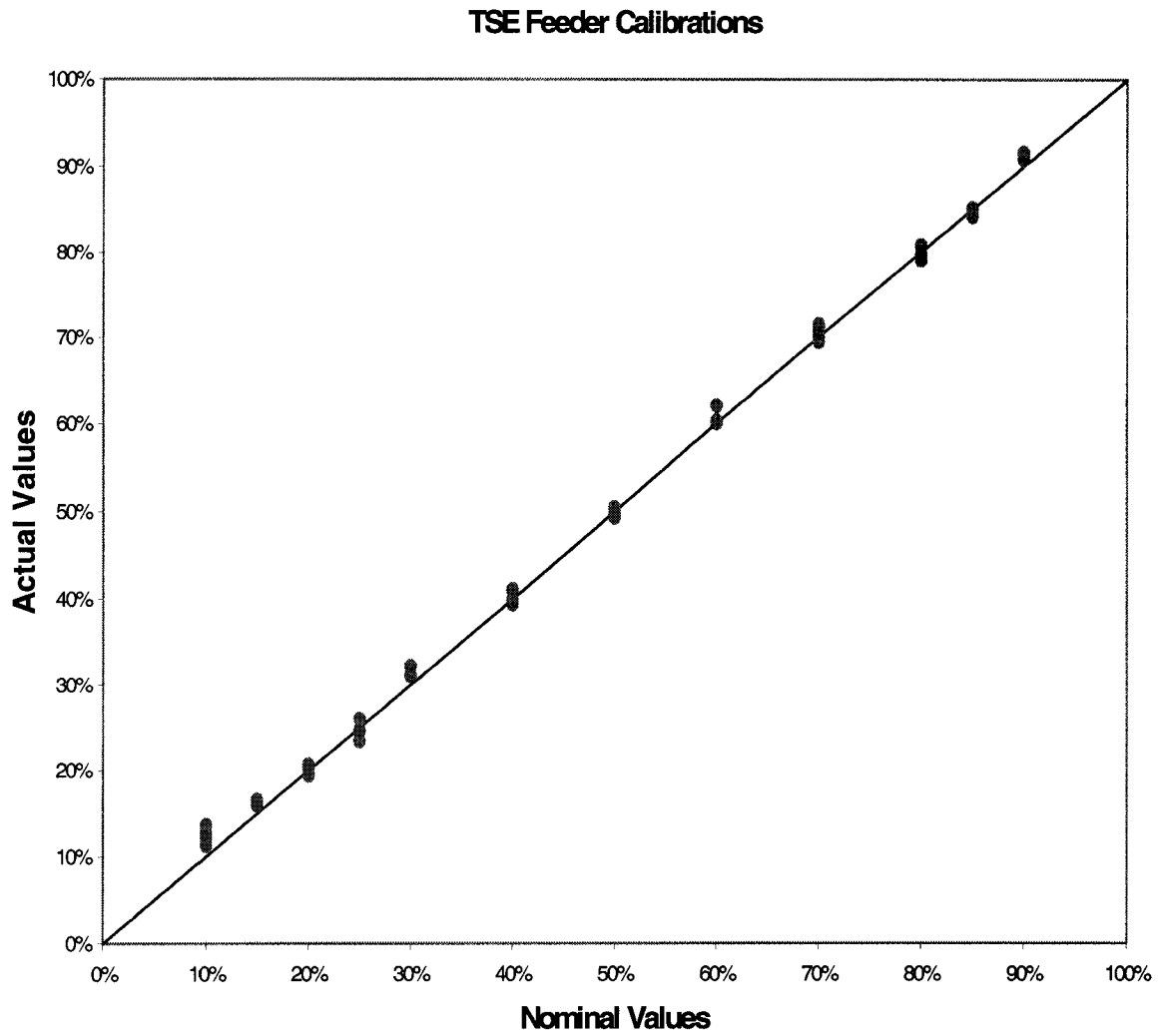*** These values are nominal values.

Figure 3-4: Twin screw extruder feeder calibrations for actual values vs. nominal values.

34

PC and 1.0 kg LCP were put into feeders #1 and #2, respectively. The flow rate of each feeder was calibrated after the machine ran for twenty minutes. When the calibration for LCP percentage exceeded 50 wt%, the hoppers for LCP and PC were switched and the initial weight was changed to 2.0 kg for LCP and 1.0 kg for PC. This is because LCP has become the principal component of the blends. It should be placed in the master hopper #1. The pellet size and density influence the flow rate of the hopper. Therefore, the initial weights of LCP and PC were different. However, the calibration procedure was exactly the same.

As can be seen in Figure 3-4, the actual points are close to the diagonal line within the range 20-70 wt% LCP. It means that the weight percentages of the blends have very small errors within this region. In the lower LCP concentration region, we increased the feeder speed up to 250 rpm to avoid the error. However, some problems in minimizing these errors persist, since there are still various intrinsic effects associated with operation of the machine at low LCP concentrations.

3.2.3.2 Blending Process

Before processing, all materials were dried overnight at 100°C in a vacuum oven to remove moisture. A Berstorff ZE-25 twin screw extruder was used for compounding. The materials were fed into the designated feeders. The rotational speed of the screws was kept constant at 80 rpm, and the melt temperature was set at different values depending on the weight percentage of LCP.

3.2.3.3 Processing Melt Temperature (T_{pm}) Measurement

The Berstorff ZE-25 twin screw extruder has five heating zones with which a temperature profile over the extruder can be established. The barrel zones are heated by means of aluminum heating elements, and can be heated or cooled by air. The

35

temperature of each zone was measured by means of a thermocouple and transmitted to the control panel. Each temperature is controlled individually. The desirable processing temperature profile could be set on the control panel.

In order to study the effect of changes in melt temperatures on thermally induced phase separation, the temperature profile along the screw barrel was varied. A twin screw extruder run time program, which is the time record program of varying processing melt temperatures, was set up at the beginning. The lowest temperature is near the inlet (hopper) and the highest temperature is near the tip of the screw. The setting of temperature profile strongly depends on the weight ratio of LCP/PC blends due to the high melting point of LCP (325°C). The higher in the LCP weight ratio, the higher will the setting be. Figure 3-5 shows a schematic plot of the processing melt temperatures for 25wt% LCP/PC blend vs. time. Once the desirable setting temperature profile is reached and the processing melt temperature has been stable for at least five minutes, the blend specimen collecting process begins. We set five minutes, because the machine is stable during this period and the consumption of the expensive resins is minimized within this time limit. This collecting time is characterized by a horizontal straight line (see Figure 3-5), which represents a stable processing melt temperature. Figure 3-5 indicates when the desired specimen could be collected and the temperature of the specimen. Specimens were collected for further studies using DSC, PLM and SEM.

3.3 Microstructural Analysis

In order to study the blend phase morphology, polarized light microscopy (PLM) and scanning electron microscopy (SEM) were used to characterize the microstructure of the blends. The main purpose of microstructural analysis is to investigate and measure the degree of miscibility, the interaction of phases and the droplet type, shape and size. In general, phase size and particle size distribution can be revealed directly by microscopy. However, it is more difficult to obtain information on partial miscibility and interfacial interaction by microscopy.

25wt%LCP/PC Blend

Temperature (°C)

330
325
320
315
310
305
300
295
290
285
280

327
323
316
313
307
302
297

0   20   40   60   80   100

Time (min)
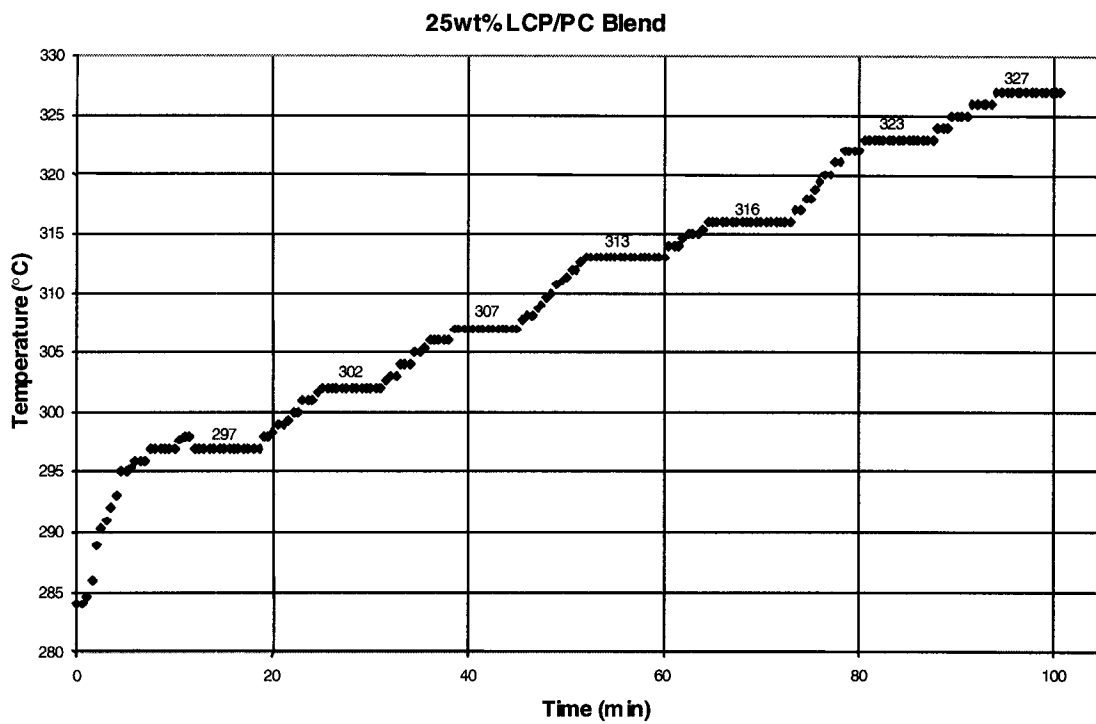
Figure 3-5: Processing melt temperatures of 25wt% LCP/PC blend as a function of time.

3.3.1 Polarized Light Microscopy (PLM)

Due to relatively simple specimen preparation and easy operation, polarized light microscopy has become one of the most important techniques in the study of polymer blend phase morphology. However, PLM with its minimum resolution (0.2 μm) can only be sufficient to study immiscible blend phase behavior. In order to improve the quality of images, the visibility of phases can be enhanced by contrast techniques, such as polarized light, phase contrast and others.

3.3.1.1 Apparatus

An Olympus® BX50 system polarized light microscopy equipped with a THMS 600/HFS 91 stage was used to observe the phase morphology of LCP/PC blends. The polarized light microscope is shown in Figure 3-6 [31]. The equipment consists of a camera (not shown), eyepiece, observation tube, revolving nosepiece, objective, condenser and hot stage which can control temperature within ± 0.1°C. The major problem of polarized light microscopy lenses is aberration and their quality which is dependent mainly on the degree of correction. In order to eliminate these negative effects and get better resolution, 20× magnification was used, because the light intensity would be diminished if higher magnifications were applied [3]. If magnification is lower than 20×, the phase morphology is hardly to seen.
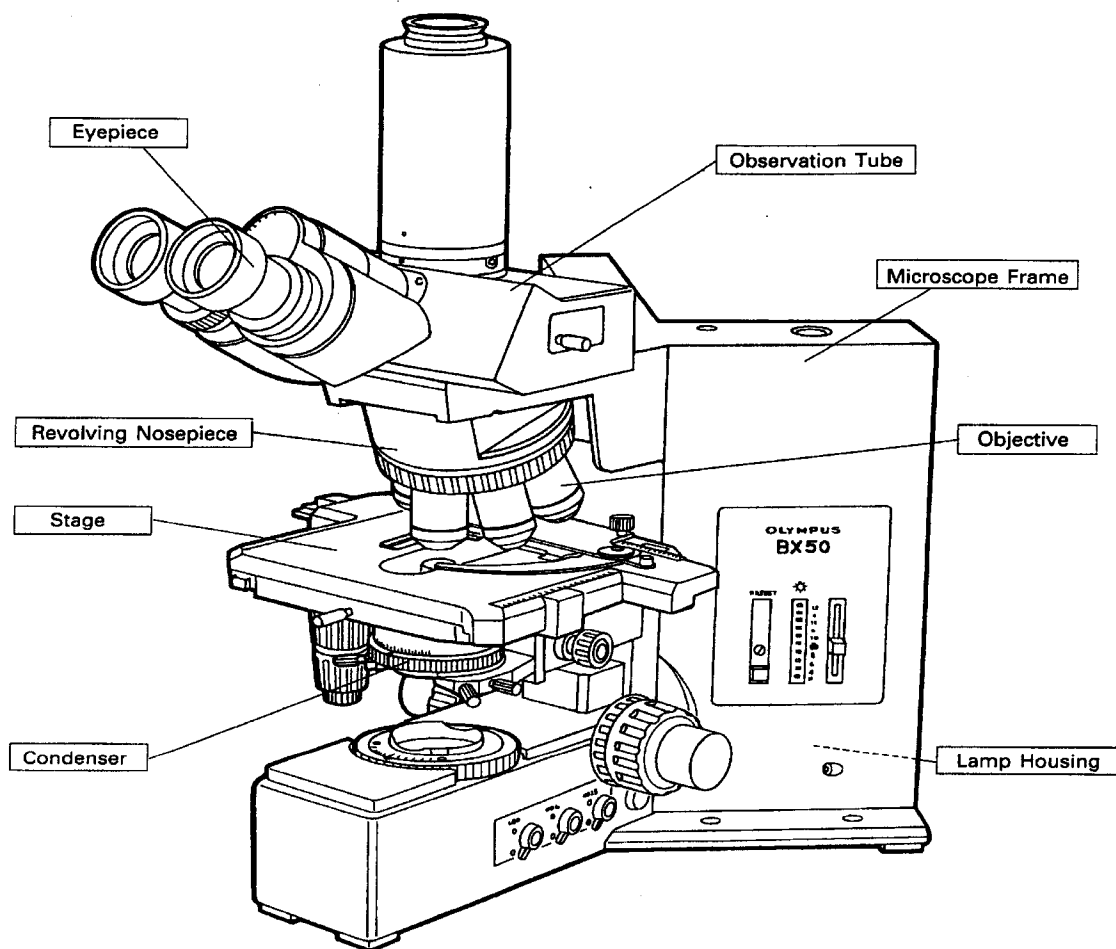

Figure 3-6: OLYMPUS® BX50 Microscopy System [31].

3.3.1.2 Sample Preparation

Like other microscopic techniques, specimen preparation for polarized light microscopy is a major problem that affects the microstructure analysis results. Therefore, specimen preparation is a very important part of microscopy as the quality and the reliability of the results are dependent on the specimen.

All samples were microtomed after extrusion in the twin screw extruder. The observed surfaces are perpendicular to the flow direction and in the central parts of each extruded sample. The discussion of the observed surfaces (Figure 3-7) will be presented in section 3.3.2.2. For accurate results, it is important that the surfaces of the stage block, window and carrier must always be kept clean, because any particles of dust will cause air gaps between the block and the window resulting in temperature errors.

3.3.1.3 Morphology of LCP/PC Blend

In order to compare the morphologies in different mixing methods, Figures 3-8 and 3-9 are presented.

Figure 3-8 shows PLM micrographs of the surfaces of 30wt% LCP blends using the Haake mixer at different temperatures. The processing conditions for these specimens are given in Table 3-2. The particles seen in this figure are the LCP rich phase because 30wt% LCP is the minor phase of the blend. It seems that there is no major difference among these photographs.

Figure 3-9 shows PLM micrographs of 30wt% LCP blends, which were prepared according to the conditions in Table 3-4. The observed surfaces are perpendicular to the flow direction and in the central parts of the extruded rods (see Figure 3-7). Figure 3-9A shows the morphology at 300°C, LCP and PC have small phases in toughened and fibrillar-like phase structure. It does not look like the typical droplet two-phase structure. However, more detailed analysis is needed to identify the exact structure. Figure 3-9B shows that LCP has fine particulate structure at 325°C, because LCP is the minor phase
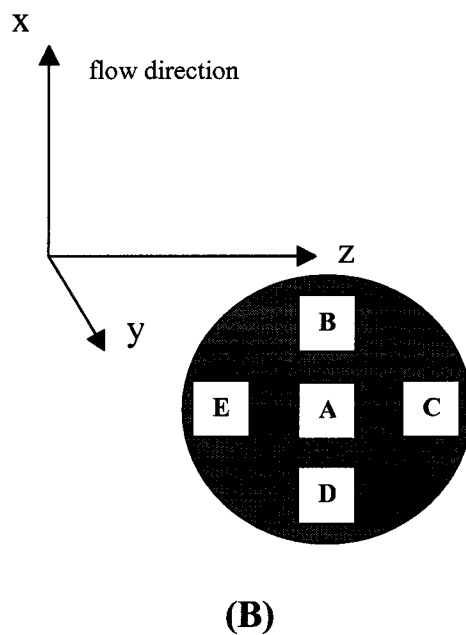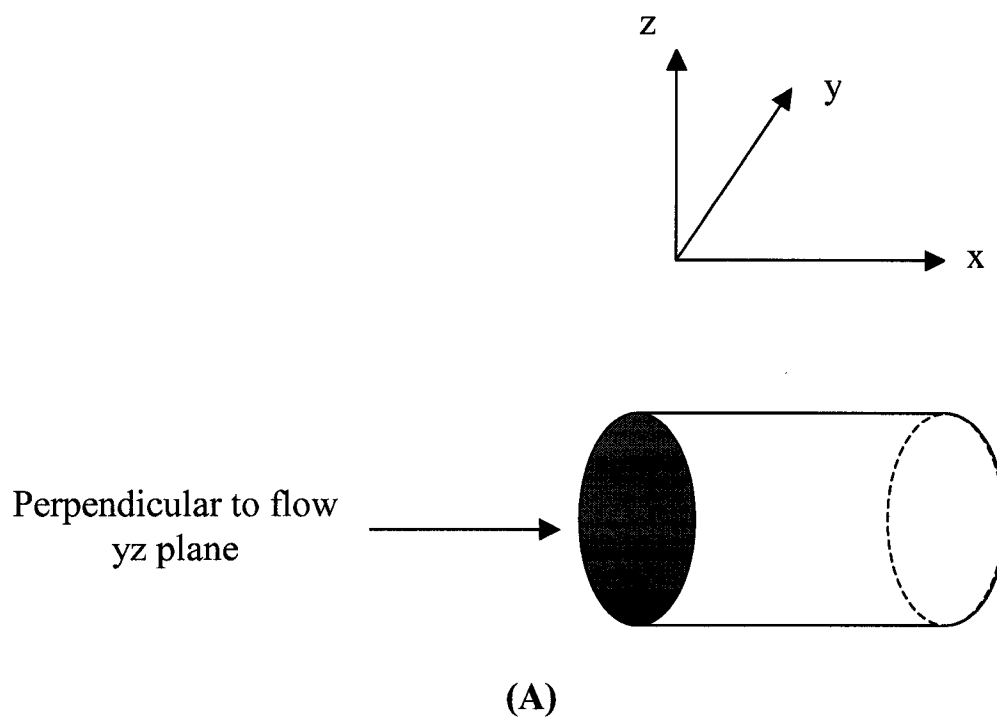
Figure 3-7: (A) Definition of the plane that is perpendicular to flow, and (B) the different locations investigated inside the twin screw extruded sample.

(A)
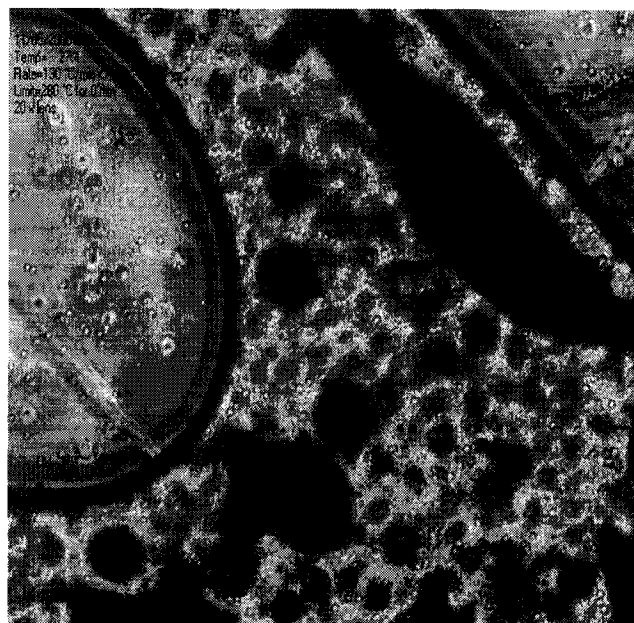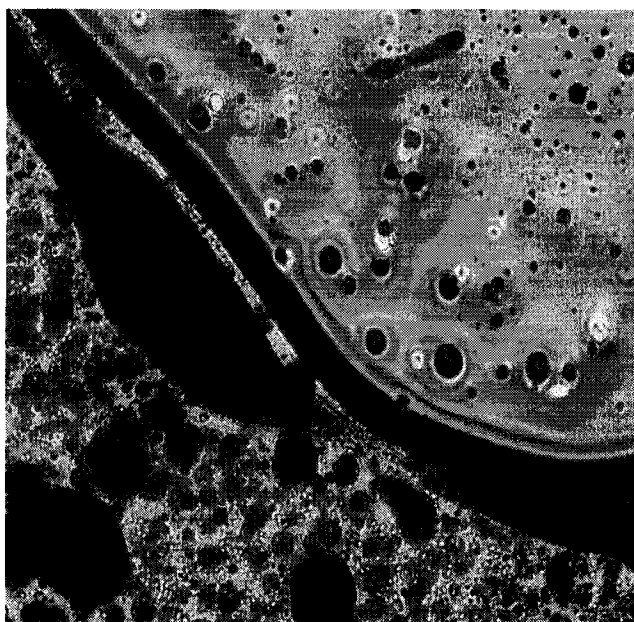
20μm

(B)

Figure 3-8: Polarized light microscopy (PLM) micrographs of the surfaces of 30wt% LCP/PC blend using Haake mixer at hot stage temperature: (A) 27°C, (B) 300°C (magnification: ×20).

41
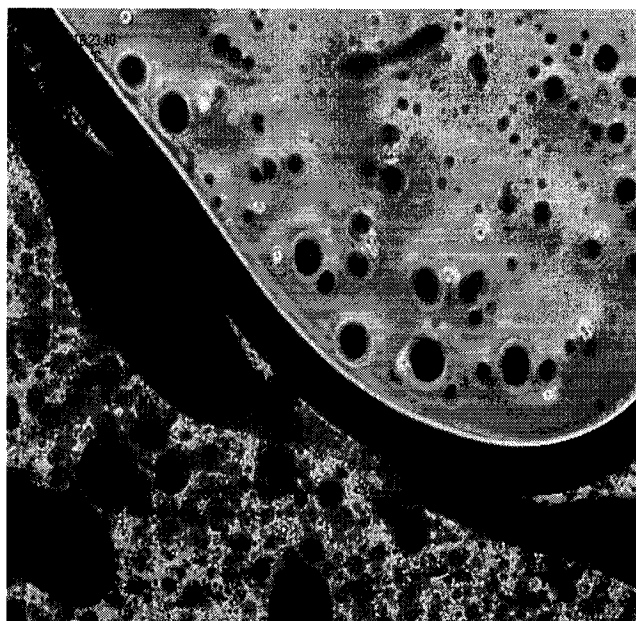
(C)
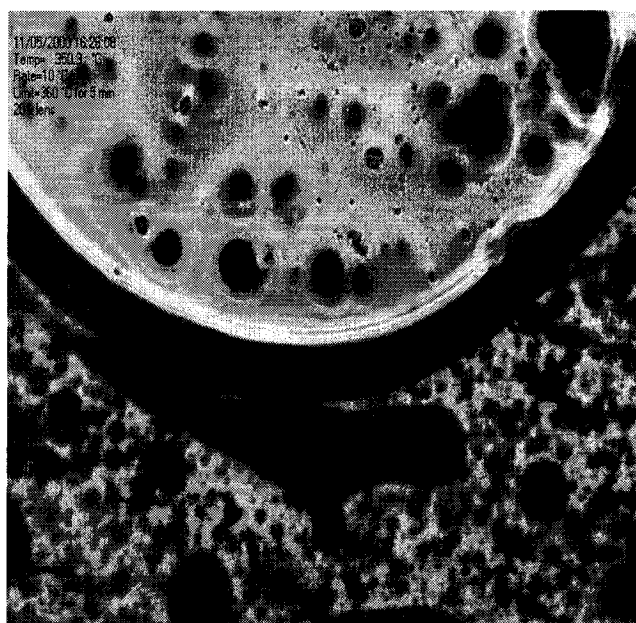
(D)   20μm

Figure 3-8: (continued) Polarized light microscopy (PLM) micrographs of the surfaces of 30wt% LCP/PC blend using Haake mixer at hot stage temperature: (C) 325°C, (D) 350°C (magnification: ×20).

(A)

(B)

(C)
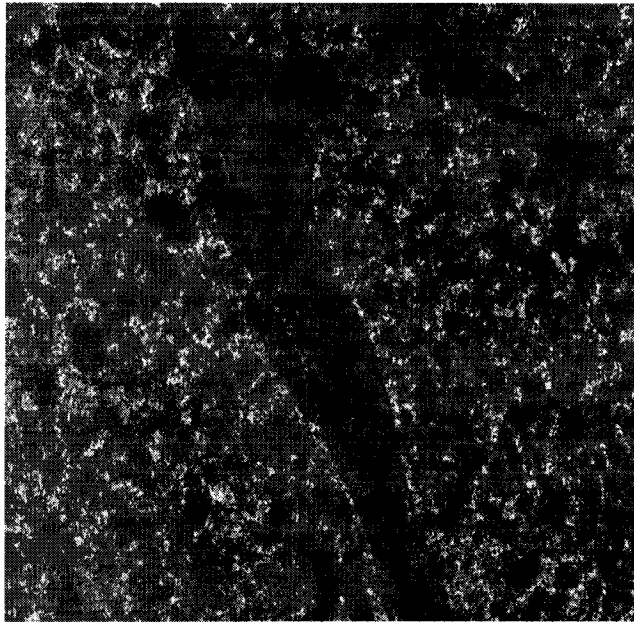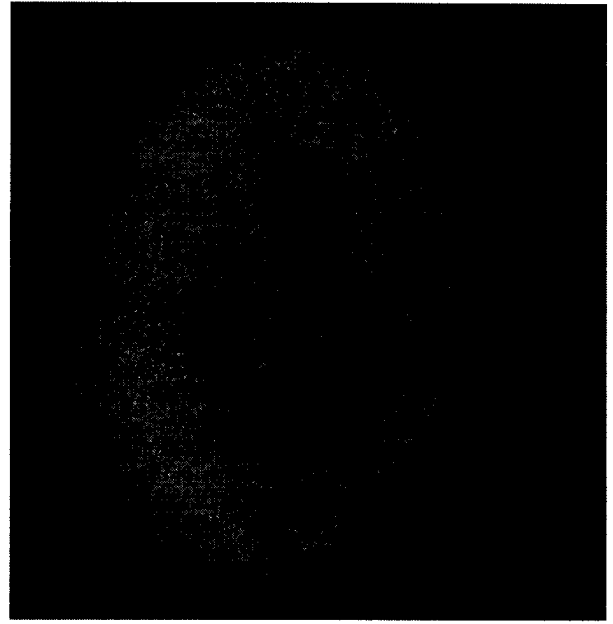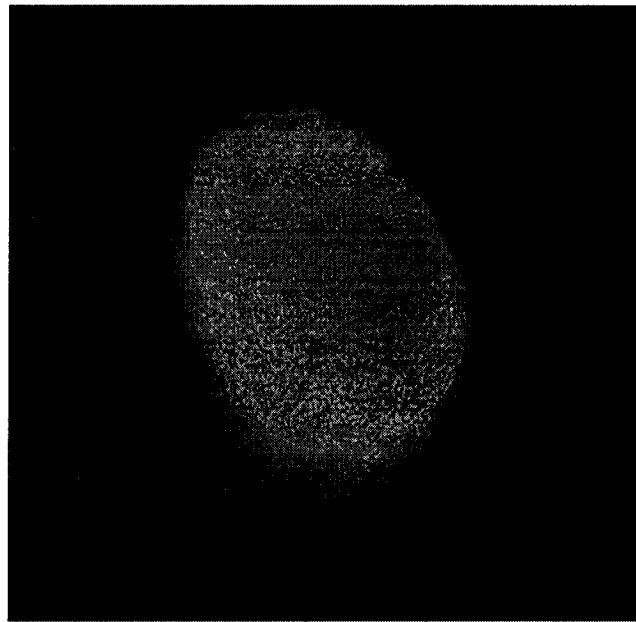
20μm
___

Figure 3-9: Polarized light microscopy (PLM) micrographs of the surfaces of 30wt% LCP/PC blend after twin screw extrusion at processing temperatures: (A) 300°C, (B) 325°C and (C) 350°C (magnification: ×20).

43

Table 3-4: Summary of Processing Conditions for 30% LCP/PC Blending Samples

| Serial #	Barrel Temperature Profile (°C)	Screw Speed (Rev Min⁻¹)	#1 Feeder Speed	#2 Feeder Ratio	Figure (3-8)
1	270-280-290-300	80	100	0.68	A
2	295-305-315-325	80	100	0.68	B
3	320-330-340-350	80	100	0.68	C

of the blend at 30 wt%. It appears like a typical droplet two-phase structure. The phase transition zones from LCP rich (droplet) to PC rich (matrix) phase can be observed. Figure 3-9C shows the blend surface at 350°C (processing temperature); photo C has smaller droplets than B, and the droplets of C are dispersed better than in B. However, both B and C have the same two-phase droplet-type morphology.

3.3.2   Scanning Electron Microscopy (SEM)

3.3.2.1   Introduction

Scanning electron microscopy (SEM) is an advanced technique that produces a microscopic image from a scanned specimen surface (5 to 10 nm in diameter) by reflecting an electron beam. The working fundamentals of the SEM instrument are shown in Figure 3-10 [32]. A scanning electron beam impinges upon the specimen surface, the signals are detected, amplified and modulated in a cathode ray tube. These reflected signals are collected and constructed to form an image. The magnification of this image that appears on the screen is the ratio of a distance on the screen and the corresponding distance on the specimen.

A Joel 840A SEM (scanning electron microscope) was used throughout the study. The samples were viewed in one direction that is perpendicular to flow, yz plane (Figure 3-7). Different locations within the extruded samples were investigated. These are illustrated in Figure 3-7B. As morphological studies are very time consuming, the focus is on the central location denoted by symbol A in the figure. We selected the central location to study the morphology because this part has the minimum flow effects during processing. On the other hand, the central part also has the maximum elongation effect. However, due to the small diameter of the studied specimen (usually 2-4 mm), we can ignore this effect. Thus, the morphology of this part can represent the phase structure of the blend. The samples were placed inside the microscope chamber under high vacuum. An accelerating voltage of 15kv and a working distance of 39 mm were used. Magnifications of 2000× and 4000× were used.

3.3.2.2   Sample Preparation

In order to obtain clean and clear surfaces where other effects, such as sample charging, signal noise, *etc*, were minimized, two kinds of sample preparation methods

45

were employed. Some samples were fractured after immersion in liquid nitrogen for at least five minutes. Others were microtomed at room temperature. Then, every sample was fixed onto a sample holder with silicone sealant so that the fractured or microtomed surface faced upwards. The next step was to coat each sample with a gold/palladium mixture. This makes them conductive and avoids sample charging that would cause deflection of the electron beam inside the microscope. The coating was applied by sputtering the metals under vacuum in a Hummer VI sputter coater.
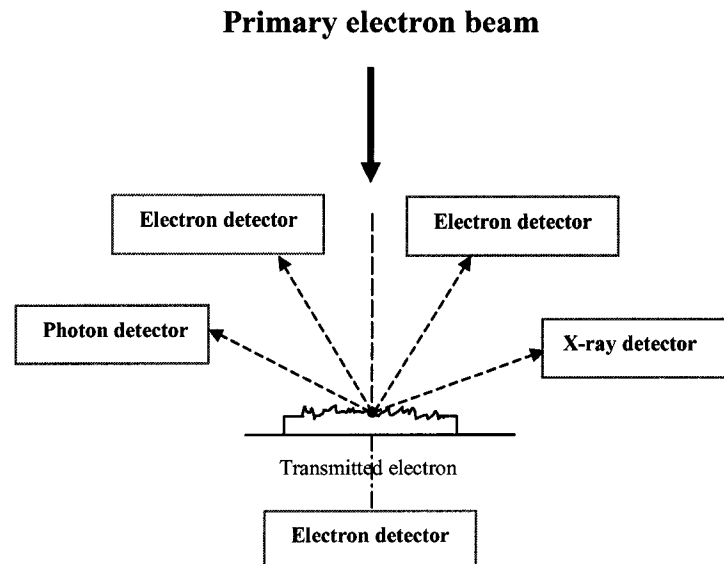
Primary electron beam

Figure 3-10: Information that can be generated in the SEM by an electron beam striking the sample [32].

3.3.2.3 Morphology of LCP/PC Blend

The SEM can be used to obtain morphological information from either immiscible or miscible blends where interfacial bonding is good and the phases are small. In Figure 3-11, it is easy to recognize the differences between morphologies A and B, which obviously has two-phase droplet-type structure. Morphology A is similar to that of Figure 3-9A. It looks like a single-phase fibrillar structure. All components are mixed together without interphase. This can be confirmed from Figure 3-12. In these two-dimensional images, morphology A has a smooth surface, which means that there is no other minor phase except the bulk phase. Meanwhile, morphology B has many holes on the surface. It means that morphology B represents a two-phase structure. The holes are LCP rich phase droplets, which were pulled out of this surface. A summary of the sample preparation conditions is given in Table 3-5. The image of fractured sample (Figure 3-11), which has three-dimensional information, is much easier to discern than that of the microtomed sample (Figure 3-12), which has only two-dimensional (2D) information. The 2D image loses some useful morphological information about the blend. Therefore, the fractured samples were used throughout the SEM study.

Table 3-5: Summary of LCP/PC Blend Sample Preparation Conditions for SEM

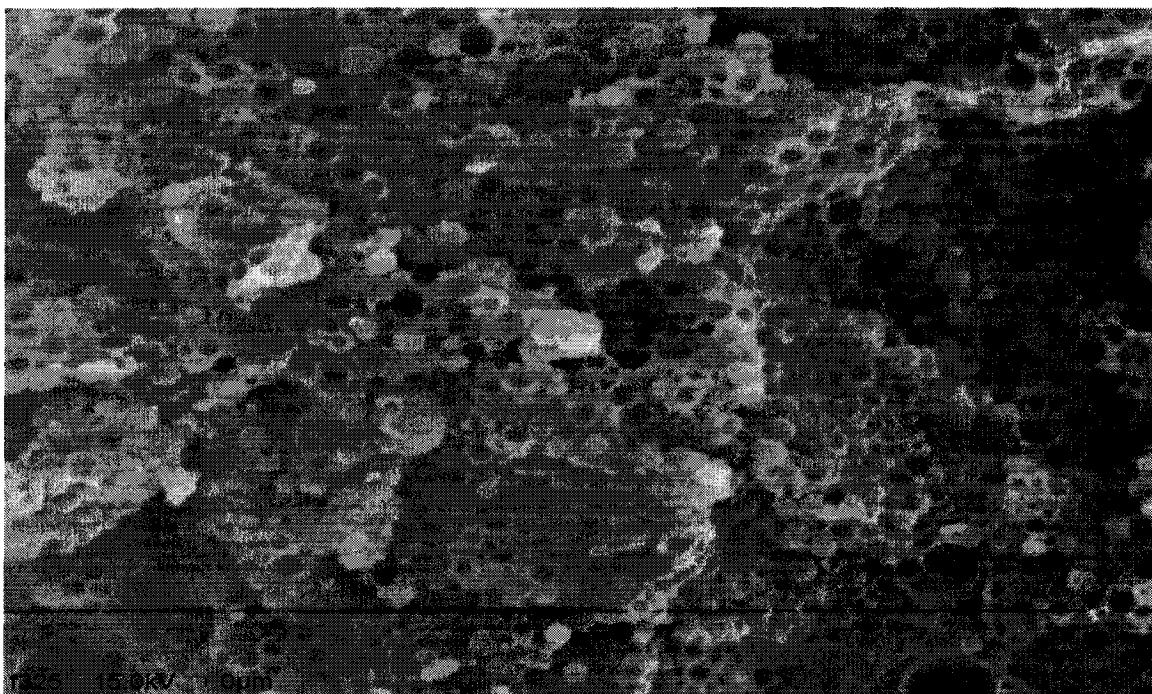| wt% LCP	Blending Conditions	Melt Temperature (°C)*	Sample Preparation	Figure
30	TSE**	300	fractured	3-11 (A)
30	TSE	325	fractured	3-11(B)
30	TSE	300	microtomed	3-12(A)
30	TSE	325	microtomed	3-12(B)

* The melt temperature refers to the final temperature in TSE near the die exit.
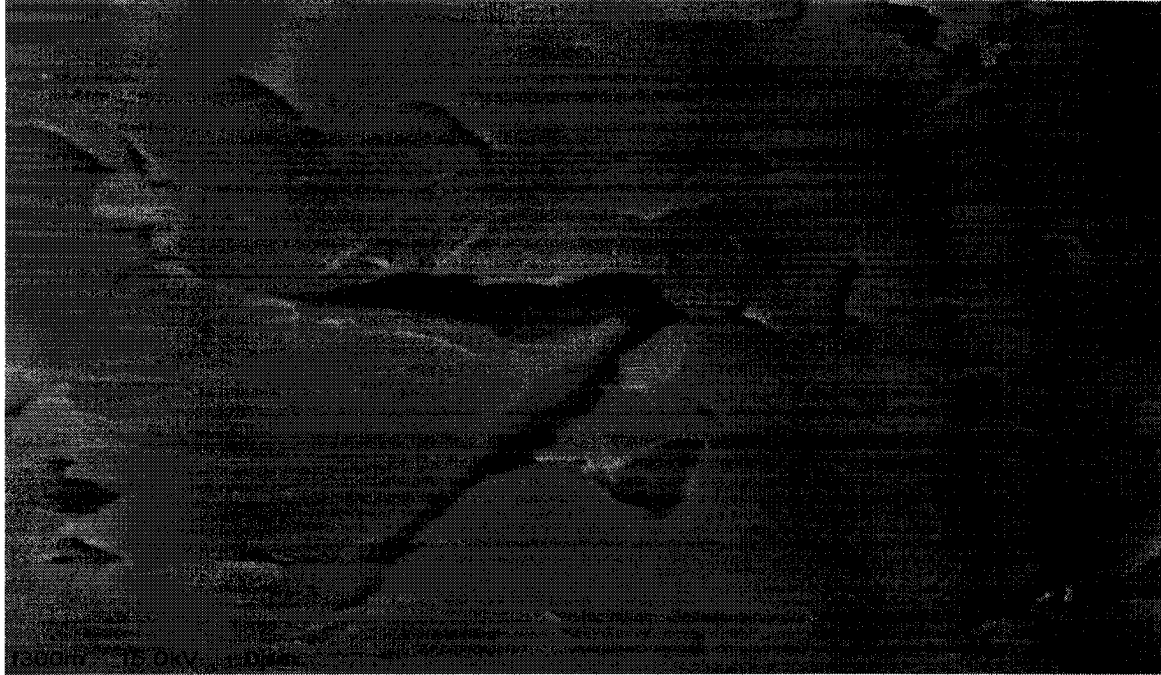** Twin Screw Extrusion (the processing condition is the same as Table 3-4).

(A)

5μm

(B)
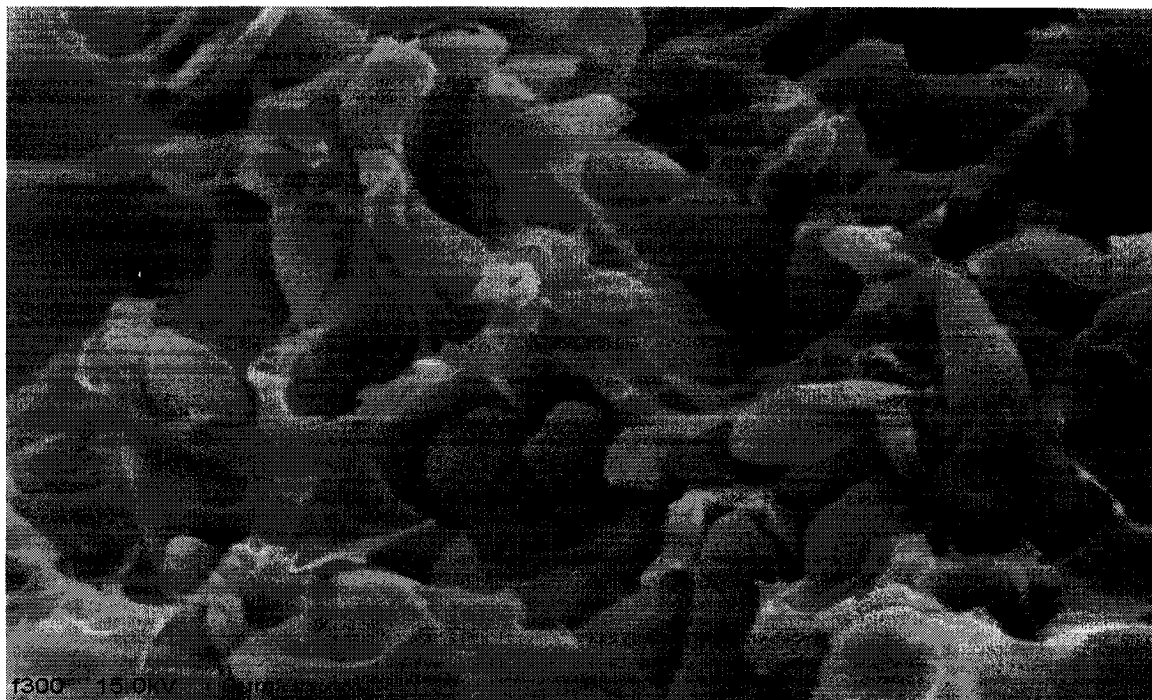
5μm

Figure 3-11: SEM micrograph of fractured 30wt% LCP blend (magnification ×2000).

(A)

5μm

(B)

5μm

Figure 3-12: SEM micrograph of microtomed 30wt% LCP blend (magnification ×2000).

3.3.2.4 Image Analysis

In order to quantify information in the SEM microphotographs, such as droplet size distribution, LECO 2005 image analysis system was used. The SEM grey image was stored in the memory of the computer and converted into a binary image. In this binary image, there were 254 color values (level 0 is black and 255 is white). However, it was difficult for the computer to perform automatic measurements on a 256 grey level image. The set of numerical data is highly dependent on the quality of the microphotograph from the SEM. Unfortunately, the SEM images were not sharp enough to perform image analysis automatically. The LCP particle gray value could not be distinguished from that of the PC matrix phase by the LECO 2005 system.

Consequently, the binary images were analyzed manually. This was a time-consuming process. In order to obtain droplet size distribution of the dispersed phase, both the numbers and diameters of the dispersed particles were measured. Finally, the statistical results and plots of particle size distribution were obtained.

3.4 Thermal Analysis

3.4.1 Differential Scanning Calorimetery (DSC) Pyris1

Differential scanning calorimetery (DSC) is one of the most commonly used techniques in thermal analysis. There are two types of DSC instruments. One type is designed to measure the differences in heat input from the differences in temperature between the specimen and the standard reference material. On the other hand, the power compensating DSC relies on the measurement of a difference in temperature. The sample and reference are heated separately, while the difference in electrical power needed to maintain equal temperatures is recorded.

The DSC Pyris1 used in this study is a power compensation type. The structure of this kind of instrument is shown in Figure 3-13 [33]. The base of the sample holder is surrounded by a reservoir of coolant, usually ice water or liquid nitrogen. The sample and reference holders are heated individually. When a temperature difference is detected between them caused by a thermal event in the specimen, energy is supplied until the temperature difference is less than a threshold 0.01 °C. Thus, the energy input per unit time is recorded as a function of temperature or time. The temperature scanning range of DSC Pyris1 is from -160 to +600 °C. Standard reference materials, such as indium and zinc are used to calibrate temperature and energy. In addition, the DSC instrument can perform scanning rates from 0.3 to 320 °C/min on heating and cooling. However, the maximum reliable scanning rate is 60 °C/min.

3.4.2 Glass Transition Temperature (T_g) Measurement

The glass transition temperature T_g of a polymer is a second-order transition that represents the polymer passing from the hard rigid solid to the rubbery state. This is an important temperature, because it indicates the transition point between the solid and rubbery states. Therefore, determination of T_g in the blend in relation to those of the pure components has become the most commonly used method for establishing miscibility in polymer-polymer blends or partial phase mixing in such blend systems [2,9]. For example, an immiscible blend will exhibit two separate T_gs between those of the pure components. This results in two phases: component A-rich phase and component B-rich phase. While a miscible polymer blend will exhibit only a single glass transition temperature between the T_g's of the pure components.

In this work, 20 °C/min heating and cooling rates were used throughout the DSC experiments. The blend samples and reference compartments were purged continuously with extra dried pre-purified nitrogen at a flow rate of 20 ml/min. The manual baseline was set up for every new experimental run. This can be done by running a heating scan from 50°C to 350°C at the rate of 20 °C/min. A baseline was run with two empty pans in both the reference and sample holders.

Pt sensors

Individual
heaters

Differential temperature control loop
Sample temperature

Average temperature control loop
Sample temperature

Recorder (temperature marking)

Programmer

Sample
holder

Differential
power (W-λW)

Power
(average)

Amplifier
(differential
temperature)

Amplifier
(average
temperature)

Average
Temperature
computer

Differential
power (W-λW)

Reference
holder

Power
(average)

Recorder
(differential power)
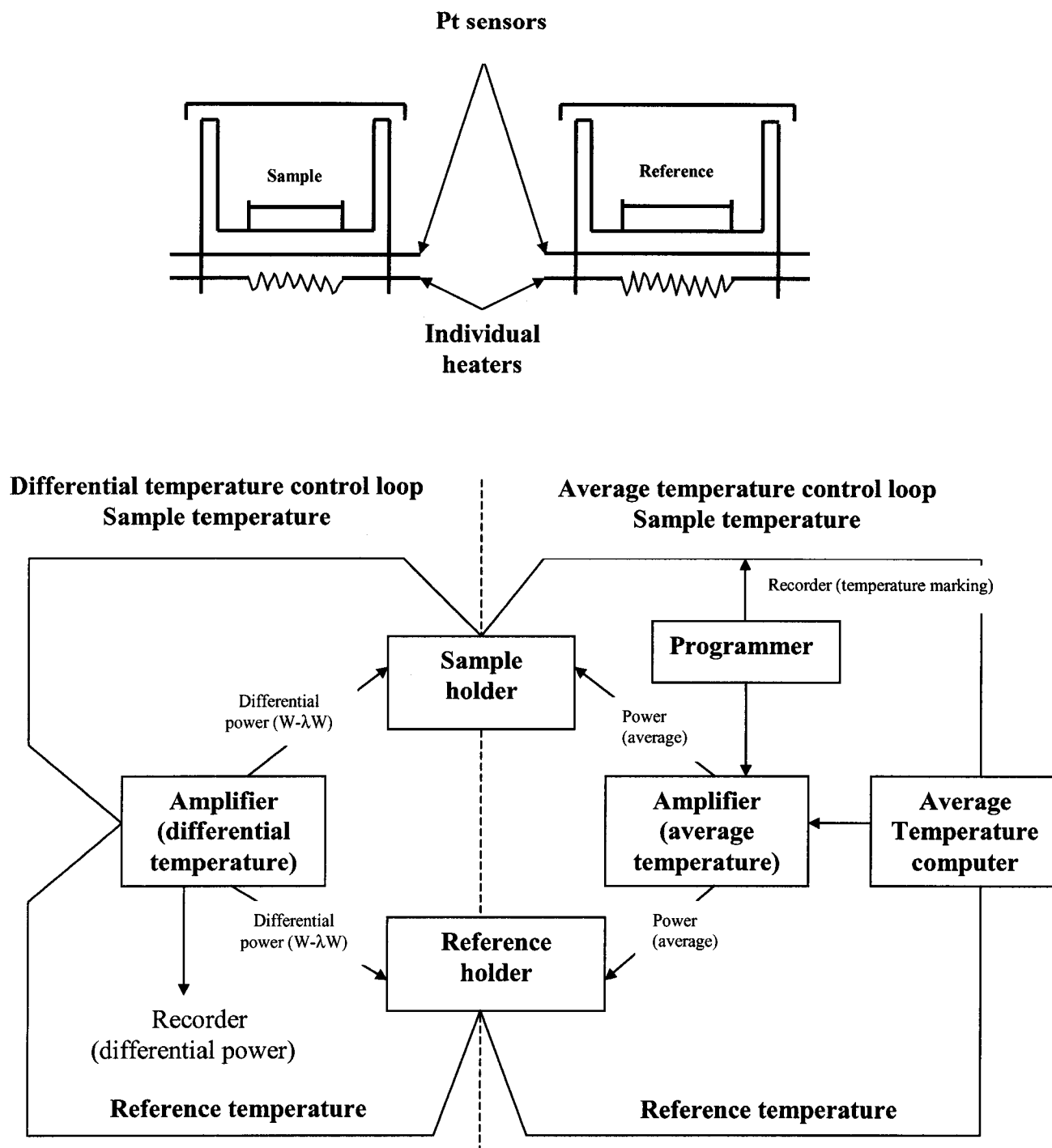
Reference temperature

Reference temperature

Figure 3-13: A schematic representation of a power compensating DSC instrument and its operation [33].

52

The DSC thermograms were normalized to take into account the weight of the samples, which varied from 5 to 8 mg. All curves and data were obtained from the second scanning, in order to eliminate the thermal history. The procedure of the automatic subtraction of the baseline and the calculation of the T_g value was used for all the runs. A Sartorius Supermicro Balance was used in conjunction with the DSC to weight blend samples with a precision of $\pm 10^{-4}$ mg.

3.4.3 Phase Transition Temperature Calculation

Nonlinear regression using Sigmaplot$^{\circledR}$ 5.0 software was employed to fit the experimental T_g data points. The Sigmoid 4 parameter regression equation was selected, it was found to fit the data successfully. It has the form:

$$y = y_0 + \frac{a}{1 + e^{-(\frac{x-x_0}{b})}} \qquad (3\text{-}1)$$

where a and b are fitting parameters, x_0 is the phase transition temperature, and y_0 is the dimensionless glass transition temperature.

The inflection point of this curve represents the phase transition temperature of the LCP/PC blend. It represents the T_g of the blend, as will be discussed in section 4.2.1. This point was obtained by setting the second derivative of Equation (3-1) equal zero.

$$y' = [\frac{a}{1 + e^{-\frac{(x-x_0)}{b}}}]' = \frac{a}{b} \times \frac{1}{[1 + e^{-\frac{(x-x_0)}{b}}]^2} \times [e^{-\frac{(x-x_0)}{b}}] \qquad (3\text{-}2)$$

$$y'' = \frac{2a}{b^2} \times [e^{-\frac{(x-x_0)}{b}}]^2 \times \frac{1}{[1 + e^{-\frac{(x-x_0)}{b}}]^3} - \frac{a}{b^2} \times [e^{-\frac{(x-x_0)}{b}}] \times \frac{1}{[1 + e^{-\frac{(x-x_0)}{b}}]^2} \qquad (3\text{-}3)$$

If $y'' = 0$, then $e^{-\frac{(x-x_0)}{b}} = 1$,

$$x = x_0 - b \ln 1 \qquad (3\text{-}4)$$

53

x_0 is the phase transition temperature of the blend under consideration.

3.5   Discussion of Experimental Techniques

The solvent casting method is not applicable to the LCP/PC blend under study, because it was not possible to dissolve the LCP used in this study in either of the mixed solvent systems (see section 3.2.2.1 and 3.2.2.2). There are a number of reasons for this problem, which are:

1. LCP, especially fully aromatic ones such as THERMX LCP LN001, are highly crystalline and resistant to solvent attack;

2. The limited solubility of LCP is the major problem; the tendency to crystallize limits the quantity that can be solubilized;

3. The complex chemical structure of copolyester LCP, including some possible cross-linked structures;

4. The molecular weight and melting point of the LCP used in this study are much higher than for other commercial grade LCP.

It has been suggested that there are some other solvents known in the literature as having at least some degree of dissolving power towards LCPs. Tennessee Eastman Kodak, the supplier of the LCP used in this study, suggested that hexafluoroisopropyl alcohol (HFIP) or mixtures of HFIP with chlorinated solvents such as methylene chloride or chloroform (volatile solvents) could dissolve the LCP at low concentrations of solute (0.5% or 0.1%). This mixture could be effective at ambient temperature if allowed sufficient time, and the application of heat would accelerate the dissolution process. However, it was decided to avoid such hazardous solvents.

The mechanical blending for LCP/PC blends was accomplished by the Haake mixer and twin screw extruder. The twin screw extruder is more suitable for the LCP/PC blends studied. From the microscopic analysis of the extruded blend samples (Figure 3-8 and 3-9), it is clearly observed that the minor LCP phase of twin screw extruded blends is more finely dispersed, that is, the average particle size is smaller than for Haake blends. In addition, the twin screw extruded blends have a more uniform dispersion of the minor phase, which represents the result of more intensive mixing action. Overall, the microscopic experimental results suggest that the twin screw extruded blends have been mixed more intensively than that using the Haake mixer.

Polarized light microscopy (PLM) and scanning electron microscopy (SEM) are the major techniques for the assessment of morphology of liquid crystalline polymers and their blends. However, we have selected only SEM as the main technique for assessing the morphology. The resolution of a SEM is typically between 10 and 30 nm, while that of the PLM is limited to 0.2 μm, which is only sufficient to study phase behavior of some immiscible blend systems. Furthermore, SEM sample preparation is relatively simple. The fractured or etched surfaces of specimens are coated with a thin layer of conductive material prior to examination, in order that the electron beam inside the SEM can deflect signals to construct an image. Finally, SEM can produce, not only detailed topographical images that are obtained by recording the scattered secondary electrons, but also large and sharp images with large topographical variations. Therefore, the final image can be converted to light intensity contrast using available techniques to coordinate the variations in absorption coefficient, sample thickness, refractive index, birefringence and so on.

In this work, we used DSC, because it is routinely performed to study polymer blend phase transition temperatures and thermodynamic characteristics. The advantages of DSC thermal analysis over other analytical methods can be summarized as follows:

1. DSC specimen preparation is relatively simple, almost any physical form is acceptable;

2. A small amount of sample (1 - 10 mg) is required;

3. The analysis can be performed over a wide temperature range;

4. Temperature can be controlled to within $\pm\,0.1\ ^{\circ}\text{C}$;

5. DSC is a suitable instrument for measuring all transition temperatures for a polymer by studying the changes of enthalpy accompanied with physical and chemical changes;

6. The run time program can vary from several minutes to several hours;

7. The DSC instrument is easy to operate.

Chapter 4

Results and Discussion

This chapter introduces a novel method to determine the thermodynamic phase diagram for LCP/PC blends. The thermally induced phase separation of the blends is discussed in detail. The experimental results are compared with theoretical results obtained using the Flory-Huggins and Cahn-Hillard theories. The reproducibility of the result and error estimation are also discussed.

4.1 Introduction

As discussed in the previous chapter, the experimental techniques selected in this study were the DSC and SEM. In DSC thermal analysis, it was found that the glass transition temperature T_g is a function of processing melt temperature T_{pm}, as defined in section 3.2.3.3. Moreover, the SEM results could be used to confirm those of DSC by observation of phase morphology. Also, the SEM results produce information regarding the microstructural morphology and its dependence on processing conditions. Thus, the above techniques are useful for obtaining the thermodynamic phase diagram, which relates the microstructural morphology of the blend to the processing melt temperature. It will be shown that the present work supports the findings of other researchers [16-23]. It also provides some novel additional contributions: (1) a practical experimental method has been established using TSE, DSC and SEM techniques to determine the thermodynamic phase diagram for the LCP/PC blend, and (2) the dependence of the blend T_gs on the processing melt temperatures T_{pm}s is evaluated carefully. The dependence of blend T_g on the processing melt temperature T_{pm} has not been considered

by other researchers. Thus, the experimental techniques and the results of this study provide more insight regarding thermally induced phase separation of the blend.

4.2 Thermodynamic Phase Diagram for LCP/PC Blends

4.2.1 Determination of Phase Transition Temperatures

In order to study the effects of thermally induced phase separation of LCP/PC blends, the thermal effect was produced by varying the processing melt temperature T_{pm}. As mentioned before, the determination of the glass transition temperatures T_g of polymer blends by thermal analysis method is a generally accepted way to evaluate the miscibility of polymer blends [2,8,10]. Therefore, the influence of processing melt temperatures T_{pm} on the blend T_g was studied. In this work, the glass transition temperature T_g is the onset value that is calculated by finding the intersection of the extrapolated tangent at the first limit and the extrapolated tangent at the inflection point (see Figure 4-1). Figure 4-1 demonstrates the typical DSC behavior near T_g for most polymers. Figure 4-2 shows the actual DSC thermograms of the blend containing 25wt% LCP, as obtained with DSC Pyris1. The calculation of the onset T_g values was automatically done by DSC (see Figure 3-2). A summary of all the processing conditions of different LCP concentrations with the corresponding T_gs detected by the DSC is given in Table 4-1.

The T_g values were plotted as a function of processing melt temperatures T_{pm}s, as shown in Figure 4-3 (A) and (B). LCP weight concentrations in the range 15%-70% were investigated. We only focused on this concentration range to avoid the complex phase behavior near the limits of the concentration range (0 and 100%). In order to clarify and simplify the analysis, the data were divided into two groups 15%-30% and 40%-70%.
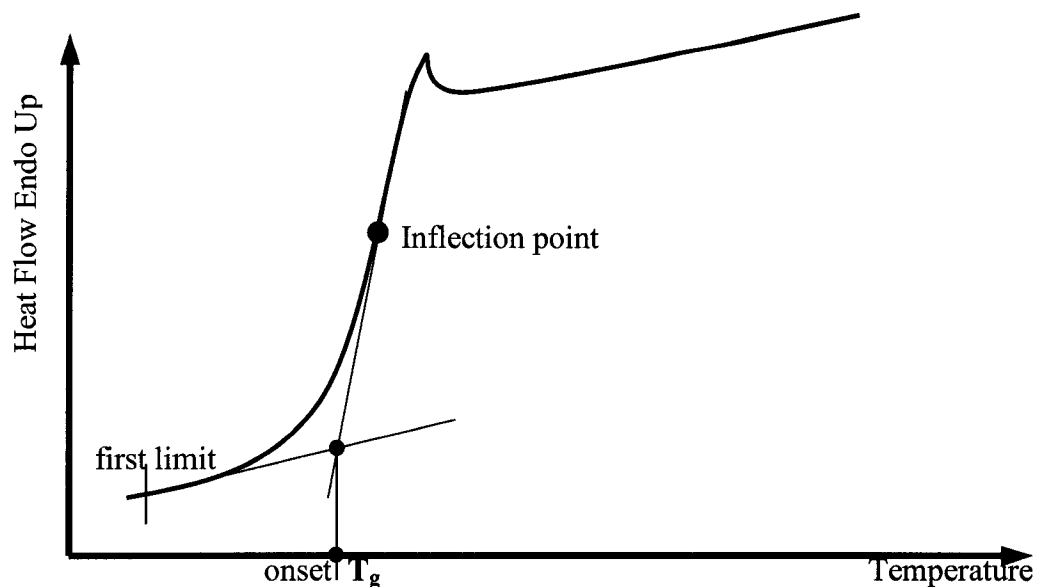
Figure 4-1:Schematic diagram of the onset glass transition temperature T_g obtained by DSC Pyris1.
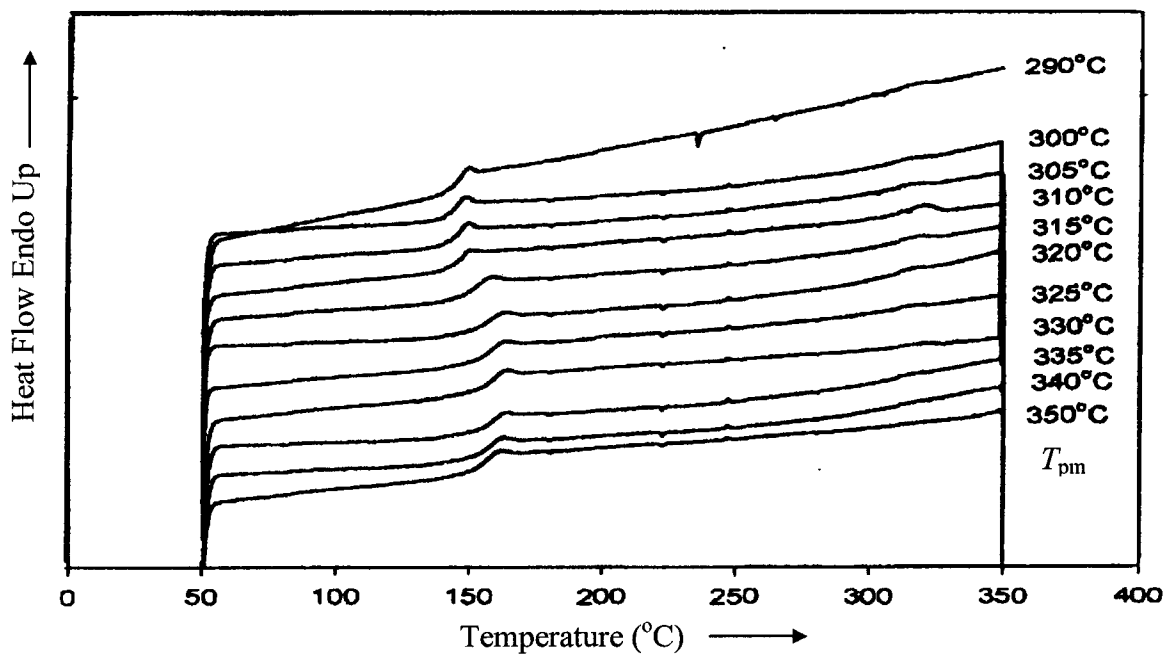

Figure 4-2: DSC thermograms of the blend containing 25 wt% LCP after being mixed for different processing melt temperatures T_{pm}s in twin screw extrusion.

Table 4-1: LCP/PC Blend Processing Conditions and their Corresponding T_g Data

wt% LCP	Processing Melt Temperature T_{pm} (°C)*								
	Onset T_g (°C)								
15	295	305	310	315	320	325	330	340	350
	142.9	143.1	143.0	144.0	146.5	147.8	146.7	147.2	149.0
20	301	307	312	317	322	328	334	337	
	146.2	147.1	149.0	151.1	153.2	152.2	153.9	154.8	
25	300	305	310	315	320	325	330	335	340
	141.4	142.1	144.1	146.2	148.5	151.9	153.0	152.3	152.0
30	290	295	300	305	310	315	325	350	
	138.4	140.3	140.6	141.3	145.6	149.2	152.3	155.7	
40	290	300	305	310	320	325	335	340	350
	139.8	139.8	138.2	139.6	151.2	150.6	152.7	152.6	152.7
50	280	290	300	310	320	325	330	335	340
	135.4	135.9	136.8	137.0	141.7	147.6	147.6	148.6	151.4
60	307	311	317	319	325	330	340		
	141.0	141.2	141.8	142.7	145.0	147.6	149.0		
70	305	311	315	319	329	332	341	345	
	138.0	140.4	140.0	139.9	143.0	147.3	148.0	148.2	

* Other processing conditions in twin screw extrusion, such as screw speed, feeder rate and so on, are the same as presented in section 3.2.3.

LCP/PC Blend T$_g$ vs. T$_{pm}$ ($^{\circ}$C)

(A)

LCP/PC Blend Tg vs. T$_{pm}$ ($^{\circ}$C)
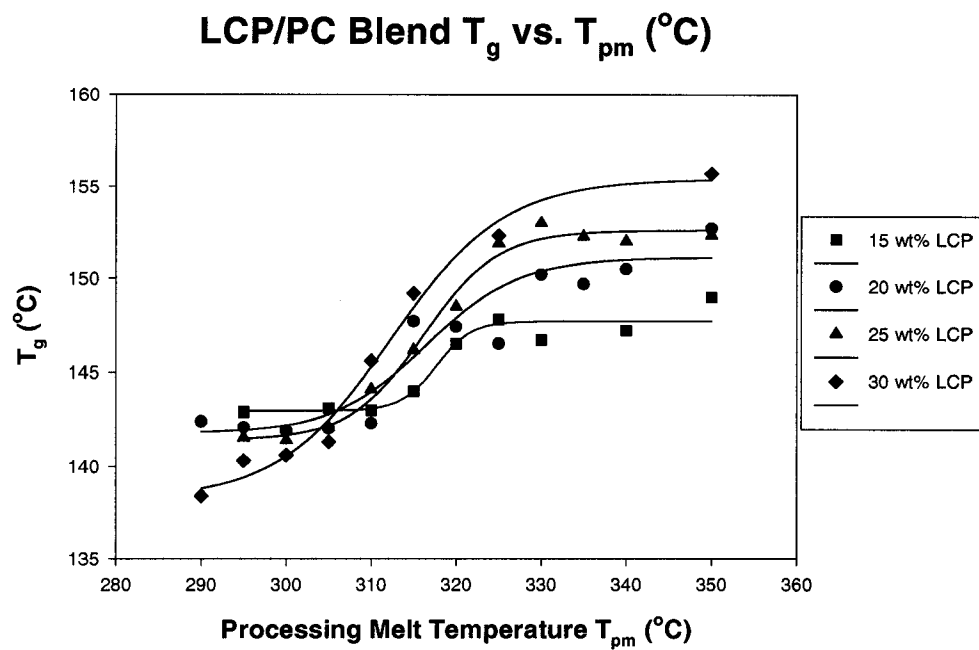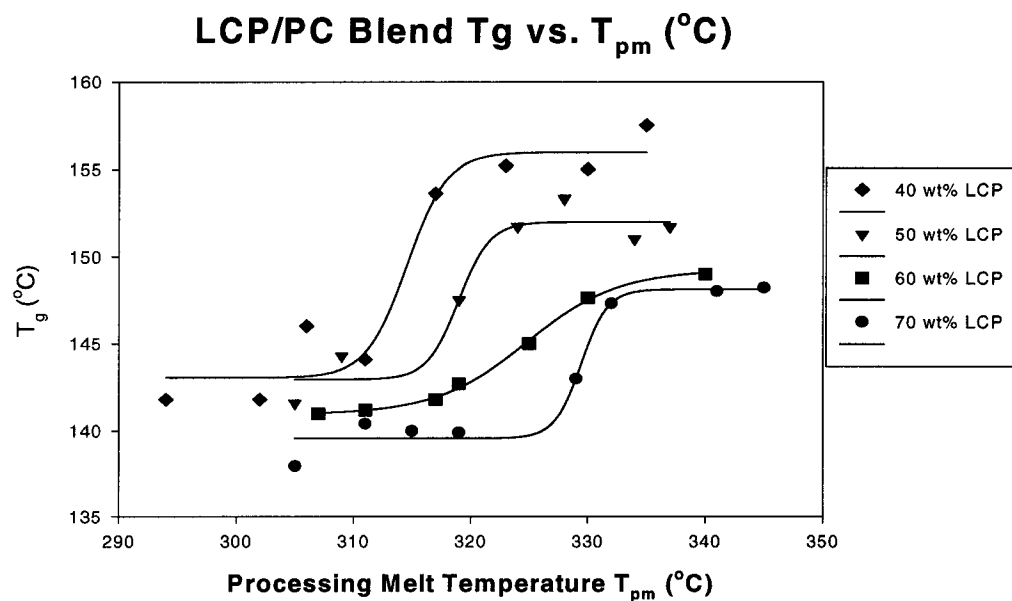
(B)

Figure 4-3: Glass transition Temperatures T_g vs. T_{pm} for different LCP wt%.

It can be seen from Figure 4-3 that the blend shows variable glass transition temperature T_g values, depending on the processing melt temperature T_{pm}. In general, T_g increases with T_{pm} for the same LCP concentration. Table 4-1 shows that the blend T_gs cross the T_g of pure PC, which is 147.6°C (see Figure 3-2A), at a certain value of T_{pm} for a given LCP concentration in the blend. The blend T_gs increase slightly when processed above this temperature. For instance, in the 25wt% blend, this temperature is located between 315°C and 320°C. The corresponding blends T_gs of this temperature range are 146.2°C and 148.5°C, respectively (see Table 4-1 item 25% columns 4 and 5). Consequently, the phase transition temperature occurs between 315°C and 320°C.

In Figure 4-3A, the inflection points of the various curves are close to each other, but it is seen that the highest inflection point value is for the 15wt% LCP blend and the lowest is for the 30wt% blend (see Table 4-2). Also, the low part of each curve becomes lower with the increase of LCP weight fraction from 15% to 30%. However, the upper part of the curve becomes higher with the increase of LCP weight fraction. Figure 4-3B and Table 4-2 show that the highest inflection point value is for the 70wt% LCP blend and the lowest is for the 40wt% blend. Both the upper and lower parts of the curve become lower with the increase of LCP weight fraction from 40% to 70%. The lower (upper) parts relate to the miscible (immiscible) blend, because the blend T_gs decreased (increased). (We shall discuss this phenomenon later in conjunction with Figure 4-4.)

The phase behavior of the blend leads to the above variations in blend T_gs. On the other hand, these variations can help us to determine the phase transition points according to the T_g criterion. If the blend has a LCST, the inflection point value for the blend T_g curves should decrease as the concentration of LCP initially increases. After reaching a certain LCP concentration, the inflection points should increase with increasing LCP concentration. In fact, this is the behavior depicted in Figure 4-3. The inflection points decrease from 15% to 30% and then increase from 40% to 70%.

Table 4-2 Summary of Calculated Transition Temperatures for LCP/PC Blend

wt% LCP	15	20	25	30	40	50	60	70
Temperature (°C)	317.7	316.5	316.2	312.4	314.6	319.0	325.0	329.4

It is well known that a miscible blend shows a single T_g intermediate between those of the pure components in isolation [9, 34]. An immiscible blend will generally exhibit two separate T_gs. In the present case, especially because a wholly aromatic LCP is one of the blend components, the T_g shifts slightly toward that of the LCP suggesting miscibility, whereas T_g of the PC phase increases suggesting generally immiscibility [26-28]. However, LCP is a highly crystalline polymer. It is difficult to observe the T_g of LCP in the blend, because of the absence of disordered LCP chains in the blend. Therefore, the T_gs obtained and discussed here are T_gs of the LCP/PC blend.

In order to obtain the two-phase transition temperatures in the blends, a nonlinear Sigmoid 4 parameter regression, Equation (3-1) discussed in section 3.4.4, was employed. This provides a good fit of the DSC experimental data points. In order to measure how well this regression model describes the data, the correlation coefficient, R^2, was determined. R^2 value near 1 indicates that the equation provides a good fit. For the present DSC data, R^2 equals 0.989.

The inflection point of the fitting curve is considered as the two-phase transition temperature, because the second derivative at this point is equal to zero. This point represents the temperature for the change from miscible to immiscible blend behavior. For instance, the two-phase transition temperature for 25 wt% LCP can be obtained by setting the second derivative of Equation (3-1) equal zero, all parameters were calculated as follows: $a = 11.17, b = 4.36, x_0 = 316.2, y_0 = 141.4$. Thus, the phase transition temperature for 25wt% LCP blend is 316.2°C. This value is located in the range 315-320°C, as discussed previously. A summary of the calculated two-phase transition temperatures is given in Table 4-2.

The variability of T_g for immiscible LCP/PC blends has been the subject of other studies [25-28]. So far, the reason for the increase of T_g is not fully understood. It has been suggested that transesterification is one of the factors [25,28]. However, the variation of free volume behavior during thermally induced phase separation could be the major cause of the fluctuating T_g of the PC-rich phase [25]. This is because of the increase of the interfaces between PC and LCP at higher processing melt temperature, which is in accordance with the consideration that the blends are immiscible. As for

miscible blends, the decrease of the interfaces between PC and LCP strengthens the solubility of each isolated component.

In order to further evaluate the T_g behavior of these blends, the T_gs of the blends were plotted as a function of LCP weight fraction. In Figure 4-4, the square points and the diamond points represent, respectively, the inflection point T_g values and the values indicated by the lower parts of the curves shown in Figure 4-3. The inflection point T_gs are constant, which means that the blends undergo phase separation and appear predominantly immiscible. These T_g values are similar to the T_g of the pure PC's. Meanwhile the lower line T_g values decrease about 8K with the increase of LCP weight fraction by 0.7. This phenomenon reflects the typical phase behavior of partially miscible blends, indicated by the shift of T_g slightly toward that of LCP, with increasing LCP concentration. (See discussion above where the lower (upper) of the curves in Figure 4-3 indicate miscible (immisible) blends.)
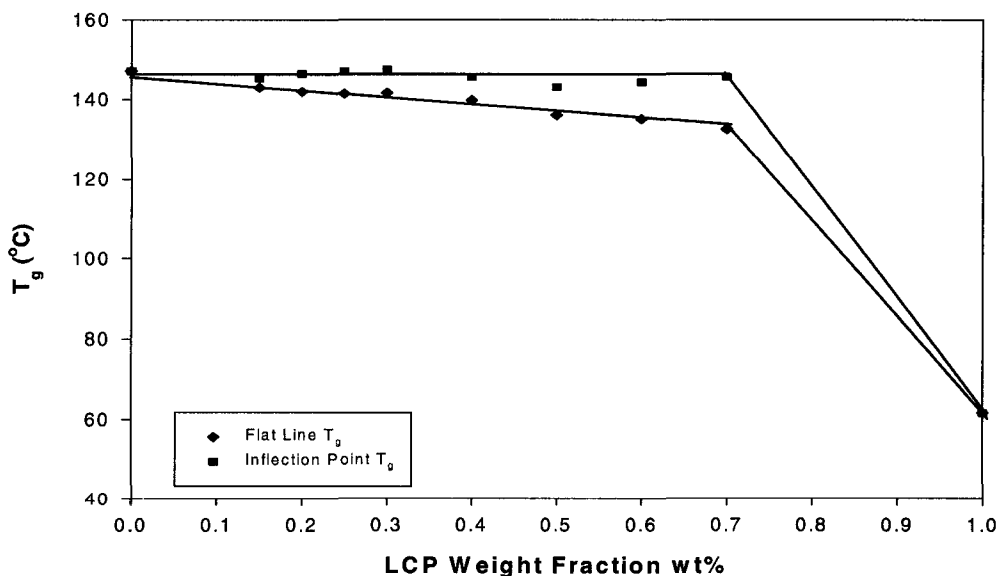
Figure 4-4: LCP/PC Blend T_g values as a function of LCP weight fraction.

4.2.2 LCP Volume Fraction Phase Diagram

The volume fraction is a typical variable used in thermodynamics to characterize multiphase polymer blends. It can be applied to many basic thermodynamic concepts and theories of composite materials and phase transformations. The volume fraction defines the fraction of the volume filled with particles. For a specimen of total volume V_T, the volume fraction $(V_V)_\alpha$ of α particles is defined as:

$$(V_V)_\alpha = \sum_{i=1}^{N} \frac{(V_i)_\alpha}{V_T} \tag{4-1}$$

where this summation is over all N particles in the volume of the specimen, V_T. The volume of α particle is given as:

$$(V_i)_\alpha = \frac{m_i}{\rho_i} \tag{4-2}$$

where m_i is the mass and ρ_i is the density of α particle, respectively. For example, the volume fraction of 1 g 15wt% LCP/PC blend can be calculated as follow:

$$\text{LCP volume } V_1 = \frac{m_{LCP}}{\rho_{LCP}} = \frac{1 \times 15\%}{1.38} = 0.1087 \text{ cm}^3$$

$$\text{PC volume } V_2 = \frac{m_{PC}}{\rho_{PC}} = \frac{1 \times (1 - 15\%)}{1.20} = 0.7083 \text{ cm}^3$$

$$\text{LCP volume fraction } (V_V)_{LCP} = \frac{V_1}{V_1 + V_2} = 13.3\%$$

A summary of the studied LCP weight fraction converted to volume fractions is given in Table 4-3.

Table 4-3: Summary of LCP Weight Fraction Converting to Volume Fraction

wt% LCP	15	20	25	30	40	50	60	70
Vol% LCP	13.3	17.9	22.5	27.1	36.7	46.5	56.6	67.0

The thermodynamic phase diagram for the LCP/PC blend (Figure 4-5) was obtained by combining the results of all experimental techniques, such as TSE, DSC and SEM. The diagram contains all experimental data points involved, including the reproducibility experiments.

The phase diagram is established on the transition temperature T versus the volume fraction ϕ of one component at constant pressure p. This diagram usually gives information about the types of phases that can exist and/or coexist with other phases formed by components of the system. As can be seen in Figure 4-5 (note that there are two overlapping points at 22.5 vol%), the blend system has a lower critical solution temperature (LCST). As discussed in section 2.3.1, two phases are formed. One is two-phase droplet-type morphology and the other is homogeneous single-phase morphology. The morphology of this blend will be discussed in the next section.

The diagram obtained in this work is similar to that of Kyu and Zhuang (Figure 2-7) [19]. In their case, they obtained the diagram via solvent casting. Figure 2-7 shows the curve to be concave upwards with a minimum at the 50/50 (weight%) concentration. The critical point is at 170°C, lower than the melting point of their PHB-PET material (T_m = 190°C) [19]. In our case, the diagram was obtained via twin screw extrusion. It has the critical point at the 30/70 (weight) LCP composition and at the temperature of 312.4°C, also lower than the melting temperature (T_m = 325°C) of our PHB-PET polymer (Table 3-1). This temperature is much higher than the T_g of pure PC, which is 147.6°C. Therefore, the segmental motion of the blend is sufficient to cause phase separation, even though the melting point of LCP is not reached. In addition, the position of the critical point is dependent on the degrees of polymerization (N_1, N_2) of both components [8]. When N_1 > N_2, the critical point shifts to the left of the diagram. When N_1 = N_2, the critical point is at the center. When N_1 < N_2, it shifts to the right of the diagram. Finally, in spite of substantial effects, we could not find the transition temperature at 10wt% LCP concentration, as Kyu and Zhuang [19] did. This is mainly because of the complex phase behavior of the blend near the limiting conditions at low LCP concentration.
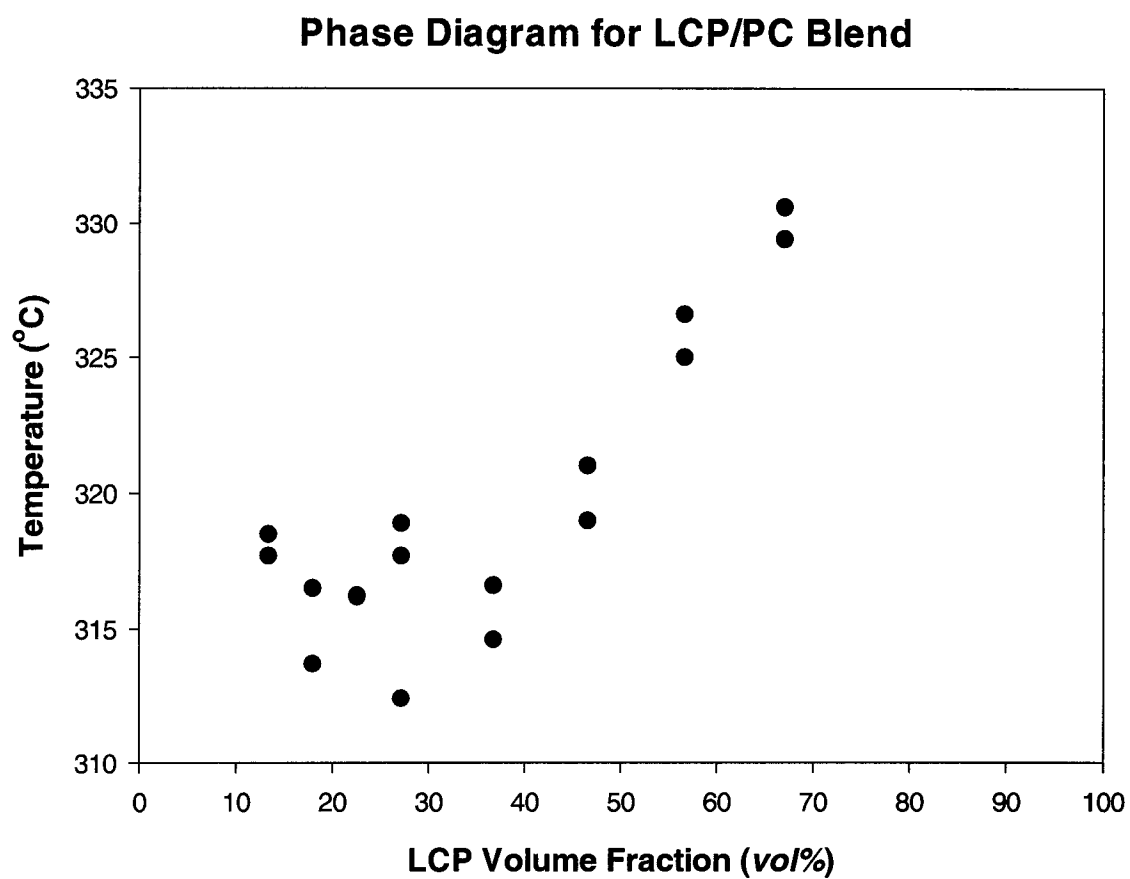
Figure 4-5: Phase Diagram for LCP/PC blend.

4.2.3 Morphology

In this section, we discuss the morphology of the blend in terms of the SEM and PLM results.

Both sides of the curve (Figure 4-5) for each LCP concentration (15%-70%) were investigated by SEM. The SEM results have confirmed those of DSC and characterized them in visible phase morphology. Figure 4-6 shows the SEM photomicrographs of fractured surfaces of extruded strands for the 30wt% LCP blend. Several observations can be made from Figure 4-6. Firstly, two types of morphology are observed. From (A) to (D), the blends show a homogenous co-continuous phase; while from (E) to (G), the blends have a dispersed droplets two-phase morphology. This phenomenon has already been discussed in section 3.3.2.3. Secondly, the LCP/PC blend undergoes thermally induced phase separation, because it transforms from a homogenous single-phase (Figure 4-6A-D) to a dispersed droplets two-phase (Figure 4-6E-G), as the blend goes from the lowest processing melt temperature (290°C) to the highest temperature (350°C). Phase separation seems to occur via spinodal decomposition, because the droplet size and shape are uniform visually. (We shall present the evidence of the droplet size distribution later in section 4.4.) The photomicrographs provide a clear visualization of the phase separation mechanism of the blend. Thirdly, the SEM microphotographs provide visible morphological evidence in support of the results of the DSC thermal analysis. As discussed in section 4.2.1, the blend T_g decreased slightly at the processing melt temperature 305°C (Figure 4-6D), reflecting a miscible blend. When the processing melt temperature increased to 315°C, the blend T_g increased and phase separation occurred (see Table 4-1 and Figure 4-6E). This confirms that the phase transition temperature is between 305°C and 315°C. In addition, the higher is the processing melt temperature, the smaller is the droplet size obtained. Recall that in section 2.3.1, the droplet size is dependent on the rate of heating or cooling and the rate of diffusion, viscosity, and chemical potential of both components. According to the Cahn-Hilliard Equation (2-9) and the Flory-Huggins Equation (2-13), the predicted wavelength at an initial concentration ϕ_0 is a function of temperature, $\lambda_m \propto T^{-\frac{1}{2}}$. Normally, $d_m \propto \lambda_m/2$, therefore
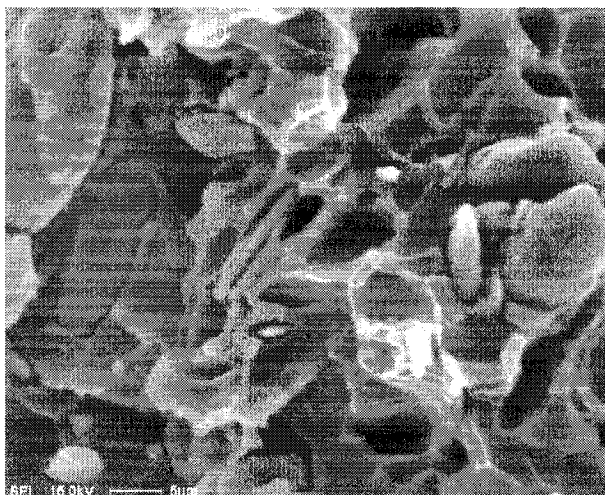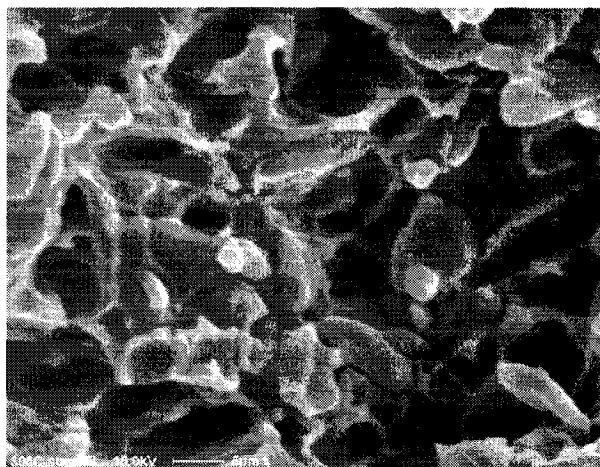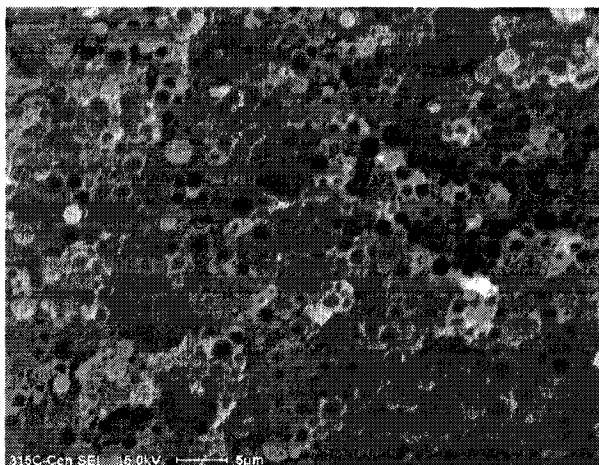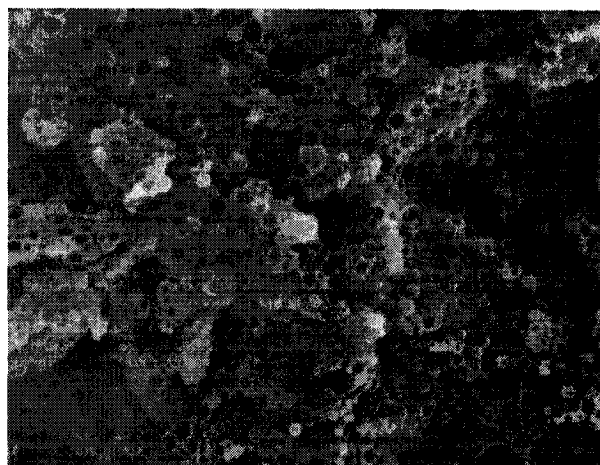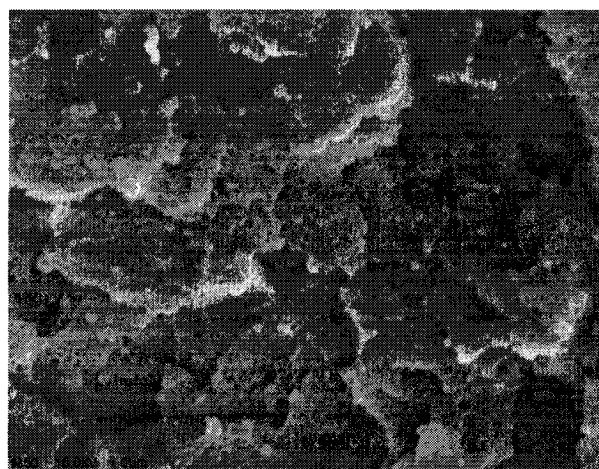
(A)
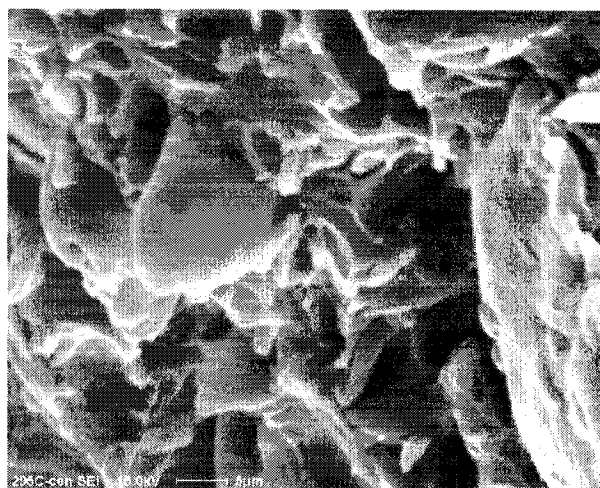
(B)
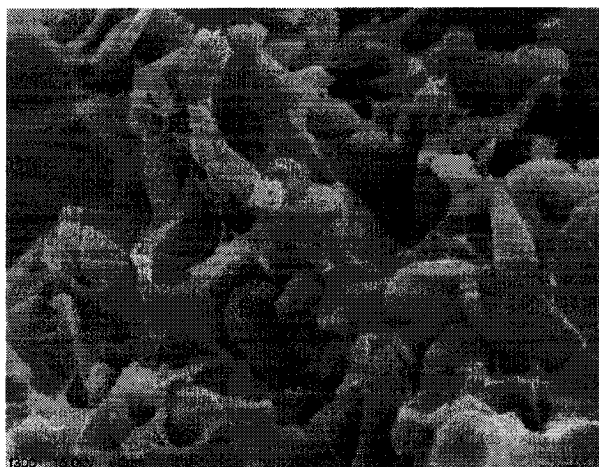
(C)

(D)

5μm

Figure 4-6: SEM micrographs of the fractured surfaces of 30 wt% LCP blend extruded in twin screw extrusion at (A) T_{pm} = 290°C, (B) T_{pm} = 295°C, (C) T_{pm} = 300°C, (D) T_{pm} = 305°C (magnification ×2000).

69

(E)

(F)

(G)

5μm

Figure 4-6 (continued): SEM micrographs of the fractured surfaces of 30 wt% LCP blend extruded in twin screw extrusion at (E) T_{pm} = 315°C, (F) T_{pm} = 325°C, (G) T_{pm} = 350°C (magnification ×2000).

the droplet size (diameter) is expected to decrease with an increase in temperature. This point will be discussed again later in section 4.4.

Another direct analysis of the blend morphology is possible with polarized light microscopy (PLM). In order to study the melt phase behavior of the LCP/PC blend, #2 specimens (Table 3-4) were microtomed in 5 μm thickness by using different heating and cooling rates using the PLM hot-stage. Figure 4-7 shows PLM micrographs of these specimens. At room temperature, as Figure 4-7A and D show, LCP has very tiny droplets because 30wt% LCP is the minor phase in the blend. In addition, the droplets are fairly well distributed in the PC rich matrix phase. Figure 4-7B shows the morphology at 340°C (heating rate 2 °C/min), LCP droplets gradually disappeared. When it was heated to 347°C (see Figure 4-7C), LCP droplets disappeared completely and there was no change in morphology when cooled down to room temperature. Another sample was used (Figure 4-7D) to repeat the same experiment but the heating rate was changed to 5 °C/min. LCP droplets gradually disappeared at around 360°C (Figure 4-7E), after that the droplets disappeared. It seems that LCP droplets will not appear again. In order to fully understand the phenomenon, a third experiment was run using 1 °C/min heating and cooling rates. Figure 4-8 shows PLM micrographs of #2 specimens (Table 3-4) microtomed in 5 μm thickness. Initially, the specimen (Figure 4-8A) was heated to 300°C as fast as possible (around 130 °C/min) and held for 2 min at 300°C. When the temperature reached 180°C, the sample began to melt (Figure 4-8B). From 300°C to 350°C, the sample was heated using 1°C/min heating rate, the droplets disappeared completely at 333°C (Figure 4-8C). Then the sample was cooled down from 350°C (Figure 4-8D) to ambient temperature at 1°C/min, but the LCP droplets did not appear again.

From Figures 4-7 and 4-8, it seems that the results of PLM contradict the DSC and SEM results. There is a major reason for this apparent behavior. The resolution of SEM (10 nm) is much higher than that of PLM (0.2 μm) [3], which is merely sufficient to study very immiscible blend phase systems. This means that the PLM could not show the droplet as the blend was heated.
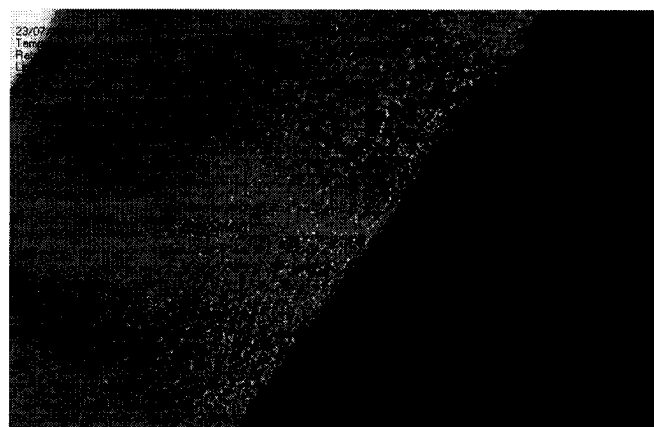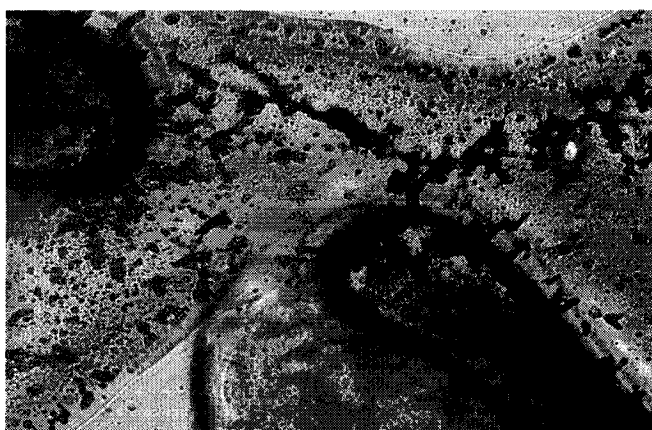
(A)
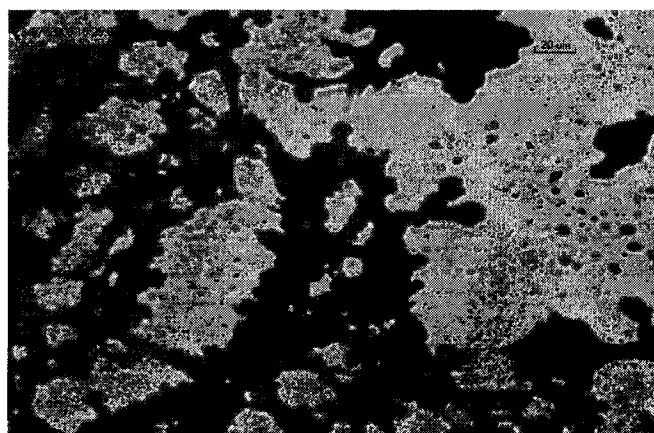
(B)

20μm

Figure 4-7: PLM micrographs of the 30 wt% LCP/PC blend in 5 μm thickness at: (A) room temperature, (B) 340°C (heating rate 2 °C/min) (magnification: ×20).

72

(C)

(D)

(E)   20µm

Figure 4-7: (continued) PLM micrographs of the 30 wt% LCP/PC blend in 5 µm thickness at: (C) 347°C (heating rate 2 °C/min), (D) room temperature, and (E) 360°C (heating rate 5 °C/min) (magnification: ×20).
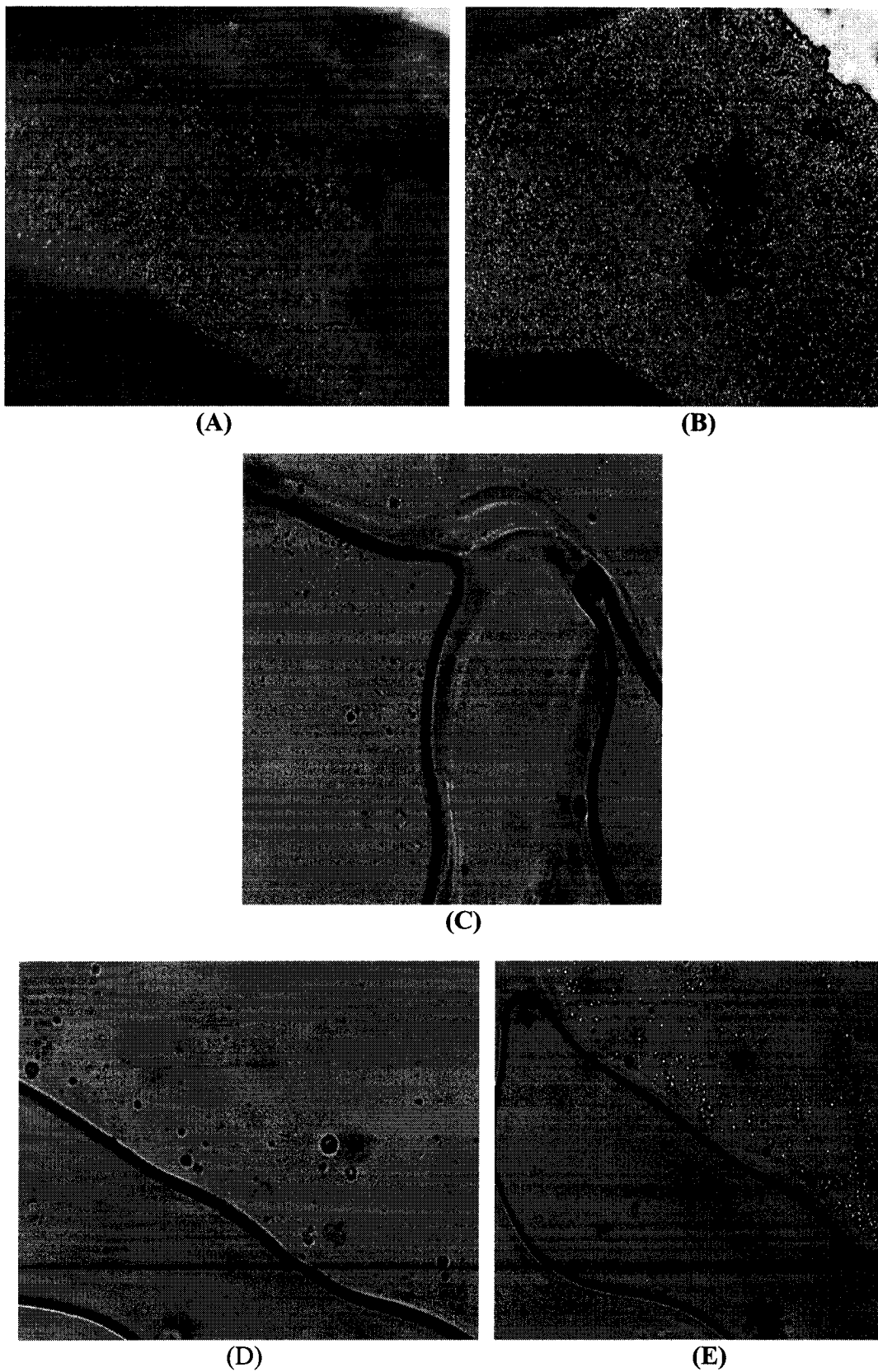
Figure 4-8: PLM micrographs of 30 wt% LCP/PC blend in 5 μm specimen thickness with 1 °C/min heating and cooling rate at: (A) room temperature, (B) 180°C, (C) 333°C, (D) 350°C, (E) 147°C (magnification: ×20).

4.2.4 Influence of Shear Rate on Phase Morphology

In explaining the morphology observed for the LCP/PC blend extruded by twin-screw extrusion, recall that phase separation via spinodal decomposition (SD) may be induced by shear, stress or pressure. In the present work, we assume that there is very little pressure change in the twin-screw extruder, so pressure effects were ignored. Figures 4-9 and 4-10 show fractured surfaces of 30 wt% LCP blend extruded at T_{pm} = 300°C and 50 wt% LCP extruded at T_{pm} = 310°C with different screw speeds. As can be seen, the morphologies are almost the same. Thus, it appears that the shear rate does not influence phase separation at these two concentrations.
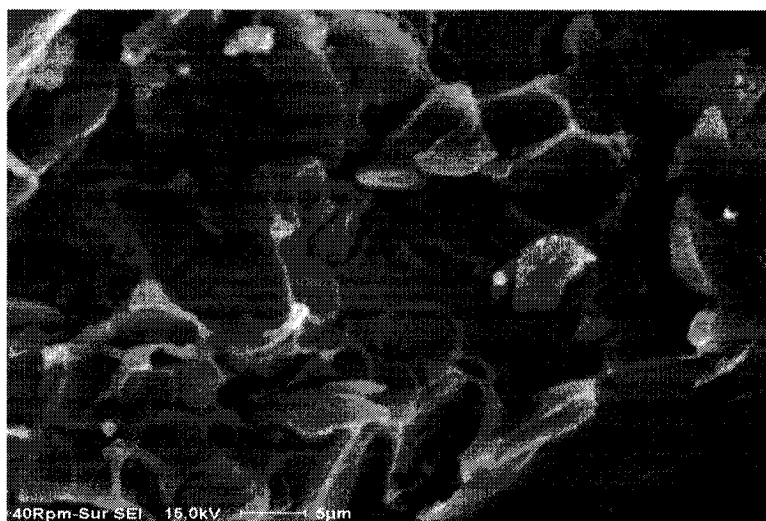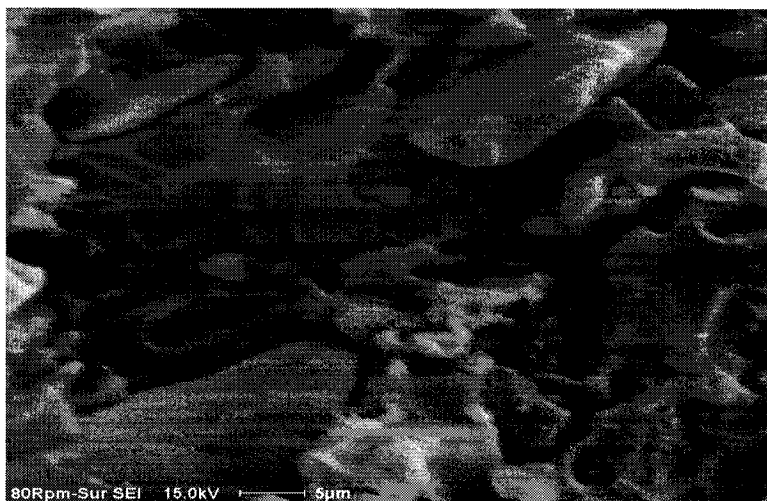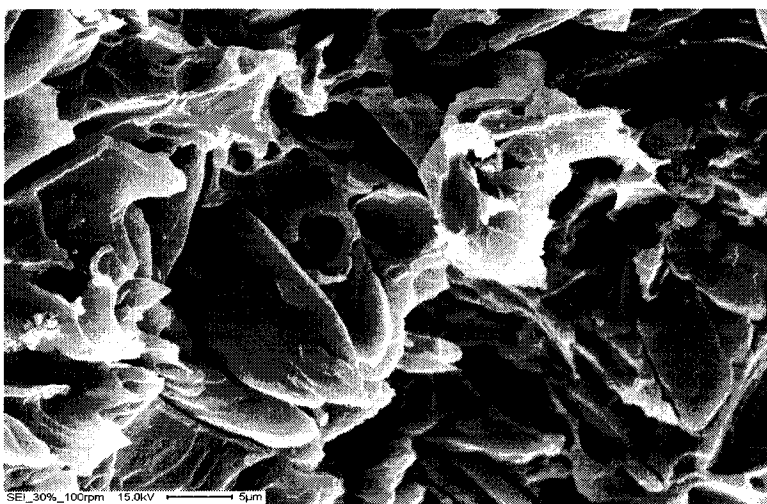
(A)
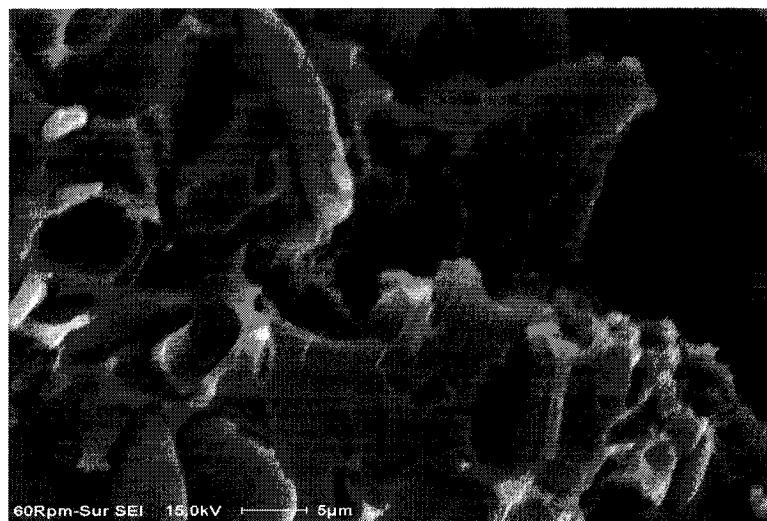
(B)

Figure 4-9: SEM micrograph of fractured surfaces of 30 wt% LCP blend extruded at T_{pm} = 300°C with different screw speed, (A) 40 rpm, (B) 60 rpm (magnification ×2000).
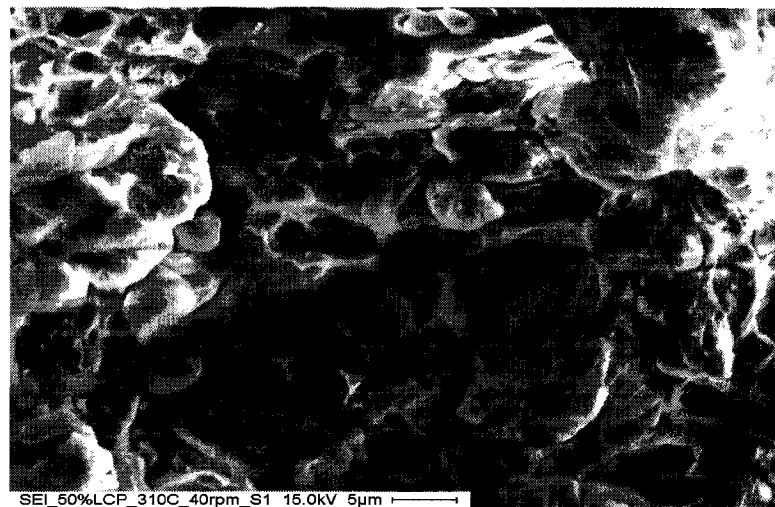
(C)

(D)

Figure 4-9: (continued) SEM micrograph of fractured surfaces of 30 wt% LCP blend extruded at T_{pm} = 300°C with different screw speed, (C) 80 rpm, (D) 100 rpm (magnification ×2000).

(A)

(B)

Figure 4-10: SEM micrograph of fractured surfaces of 50 wt% LCP blend extruded at $T_{pm} = 310^\circ C$ with different screw speed, (A) 40 rpm, (B) 60 rpm (magnification ×2000).
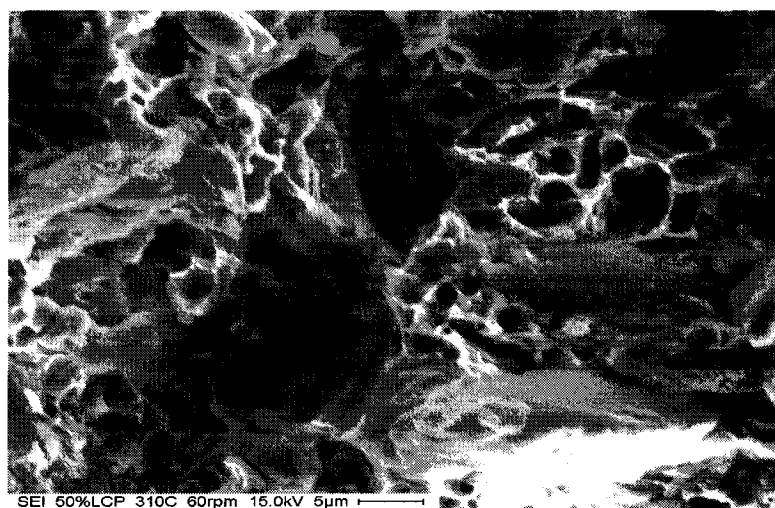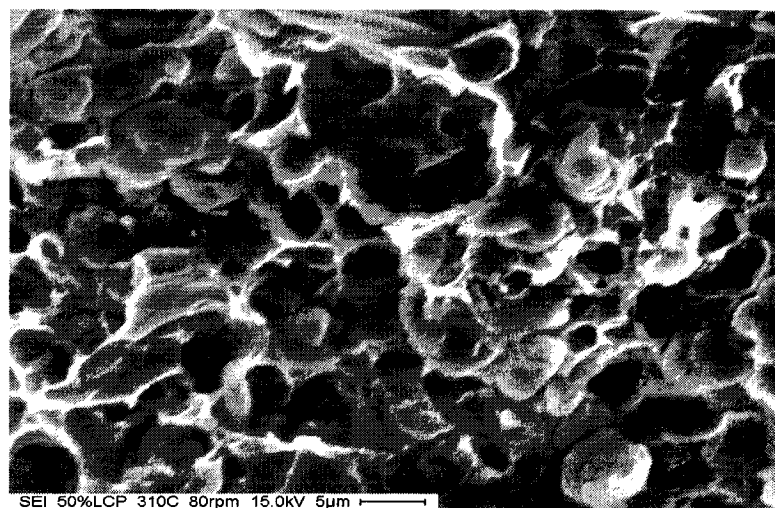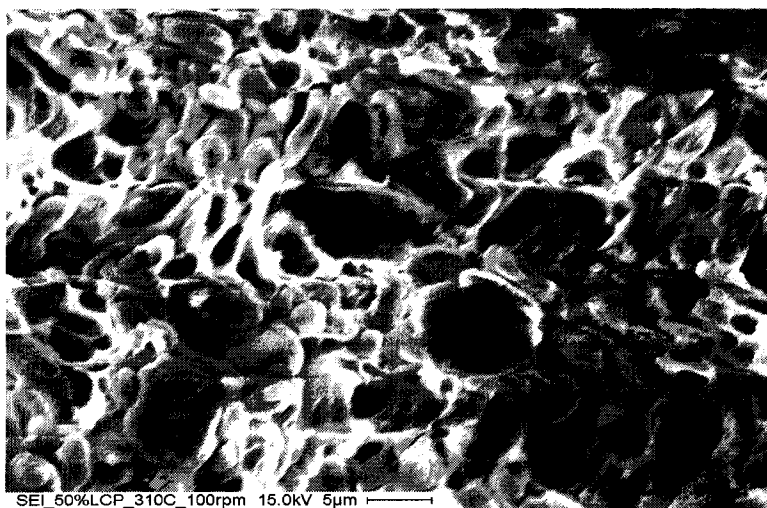
(C)

(D)

Figure 4-10: (continued) SEM micrograph of fractured surfaces of 50 wt% LCP blend extruded at T_{pm} = 310°C with different screw speed, (C) 80 rpm, (D) 100 rpm (magnification ×2000).

4.2.5 Error Estimation for the Phase Diagram

As shown in Figure 4-5, many experiments were repeated. All experimental data are plotted in this figure. Some LCP concentrations show small deviations, which others show higher deviation. The largest discrepancy occurred in the 27.1vol% LCP concentration. There are three major reasons causing errors in determining the phase diagram.

1. It is difficult to precisely control the processing melt temperature in the twin screw extruder, the melt temperature recorded was not the real value near the exit of the die. Usually there is around $\pm 5^{\circ}C$ difference. This factor causes temperature error (Y-axis error bar) in the phase diagram.

2. The calibration curve for the twin screw extruder feeders is not constant. Therefore, the blend weight ratio (LCP/PC) could vary from the estimated value. This may cause LCP volume fraction error (X-axis error bar) in the phase diagram.

3. The final results (phase diagram) involve many experimental steps, such as sample preparation and thermal analysis. Significant cumulation errors could result in the final phase diagram.

The phase diagram with error bars is shown in Figure 4-11. The dots represent the average value at each concentration. A quadratic curve was fitted to these points.
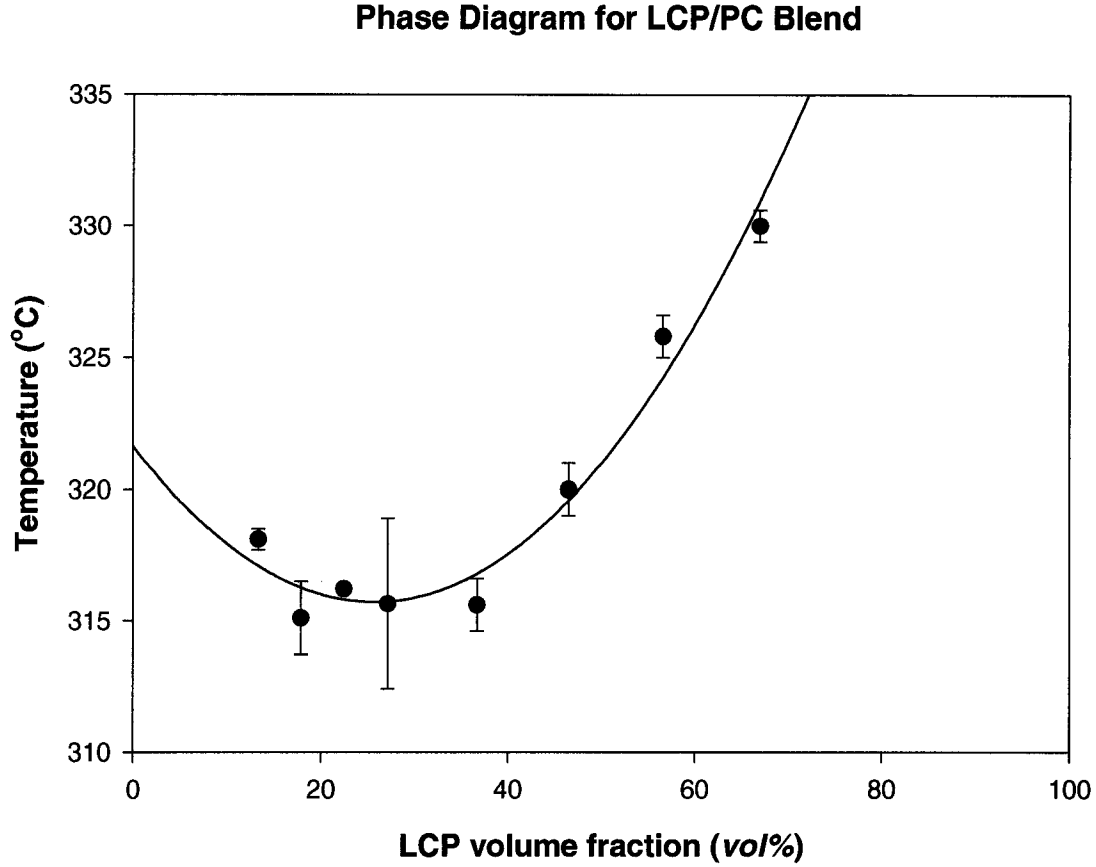
Phase Diagram for LCP/PC Blend

Figure 4-11: Phase diagram for LCP/PC blend prepared by twin screw extrusion, determined by DSC thermal analysis and calculation. The solid line is a quadratic fitting curve for the experimental data. The dots are the experimental data with error bars.

4.3 Flory-Huggins Theory Phase Diagram for LCP/PC Blend

As mentioned in Section 2.4.2, the Flory-Huggins (F-H) free energy equation has been quite successful in phase equilibrium studies [8,14]. Based on the condition that the second derivative of Equation (2-13) with respect to volume fraction equals zero, the χ-ϕ relationship equation can be expressed as,

$$\phi_1^2 + (\frac{N_1 - N_2}{2N_1 N_2 \chi} - 1)\phi_1 + \frac{1}{2N_1 \chi} = 0 \qquad (4\text{-}3)$$

81

where N_1, N_2 are the degrees of polymerization of components 1 and 2, respectively, ϕ_1 is the volume fraction of component 1 and χ is the polymer-polymer interaction parameter. Equation (4-3) can be expressed in another form,

$$\chi = \frac{1}{2N_1\phi} + \frac{1}{2N_2(1-\phi)}$$ (4-4)

The degree of polymerization N can be calculated by,

$$N = M_n / M_o$$ (4-5)

where M_n is the number average molar mass of the polymer and M_o is the corresponding structural unit molar mass of this polymer. In this work, LCP and PC are components 1 and 2, respectively. In Table 3-1, M_{n1} = 10,365 g/mol, M_{01} = 182 g/mol, $N_1 = M_{n1}/ M_{01}$ = 57; M_{n2} = 24,500 g/mol (average value), M_0 = 254 g/mol, N_2 = 96.

The experimental χ values can be obtained by substituting the experimental volume fraction of Table 4-3 into Equation (4-4). These χ values, with their corresponding processing melt temperature T_{pm}, are given in Table 4-4,

Table 4-4: Summary of Experimental χ Values

Vol% LCP	13.3	17.9	22.5	27.1	36.7	46.5	56.6	67.0
χ	0.0720	0.0553	0.0457	0.0395	0.0321	0.0286	0.0275	0.0289
T_{pm} (°C)	317.7 318.5	316.5 313.7	316.23 316.19	317.7 318.9 312.4	314.6 316.6	319.0 321.0	325.0 326.6	329.4 330.6

As discussed in Section 2.4.2, the temperature dependence of χ relation is given by (Equation 2-12):

$$\chi(T) = a + \frac{b}{T}$$ (2-12)

The experimental χ values are plotted as a function of reciprocal T_{pm} shown in Figure 4-12. The best linear fit for Equation (2-12) was used. This fitting also needs to have a good agreement with the phase diagram given by Equation (4-3). However, because of the wide scatter of these data, it is not possible at this time to confirm the general validity. Consequently, the fitting equation is not a perfect one and is given by:

$$\chi(T) = 1.025 - \frac{583}{T} \tag{4-6}$$

At the critical point, the volume fraction ϕ_c and interaction parameter χ_c are calculated by Equations (2-14 and 2-15),

$$\phi_c = 0.566 \,;\, \chi_c = 0.0275.$$

From Equation (4-6), the χ values were recalculated by scanning the temperatures from 584K to 608K (311°C-335°C) with a step 0.05K. Then these χ values were substituted into Equation (4-3) to calculate the volume fractions ϕ of component 1. In order to compare the theoretical and experimental phase diagrams, these calculated volume fractions were plotted in a T-ϕ phase diagram as shown in Figure 4-13. The curve appears concave with a minimum at 56.6 vol% LCP concentration at 311.4°C, while the experimental curve (Figure 4-11) has a minimum at the 27.1vol% LCP concentration at 312.4°C. The two curves have almost the same critical temperature but different critical concentrations ϕ_c. The simulated curve is shifted to the right. As mentioned in section 4.2.2, when $N_1 < N_2$, the curve will shift to the right of the diagram. It also should be noted that the simulated curve has a steep slope at lower LCP concentrations (<10vol% LCP). This situation brings about practical difficulties in either finding a transition temperature or controlling the errors at low LCP volume fraction (<10vol% LCP).
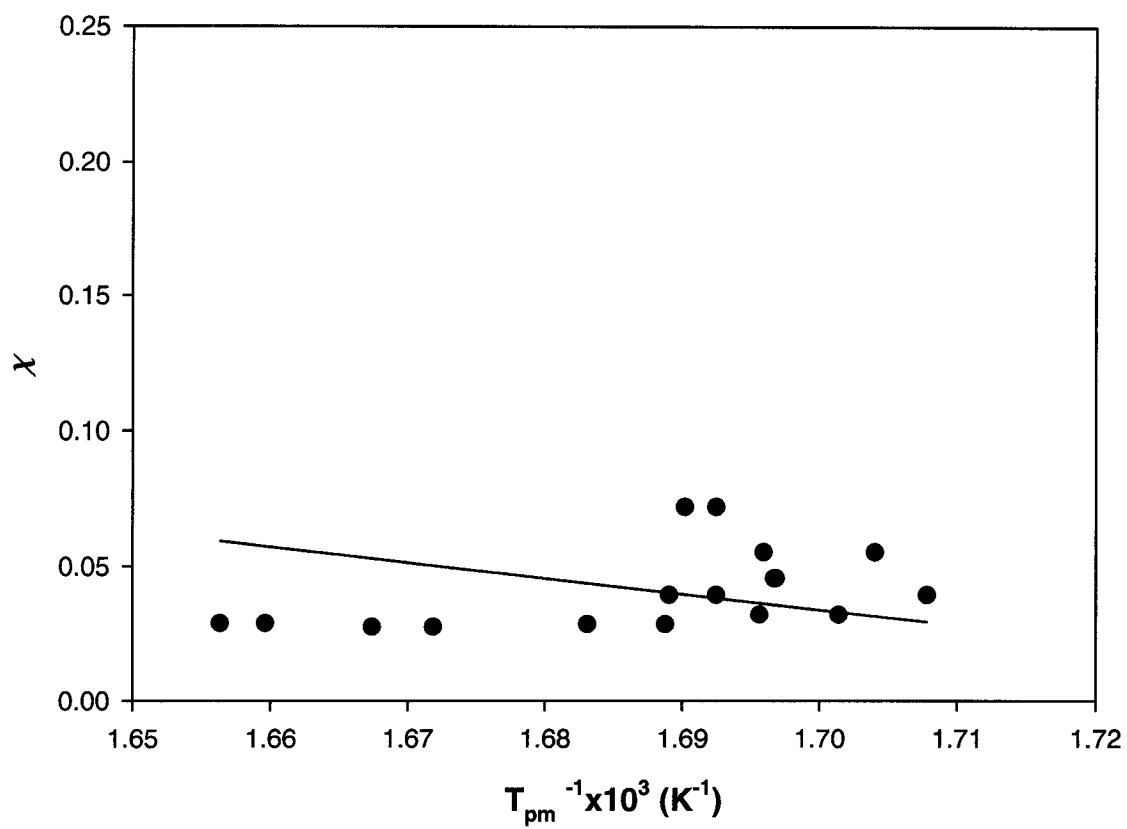
Figure 4-12: Curve fitting for experimental χ values. The solid line is given by Equation (4-6). The dots are the experimental data.
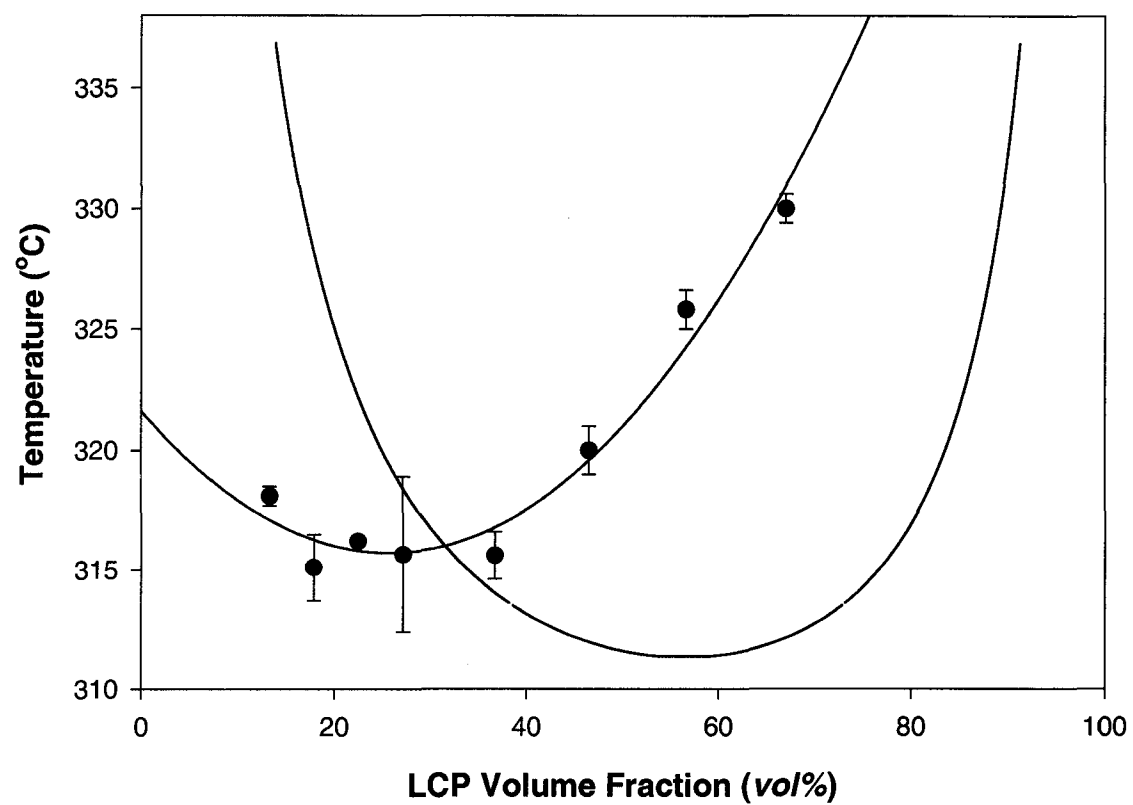
Figure 4-13: Phase diagram for LCP/PC blends. Left: the experimental phase diagram with error bars, right: simulated phase diagram derived from Flory-Huggins theory.

4.4 Droplet Size Distribution for LCP/PC Blend

As discussed in section 2.4.1, the Cahn-Hilliard Equation (2-9) can be used to calculate the wavelength at an initial concentration ϕ_0. Based on Equations (2-9) and (2-13), we can obtain the T-λ_m relationship as follow,

$$\lambda_m = 2\sqrt{2}\pi\, (\frac{k_B}{\kappa v})^{-\frac{1}{2}} \{-\frac{T}{2}[\frac{1}{N_1\phi_0} + \frac{1}{N_2(1-\phi_0)} - 2\chi]\}^{-\frac{1}{2}} \qquad (4\text{-}7)$$

where k_B is Boltzmann's constant, v is the volume of a cell or segment, κ is the gradient energy parameter, ϕ_o is the initial average concentration, N_1 and N_2 are the degree of polymerization of components 1 and 2, respectively, χ is the Flory-Huggins interaction parameter, T is temperature and λ_m is the wavelength.

It has been assumed that $(\frac{k_B}{\kappa v})^{-\frac{1}{2}}$ is constant at an initial concentration ϕ_0 and temperature. The dimensionless wavelength is given as:

$$\lambda_m^* = \lambda_m /(\frac{k_B}{\kappa v})^{-\frac{1}{2}} \qquad (4\text{-}8)$$

We selected some data in section 4.3 for calculation, $N_1 = 57$, $N_2 = 96$, $\chi = 1.025-583/T$ (Equation 4-6). In the case of 30wt% LCP (27.1 vol% LCP $\phi_0 = 0.271$), the calculation results of λ_m^* are given in Table 4-5.

Table 4-5: Summary of Calculated Dimensionless Wavelength for 30% LCP Blend

Processing Melt Temperature T_{pm} (°C)	325	330	340	350
λ_m^*	3.678*	2.697*	1.944*	1.598*

In this table, the dimensionless wavelength decreases when the processing melt temperature increases. It means that at higher processing melt temperature T_{pm}, smaller droplet size obtained. Figure 4-14 shows the SEM micrographs of 30wt% LCP blend at
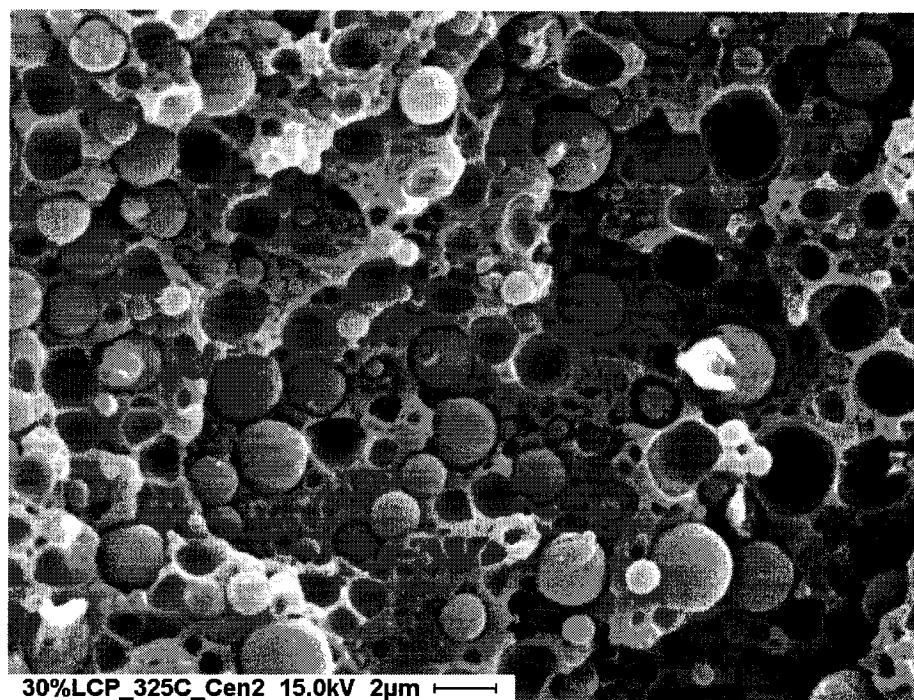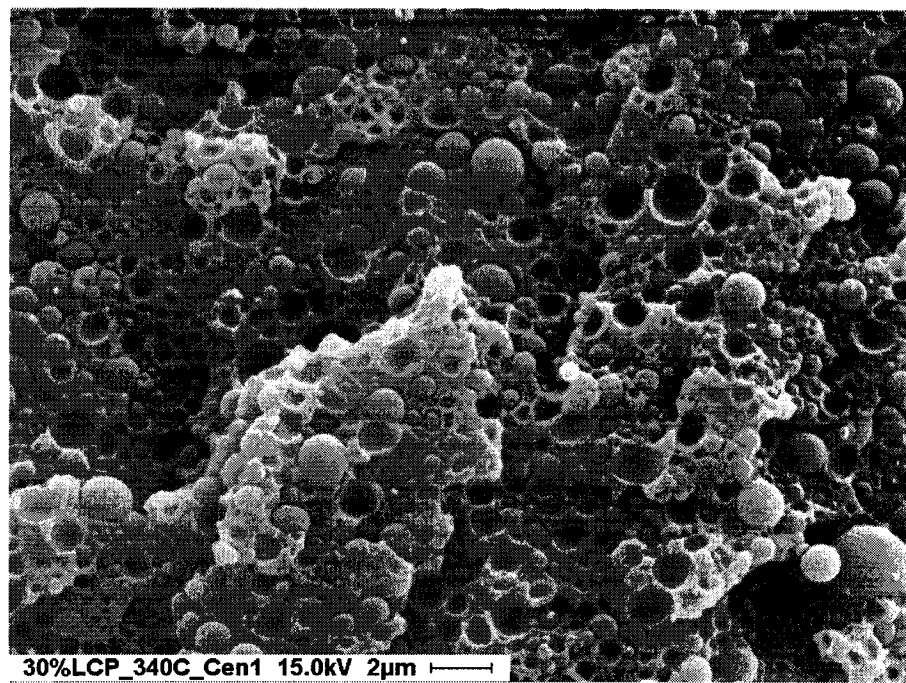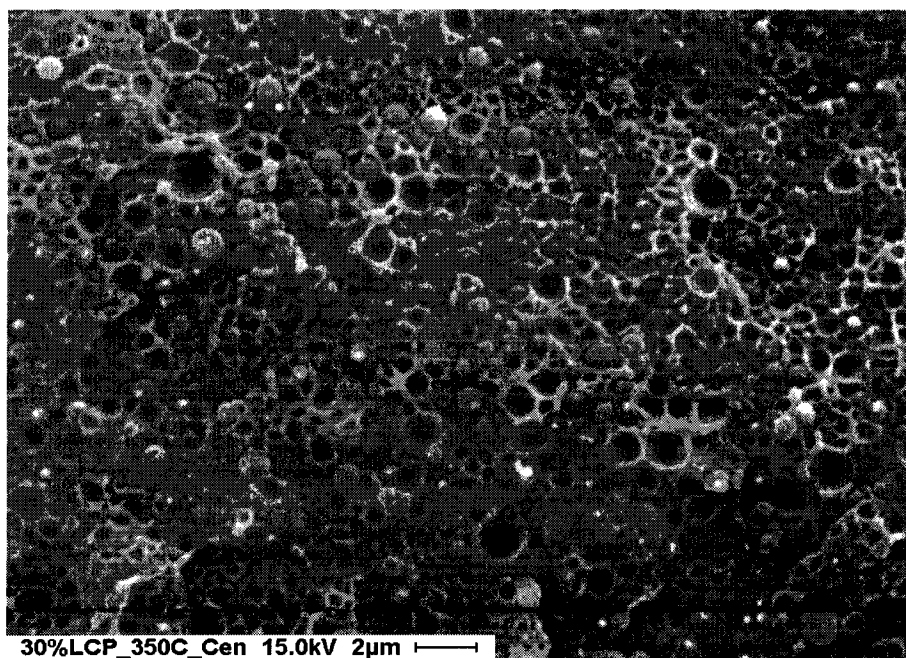
(A)
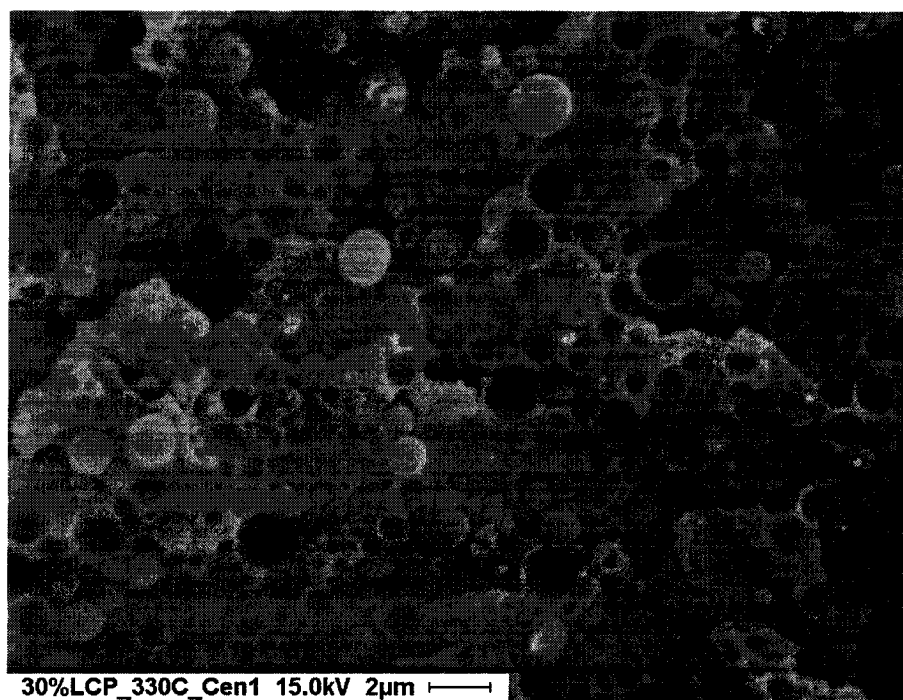
(B)

Figure 4-14: SEM micrographs of 30 wt% LCP blend at different processing melt temperature (A) $T_{pm} = 325^{\circ}C$, (B) $T_{pm} = 330^{\circ}C$ (magnification ×4000).

(C)

(D)

Figure 4-14 (continued): SEM micrographs of 30 wt% LCP blend at different processing melt temperature (C) T_{pm} = 340°C, (D) T_{pm} = 350°C (magnification ×4000).

different T_{pm}. The droplet size becomes smaller with the increase of processing melt temperature T_{pm}, as indicated by the above analysis.

In order to quantify the above observations, the droplet size distribution of the blend was determined. The distributions can be described by a variety of averages, such as number-average and weight-average. The number-average droplet size $<D>_n$ is defined by:

$$<D>_n = \frac{\sum N_i D_i}{\sum N_i}$$ (4-9)

where N_i is the number of ith particles with droplet diameter D_i. The brackets $<>$ indicate that it is an average value. The weight-average droplet size $<D>_w$ is obtained by,

$$<D>_w = \frac{\sum N_i D_i^2}{\sum N_i D_i}$$ (4-10)

The breadth of the distribution can be gauged by establishing the particle distribution or polydispersity index PD, which can be defined as,

$$PD = \frac{<D>_w}{<D>_n}$$ (4-11)

As mentioned in section 3.3.2.4, the images (Figure 4-14) were analyzed manually. Figure 4-15 shows the plot of droplet size distribution of these images (Figure 4-14). A summary calculation of $<D>_n$, $<D>_w$ and PD for this blend is given in Table 4-6.

In Figure 4-15 A, the blend has the largest number of the smallest droplets (≤ 0.27 μm) at 350°C. However, the blend has the largest droplets (≥ 3.33 μm) at 325°C. Figure 4-15B is a scatter plot of droplet size distribution. The peak of each curve decreases with a decrease of temperature. This confirms that the higher temperature, the smaller droplet size.

In Table 4-6, the PD values are almost the same. This suggests that there is no major difference in the breadth of the distribution. The $<D>_n$ and $<D>_w$ decrease when the processing melt temperatures increase.

Droplet Size Distribution for 30wt% LCP Blend

(A)

Droplet Size Distribution for 30wt% LCP Blend
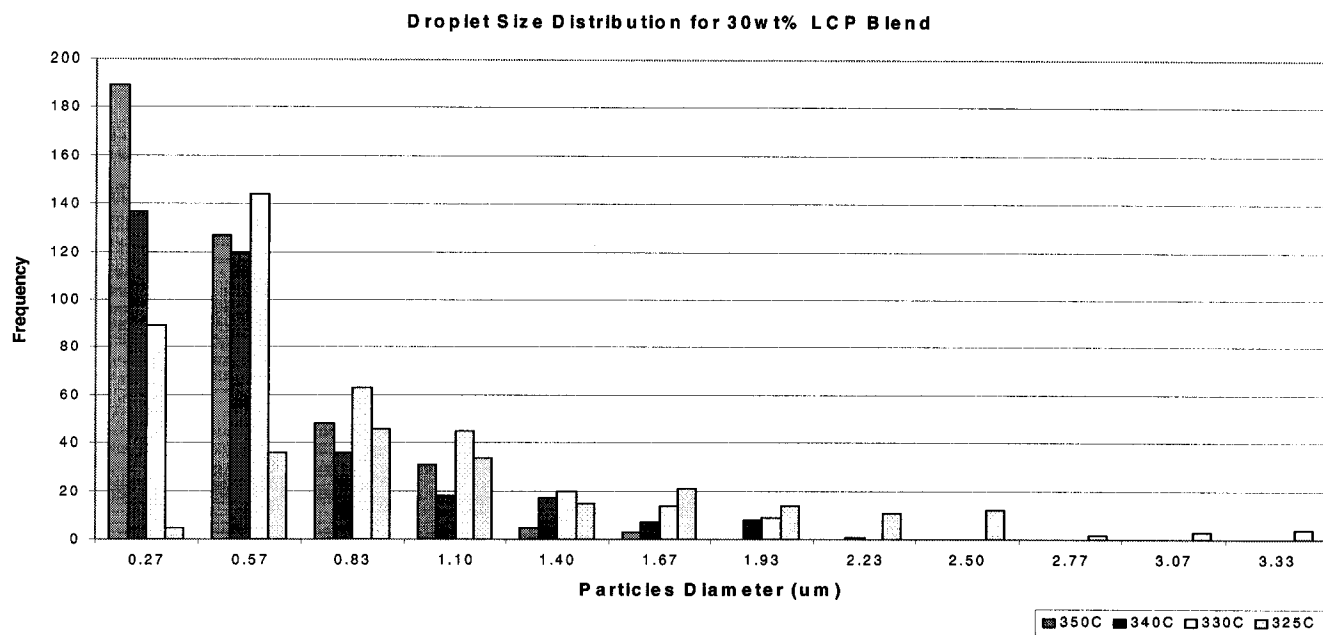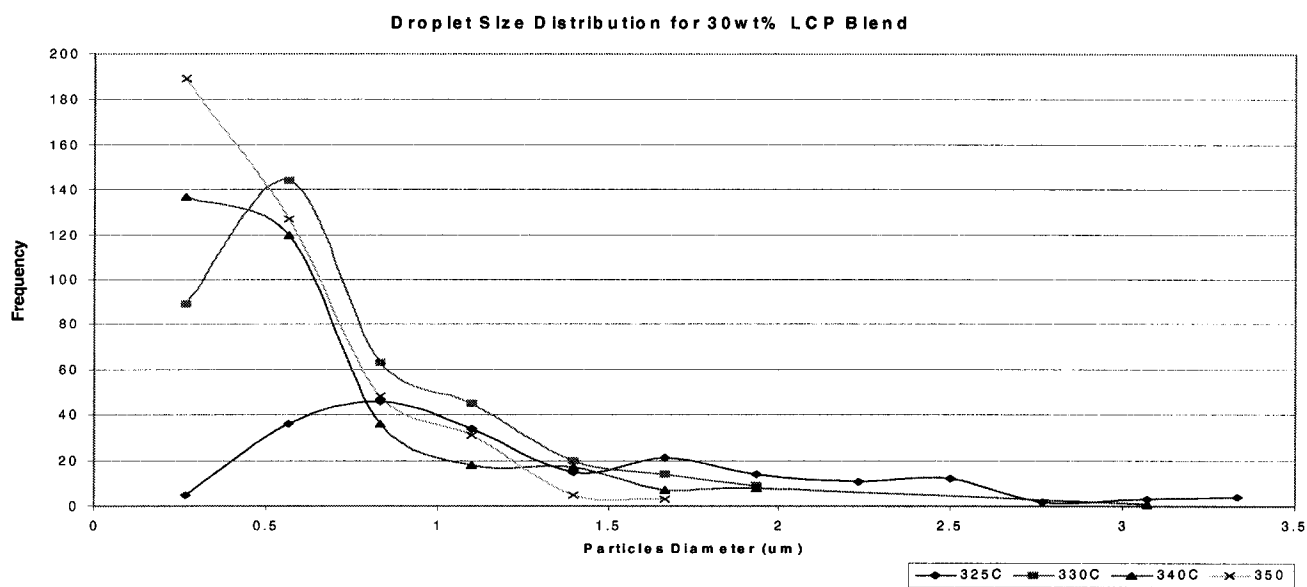
(B)

Figure 4-15: Droplet size distribution for 30wt% LCP/PC blend (A) bar chart of particle number vs. diameter, (B) Scatter curve of particle number vs. diameter.

Table 4-6: Summary of Calculated $\langle D \rangle_n$, $\langle D \rangle_w$ and PD for 30% LCP Blend

Temperature (^{o}C)	$\langle D \rangle_n$	$\langle D \rangle_w$	PD
325	1.30	1.68	1.30
330	0.719	0.951	1.32
340	0.603	0.881	1.46
350	0.517	0.687	1.33

Chapter 5

Conclusions and Recommendations

The experimental results indicate that the techniques developed are successful for the purpose of obtaining the phase diagram for LCP/PC blends, which is known to undergo thermally induced phase separation via spinodal decomposition [18,19]. The DSC results and the fitting equation developed appear to provide a reliable method for determining the thermodynamic binary phase diagram. Furthermore, the SEM results support and confirm the DSC results and provide reliable phase morphology evidence. Thus, the results suggest that the proposed novel technique, involving twin screw extrusion coupled with DSC and SEM characterization, is suitable to generate blend behavior information about the thermally induced phase separation via spinodal decomposition.

The experimental techniques produced results which appear to be in agreement with those predicted by theory and generally, with experimental results reported by other researchers [16-29]. Some of the more pertinent conclusions that have been derived from these results are as follows:

1. Polycarbonate (PC) and liquid crystalline polymer (LCP) can form either miscible or immiscible blends under different processing conditions in twin screw extrusion.

2. The influence of blending process melt temperature T_{pm} in twin screw extrusion on the glass transition temperatures (T_{g}s) of the blends was investigated. The blends show variable T_{g}s, depending on the processing melt temperatures. This

observation has led to the development of a novel method to determine the thermodynamic phase diagram for the polymer blend system under consideration.

3. The LCP/PC blend is unstable and undergoes thermally induced phase separation via spinodal decomposition with a characteristic lower critical solution temperature (LCST).

4. As evidenced by DSC and SEM measurements, the processing melt temperature T_{pm} in twin screw extrusion appears to have a significant influence on phase morphology of the blends, while the screw speed (shear rate) does not.

5. At a given LCP concentration, higher processing melt temperature (T_{pm}) produce smaller droplet sizes.

Finally, knowledge of the temperature and concentration dependencies (T-ϕ) in the phase diagram provides important information which can be used to manipulate the properties of the polymer blend system. Phase morphology of the blend and its corresponding mechanical properties can be manipulated by using this T-ϕ phase diagram. It is suggested that a relationship between the morphology and the mechanical properties can be further investigated using different polymer processing methods, such as injection molding. Finally, the behavior of the blend at the lower and higher LCP concentration ranges, below 15wt% and above 70wt%, should be investigated.

References

1. L. H. Sperling, *Polymeric Multicomponent Materials: An Introduction*, John Wiley & Sons, New York (1997).

2. L. A. Utracki, *Polymer Alloys and Blends: Thermodynamics and Rheology*, Hanser Publishers, New York (1989).

3. M. J. Folkes and P. S. Hope, (ed.), *Polymer Blends and Alloys*, Blackie Academic & Professional, London (1993).

4. W. Brostow, (ed.), *Mechanical and Thermophysical Properties of Polymer Liquid Crystals*, Chapman and Hall, London (1998).

5. J. F. Masson, *Cellulose/Synthetic-polymer Blends*, Ph.D. Thesis, McGill University (1990).

6. E. Kiran, *NATO ASI Series E Applied Sciences – Advanced Study Institute*, **366**, 167 (2000).

7. M. A. Van Dijk and A. Wakker, *Concepts of Polymer Thermodynamics*, Technomic Publishing Co., Lancaster, PA (1997).

8. J. M. G. Cowie, *Polymers: Chemistry and Physics of Modern Materials*, Chapman and Hall, New York (1991).

9. O. Olabisi, L. M. Robeson and M. T. Shaw, *Polymer-Polymer miscibility*, Academic Press, New York (1979).

10. J. W. Cahn, *J. Chem. Phys.,* **42**, 93 (1965).

11. J. W. Cahn and J. E. Hilliard, *J. Chem. Phys.,* **28**, 258 (1958).

12. P.J. Flory, *J. Chem. Phys.,* **10**, 51 (1942).

13. M. L. Huggins, *Ann. NY Acad. Sci.,* **43**, 1 (1942).

14. P. J. Flory, *Principles of Polymer Chemistry*, Cornell University, Ithaca (1953).

15. K. Binder, in *Materials Science and Technology*, edited by R. W. Cahn, P. Haasen and E. J. Kramer, Volume 5, Chapter 7, VCH, New York (1991).

16. M. Kimura and R. S. Porter, *J. Polym. Sci., Polym. Phys. Ed.,* **22**, 1697 (1984).

17. P. Zhuang, T. Kyu, and J. L. White, *SPE ANTEC Tech. Papers*, **34**, 1237 (1988).

18. A. Nakai, T. Shiwaku, H. Hasegawa, and T. Hashimoto, *Macromolecules*, **19**, 3008 (1986).

19. T. Kyu and P. Zhuang, *Polym. Commun.,* **29**, 4, 99 (1988).

20. M. J. Seurin, J. M. Gill, A. T. Bosch, and P. Sixou, *Polymer,* **25**, 1073 (1984).

21. K. Friedlich, M. Hess, and R. Kosfield, *Makromol. Chem., Macromol. Symp.,* **16**, 251 (1988).

22. R. Kosfield, K. Friedlich, and M. Hess, 18th Euro-physics Conference on Macromolecular Physics, **11c**, 81 (1987).

23. M. Hess, K. Friedlich, and R. Kosfield, Int Conf. Liq. Cryst. Polym., Bordeaux, France, Paper 7P8 (July 1987).

24. S. Huang, A. C. Griffin, and R. S. Porter, *Polym. Eng. Sci.,* **29**, 55 (1989).

25. T. T. Hsieh, C. Tiu, K. H. Hsieh, and G. P. Simon, *J. Appl. Polym. Sci.,* **77**, 2319 (2000).

26. T. M. Malik, P. J. Carreau and N. Chapleau, *Polym. Eng. Sci.,* **29**, 600 (1988).

27. D. E. Turek, G. P. Simon, and C. Tiu, *Polym. Eng. Sci.,* **35**, 52 (1995).

28. K. Engberg, O. Stromberg, J. Martinsson, and U. W. Gedde, *Polym. Eng. Sci.,* **34**, 1336 (1994).

29. H. S. Lee, W. H. Jung and W. N. Kim, *Polymer Bulletin,* **37**, 4, 503 (1996).

30. Instructions Manual berstorff ZE-25, twin screw extruder, Charlotte, N.C. (1991).

31. Instructions Manual BX50, System Microscope, Olympus (1999).

32. J. F. Rabek, *Experimental Methods in Polymer Chemistry,* John Wiley & Sons (1980).

33. E. A. Turi, (edi.), *Thermal Characterization of Polymeric Materials,* Academic Press (1997).

34. D. R. Paul and S. Newman, *Polymer Blends,* Academic, New York (1978).

35. D. Patterson and A. Robard, *Macromolecules,* **11**, 690 (1978).

36. L. P. McMaster, *Macromolecules,* **6**, 760 (1973).
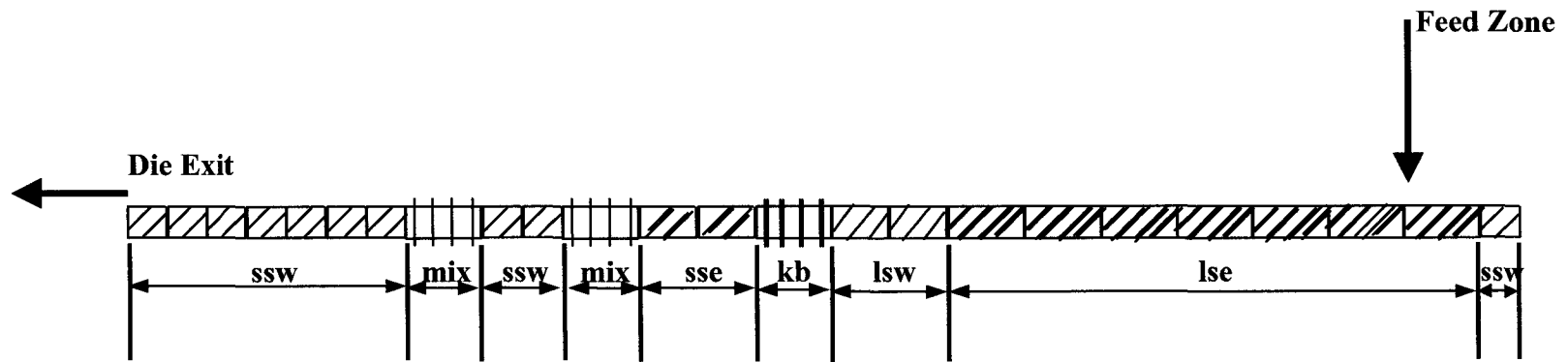
Screw Arrangement of Twin Screw Extruder

Figure A-1: Schematic design of the screw arrangement for twin screw extrusion. The initial words represent: ssw- short self-wiping, mix- toothed block mixing element, sse- short standard element, kb- 90° double threaded kneading block, lsw- long self-wiping, and lse- long standard element. ssw, sse, lsw, and lse are double-threaded conveying elements.